

INFORMATION TO USERS

This manuscript has been reproduced from the microfilm master. UMI films the text directly from the original or copy submitted. Thus, some thesis and dissertation copies are in typewriter face, while others may be from any type of computer printer.

The quality of this reproduction is dependent upon the quality of the copy submitted. Broken or indistinct print, colored or poor quality illustrations and photographs, print bleedthrough, substandard margins, and improper alignment can adversely affect reproduction.

In the unlikely event that the author did not send UMI a complete manuscript and there are missing pages, these will be noted. Also, if unauthorized copyright material had to be removed, a note will indicate the deletion.

Oversize materials (e.g., maps, drawings, charts) are reproduced by sectioning the original, beginning at the upper left-hand corner and continuing from left to right in equal sections with small overlaps. Each original is also photographed in one exposure and is included in reduced form at the back of the book.

Photographs included in the original manuscript have been reproduced xerographically in this copy. Higher quality 6" x 9" black and white photographic prints are available for any photographs or illustrations appearing in this copy for an additional charge. Contact UMI directly to order.

UMI

A Bell & Howell Information Company
300 North Zeeb Road, Ann Arbor, MI 48106-1346 USA
313:761-4700 800:521-0600

Order Number 9518460

Structure and function of unmodified *E. coli* valine-tRNA

Yue, Dongxian, Ph.D.

Iowa State University, 1994

Copyright ©1994 by Yue, Dongxian. All rights reserved.

U·M·I

300 N. Zeeb Rd.
Ann Arbor, MI 48106

Structure and function of unmodified *E. coli* valine-tRNA

by

Dongxian Yue

A Thesis Submitted to the
Graduate Faculty in Partial Fulfillment of the
Requirements for the Degree of
DOCTOR OF PHILOSOPHY

Department: Biochemistry and Biophysics
Major: Biochemistry

Approved:

Signature was redacted for privacy.

In Charge of Major Work

Signature was redacted for privacy.

For the Major Department

Signature was redacted for privacy.

For the Graduate College

Iowa State University
Ames, Iowa
1994

Copyright © Dongxian Yue, 1994. All rights reserved.

DEDICATION

To My Parents

TABLE OF CONTENTS

ABBREVIATIONS	xv
ABSTRACT	xvii
CHAPTER 1. INTRODUCTION	1
Function of tRNA	1
General structure of tRNA	3
Mg ²⁺ binding to tRNA	6
tRNA modifications	8
Unmodified tRNA	10
¹ H NMR studies of tRNA	10
¹⁹ F NMR studies of tRNA	12
tRNA identity	13
Codon-anticodon interaction	16
CHAPTER 2. MATERIALS AND METHODS	17
Materials	17
Methods	18
Purification of oligonucleotide GUAA	18

<i>In vitro</i> transcription of tRNA ^{Val} by T7 RNA polymerase	19
HPLC purification of transcribed tRNA	20
Site-directed mutagenesis	21
Overexpression of native tRNA ^{Val}	21
Aminoacylation kinetics	25
¹ H NMR spectroscopy	27
¹⁹ F NMR spectroscopy	29
CHAPTER 3. RESULTS	31
Structure comparison between native and transcribed tRNA ^{Val}	31
Solution structure in excess Mg ²⁺	32
Structure of unmodified tRNA ^{Val} at low Mg ²⁺ concentration	48
pH effect on native and <i>in vitro</i> transcribed tRNA ^{Val}	58
Recognition of the anticodon loop of <i>E. coli</i> tRNA ^{Val} by VRS	65
Anticodon variants	65
Anticodon loop deletion and position-shift mutants	65
Anticodon contributes to the binding of tRNA ^{Val} to VRS	67
Other mutants in the anticodon loop	68
Effect of positions 32 and 38 on anticodon loop structure	70
Aminoacylation activity of tRNA ^{Val} variants at positions 32 and 38	70
Evidence for conformational changes in tRNA ^{Val} mutant G38	70
Possible formation of an extra base pair between C32 and G38	73

Effects on tRNA ^{Val} structure of substitution of A38 with G38	75
¹⁹ F NMR studies of dynamics of the anticodon loop	79
Codon-anticodon interactions studied by ¹ H NMR	94
GUAA binding to tRNA ^{Val} : imino ¹ H NMR study	94
Structure of GUAA upon binding to tRNA ^{Val}	95
CHAPTER 4. DISCUSSION	108
REFERENCES	124
ACKNOWLEDGMENTS	130

LIST OF TABLES

Table 3.1:	Imino proton assignments in <i>E. coli</i> tRNA ^{Val}	43
Table 3.2:	Aminoacylation kinetics of anticodon variants	66
Table 3.3:	Aminoacylation Kinetics of nonanticodon variants	69
Table 3.4:	Proton assignments of free GUAA	104

LIST OF FIGURES

Figure 1.1:	Secondary and tertiary structure of tRNA. (A) Invariant nucleotides in the cloverleaf structure are indicated. (B) The L-shaped model of tertiary structure	5
Figure 1.2:	Mg ²⁺ and spermine binding sites located in the x-ray crystal structure of yeast tRNA ^{Phe}	7
Figure 2.1:	Aromatic and 1' sugar proton region of ¹ H NMR spectrum of GUAA in D ₂ O at 6 °C	20
Figure 2.2:	Expression of <i>E. coli</i> tRNA ^{Val} . (Δ) TG1 cell transformed with pVALT7 without induction by IPTG. (○) BL21(DE3) containing pVAL119-21 with induction by 0.3 mM IPTG. (□) BL21(DE3) containing pVALT7 with induction by 0.3 mM IPTG	23
Figure 2.3:	Imino ¹ H NMR spectra of commercial (A) and overexpressed (B) <i>E. coli</i> tRNA ^{Val} in buffer containing 10 mM phosphate, pH 7, 100 mM NaCl, 15 mM MgCl ₂ at 22 °C	26

- Figure 3.1: Model of the secondary structure (a) and tertiary (b) interactions of *E. coli* tRNA^{Val} based on the crystal structure of yeast tRNA^{Phe}. The positions of 7 modified nucleosides are indicated in the secondary structure 33
- Figure 3.2: Imino ¹H NMR spectra of native (a) and *in vitro* transcribed tRNA^{Val} (b) in buffer (10% D₂O) containing 10 mM sodium phosphate, pH 7.0, 15 mM MgCl₂, 100 mM NaCl at 22 °C . . . 34
- Figure 3.3: Imino proton region of two-dimensional NOESY NMR spectrum of the *in vitro* transcript in buffer containing 10 mM sodium phosphate, pH 7.0, 15 mM MgCl₂, 100 mM NaCl at 22 °C. The cross peaks are labeled with the letters of the parent peaks 36
- Figure 3.4: Downfield region of ¹H NMR one-dimensional difference NOE spectra of the unmodified tRNA at the same solution conditions and temperature as in Figure 3.2. The NOE partners of each saturated peak are indicated. (a) peak Q has been saturated. (b) peak C has been saturated. (c) peak E has been saturated. (d) peak P has been saturated. (e) peak X has been saturated. (f) peak M has been saturated 37
- Figure 3.5: Imino ¹H NMR spectrum of tRNA^{Val} variant U30A40 obtained in the same solution conditions and temperature as in Figure 3.2 41

- Figure 3.6: Difference in chemical shift of assigned peaks in the imino proton spectra of unmodified and modified *E. coli* tRNA^{Val}. A positive value of the chemical shift difference indicates an upfield shift of the resonance in unmodified tRNA 45
- Figure 3.7: ¹H NMR spectra of native *E. coli* tRNA^{Val} obtained at different temperatures. The solution conditions were as in Figure 3.2. (a) 22 °C. (b) 35 °C. (c) 47 °C. (d) 60 °C 46
- Figure 3.8: ¹H NMR spectra of unmodified *E. coli* tRNA^{Val} obtained at different temperatures. The solution conditions were as in Figure 3.2. (a) 8 °C. (b) 22 °C. (c) 47 °C. (d) 60 °C 47
- Figure 3.9: Expanded region of the ¹H NMR spectra of tRNA in H₂O (10% D₂O) with 10 mM sodium phosphate in the absence of added Mg²⁺ at 22 °C. (a) Native *E. coli* tRNA^{Val}. (b) *E. coli* tRNA^{Val} transcribed *in vitro* 50
- Figure 3.10: Mg²⁺ titration of unmodified *E. coli* tRNA^{Val}. Downfield region of the ¹H NMR spectra of the *in vitro* transcript at 22 °C. The solution conditions were as in Figure 3.2 except Mg²⁺ was added to attain the indicated Mg²⁺/tRNA ratio, γ . (a) $\gamma = 1$. (b) $\gamma = 4$. (c) $\gamma = 6$. (d) $\gamma = 10$. (e) $\gamma = 18$. (f) $\gamma = 40$ 51

- Figure 3.11: Plot of the chemical shift of the downfield ^1H NMR peaks as a function of the $\text{Mg}^{2+}/\text{tRNA}$ ratio. A dotted line joining two points indicates that there two resonances attributable to a particular proton, corresponding to two conformations (with and without bound Mg^{2+}) of tRNA. The disappearance of a solid line at a particular $\text{Mg}^{2+}/\text{tRNA}$ ratio indicates the disappearance of a peak 53
- Figure 3.12: Downfield region of ^1H NMR one-dimensional difference NOE spectra of the unmodified tRNA at the same solution conditions and temperature as in Figure 3.9. The NOE partners of each saturated peak are indicated. Other apparent NOEs that have not been labeled are believed to be artifacts of power spillover or incomplete cancellation, or else could not be unequivocally assigned. (a) Peak A has been saturated. (b) Peak v has been saturated. (c) Peak c' has been saturated 56
- Figure 3.13: Expanded region of ^1H NMR spectra of unmodified *E. coli* tRNA^{Val} obtained at different temperatures The solution conditions were as in Figure 3.9. (a) 8 °C. (b) 22 °C. (c) 47 °C. (d) 60 °C. The labeled peaks are assigned as follows: A (U67), h'' (G42), j (G63), Q (G49), S (U64), v (G50) 57
- Figure 3.14: pH titration of unmodified tRNA^{Val} in the absence of Mg^{2+} . (A) pH 4.2. (B) pH 4.5. (C) pH 4.7. (D) pH 5.1. (E) pH 7.0 60

Figure 3.15: pH titration of native tRNA ^{Val} shown by the downfield region of the ¹ H NMR spectra in the absence of Mg ²⁺ at 22 °C. (a) pH 4.2. (b) pH 4.6. (c) pH 7.0	61
Figure 3.16: Analysis of the extremely low field peaks in the ¹ H NMR spectrum of unmodified tRNA ^{Val} at 10 °C. (A) One-dimensional difference spectrum when peak 1 has been saturated. (B) The control spectrum of unmodified tRNA ^{Val} obtained at low Mg ²⁺ , pH 4.2 and at 10 °C	63
Figure 3.17: Proposed structure of AA+ base pair	64
Figure 3.18: Time course of aminoacylation of wild type and mutant tRNA ^{Val} . The tRNA concentration is 2 μM	67
Figure 3.19: Inhibition of aminoacylation of wild type tRNA ^{Val} by tRNA ^{Val} mutants G35 and and -ACCA	68
Figure 3.20: Comparison of gel mobility of wild type tRNA ^{Val} and mutant G38	71
Figure 3.21: ¹⁹ F NMR spectra of wild type FU-tRNA ^{Val} (A) and FU-G38 variant (B) obtained in standard buffer at 22 °C	72
Figure 3.22: Imino ¹ H NMR spectra of tRNA ^{Val} mutant G38 (A), wild type tRNA ^{Val} (B) and the difference spectrum (C) obtained by subtracting B from A. Spectra were recorded in 15 mM Mg ²⁺ at 22 °C. The position of extra intensity in the difference spectrum is indicated by an arrow	74

- Figure 3.23: Imino ^1H NMR spectra of overexpressed tRNA^{Val} mutant G38 (A) and native tRNA^{Val} (B) and the difference spectrum (C) obtained by subtracting B from A. Spectra were recorded in 15 mM Mg^{2+} at 22 °C. The position of extra intensity in the difference spectrum is indicated by an arrow 76
- Figure 3.24: Imino ^1H NMR spectra of tRNA^{Val} mutant G38 (A) and wild type tRNA^{Val} (B) obtained in the absence of Mg^{2+} at 22 °C 78
- Figure 3.25: Imino ^1H NMR spectra of tRNA^{Val} mutant G38 (A) and wild type (B) obtained in the absence of Mg^{2+} at 60 °C 80
- Figure 3.26: ^{19}F NMR spectra of wild type FU-tRNA^{Val} obtained in standard buffer at different temperatures. (A) 47 °C. (B) 35 °C. (C) 22 °C 82
- Figure 3.27: ^{19}F NMR spectra of FU-tRNA^{Val} mutant U32 obtained in standard buffer at different temperatures. (A) 47 °C. (B) 35 °C. (C) 22 °C 83
- Figure 3.28: ^{19}F NMR spectra of mutant FU-tRNA^{Val} U32G38 obtained in standard buffer at different temperatures. (A) 47 °C. (B) 35 °C. (C) 22 °C 85
- Figure 3.29: ^{19}F NMR spectra of FU-tRNA^{Val} mutant U38 obtained in standard buffer at different temperatures. (A) 47 °C. (B) 35 °C. (C) 22 °C 87

Figure 3.30:	^{19}F NMR spectra of FU-tRNA ^{Val} mutant U38G32 obtained in standard buffer at different temperatures. (A) 47 °C. (B) 35 °C. (C) 22 °C	88
Figure 3.31:	^{19}F NMR spectra of FU-tRNA ^{Val} mutant U38A32 obtained in standard buffer at different temperatures. (A) 47 °C. (B) 35 °C. (C) 22 °C	90
Figure 3.32:	^{19}F NMR spectra of FU-tRNA ^{Val} mutant U32U38 obtained in standard buffer at different temperatures. (A) 47 °C. (B) 35 °C. (C) 22 °C	91
Figure 3.33:	^{19}F NMR spectra of FU-tRNA ^{Val} mutant U32C38 obtained in standard buffer at different temperatures. (A) 47 °C. (B) 35 °C. (C) 22 °C	93
Figure 3.34:	Imino ^1H NMR spectra of GUAA binding to native tRNA ^{Val} in the presence of 15 mM Mg^{2+} . The molar ratio of GUAA to tRNA is 3 (A), 2 (B), 1 (C) and 0 (D)	96
Figure 3.35:	Portion of two-dimensional NOESY spectrum of GUAA measured at 6°C in D_2O containing 10 mM phosphate, 100 mM NaCl and 15 mM MgCl_2 , showing NOE cross peaks from aromatic protons to sugar protons	98

Figure 3.36: Portion of two-dimensional ROESY spectrum of GUAA measured at 6 °C in D₂O containing 10 mM phosphate, 100 mM NaCl and 15 mM MgCl₂, showing NOE cross peaks from the aromatic protons to the sugar protons and 1' of sugar proton to other sugar protons 100

Figure 3.37: Model of GUAA as an A-form right-handed helix 101

Figure 3.38: Portion of two-dimensional TOCSY spectrum of GUAA at 6 °C in D₂O containing 10 mM phosphate, 100 mM NaCl and 15 mM MgCl₂, showing NOE cross peaks between sugar protons 105

Figure 3.39: Portion of two-dimensional transfer NOE spectrum of GUAA in D₂O containing 10 mM phosphate, 100 mM NaCl and 15 mM MgCl₂ at 6 °C, showing NOE cross peaks between aromatic and 1' sugar protons 107

ABBREVIATIONS

Y base	wybutosine
Q	queosine
I	inosine
m ⁷ G	7-methylguanosine
m ⁶ A	N ⁶ -methyl adenosine
s ⁴ U	4-thiouracil
D	dihydrouracil
cmo ⁵ U	uridine-5-oxyacetic acid
Ψ	pseudouridine
T	ribothymidine
NMR	nuclear magnetic resonance
FU	5-fluorouracil
NOE	nuclear Overhauser effect
Tris	tris-[hydroxymethyl]-aminomethane
DTT	dithiothreitol
EDTA	ethylenediaminetetraacetic acid
LB	Luria-Bertini
DEAE	diethylaminomoethyl

VRS	valyl-tRNA synthetase
FUTP	5-fluorouridine-5'-triphosphate
ppm	parts per million
Hepes	N-2-hydroxyethylpiperazine-N'-2-ethanesulfonic acid
NOESY	nuclear Overhauser enhancement spectroscopy
IPTG	isopropyl- β -D-thiogalactoside
Echo 11	1D spectrum using echo 11 pulse sequence
TOCSY	total correlation spectroscopy
ROESY	rotating-frame Overhauser enhancement spectroscopy
ROE	rotating-frame Overhauser effect
TBAF	tetrabutylammonium fluoride
THF	tetrahydrofuran
T ₁	spin-lattice relaxation time
T ₂	spin-spin relaxation time
PAGE	polyacrylamide gel electrophoresis
HPLC	high performance liquid chromatography
cpm	counts per minute
TEAA	tetrabutylammonium acetate

ABSTRACT

The effects of nucleoside modifications on *E. coli* tRNA^{Val} structure have been probed by imino ¹H NMR. The NMR data shows that the structure of *in vitro* transcribed (unmodified) and native (modified) tRNA^{Val} are very similar in 15 mM Mg²⁺. Temperature dependence of the spectra reveals that nucleoside modifications stabilize tertiary interactions between T and D loops. On removal of Mg²⁺, unmodified tRNA^{Val} undergoes remarkable structural changes which are not observed in native tRNA^{Val}. There is near total disruption of the D stem and of tertiary interactions. A new strong interaction occurs between the A6U67 base pair (acceptor stem) and the G50U64 wobble base pair (T stem). This interaction remains intact and forms a stable structural core even at 60 °C. These conformational changes are correlated with the decreased strength of Mg²⁺ binding in unmodified tRNA^{Val}. However, in the absence of Mg²⁺, mutant G38 has a stable structural core in the acceptor stem and the anticodon stem, unlike that found in wild type tRNA^{Val}. Such structural changes are caused by a base pair formation between G38 and C32. This may also account for the reduction in catalytic efficiency of G38 mutant. tRNA^{Val} position 35 mutants do not inhibit aminoacylation of wild type tRNA^{Val}, suggesting that valyl-tRNA synthetase discrimination is affinity-based.

¹⁹F NMR studies of FU-tRNA^{Val} mutants of positions 32 and 38 provide evi-

dences for GU base pair formation between G38 and U32, but not between G32 and U38. Unexplained chemical shift positions for residues FU32 and FU33 are found in the ^{19}F NMR spectrum of mutant U32C38.

Most resonances in the ^1H NMR spectrum of codon containing tetranucleotide GUAA have been assigned. Transfer NOE experiments have been initiated to determine the structure of GUAA when bound to tRNA^{Val}.

CHAPTER 1. INTRODUCTION

This thesis is aimed at getting more insights into the structure and function relationships of *E. coli* tRNA^{Val}. First, the structures of native (modified) and *in vitro* transcribed (unmodified) tRNA^{Val} were compared in the presence and absence of Mg²⁺. Second, the recognition of anticodon loop of tRNA^{Val} by VRS was analyzed by aminoacylation kinetics. Third, the effects of positions 32 and 38 on tRNA^{Val} structure were probed by imino ¹H and ¹⁹F NMR.

Function of tRNA

In 1955, Francis Crick predicted the existence of an adaptor molecule in protein biosynthesis. This adaptor molecule links the genetic information in DNA to protein. Two years later the adaptor molecules were discovered by Hoagland and his colleagues (Hoagland *et al.*, 1957). These adaptor molecules are a group of small RNAs called transfer RNA (tRNA). tRNAs exist in every cell and are essential for cell survival.

tRNA is central to protein biosynthesis. As an adaptor molecule between amino acids and the genetic code, tRNA is first aminoacylated with its cognate amino acid at the 3' CCA end, then the resulting aminoacyl-tRNA recognizes its codon in mRNA by base pairing. Because amino acids do not interact directly with their

corresponding codons, the accuracy of protein biosynthesis is governed by the recognition processes involving tRNA. Thus each tRNA must have its unique structural elements for accurate recognition.

During protein synthesis, tRNA interacts with many proteins and nucleic acids. The initiation of protein synthesis involves N-formylmethionyl tRNA^{fMet} binding to the initiation factors (IFs), IF-1, IF-2 and IF-3 and GTP are required for the formation of an initiation complex with fMet-tRNA^{fMet} bound at the P-site of the ribosome. Then the ternary complex formed by aminoacyl-tRNA, elongation factor EF-Tu and GTP comes to the A-site of the ribosome. Peptide bond formation is then catalyzed by peptidyl transferase, which ligates the amino group of the aminoacyl-tRNA in the A-site and the carboxyl group of the amino acid in the P-site. Hydrolysis of the acyl-ester bond of the aminoacyl-tRNA supplies the energy for peptide bond formation. Then the free tRNA moves to the E-site and then releases from the ribosome, the peptidyl-tRNA is translocated from the A-site to P-site. Then a new codon in mRNA appears at the A-site and this A-site is ready to accept another aminoacyl-tRNA corresponding to the new codon. When termination codons, UAA, UGA or UAG appear in the A-site, protein synthesis stops due to lack of corresponding aminoacyl-tRNA. The ester-bond of peptidyl-tRNA is hydrolyzed with the help of release factors to release the peptide chain. Because all tRNAs interact with the same protein synthesis machinery, they must be very similar in some aspects. These include the L-shape and size of all tRNAs and the invariant and semiinvariant bases in all tRNAs.

Besides direct involvement in protein biosynthesis, tRNA plays other important roles. Aminoacyl-tRNA was found to play a role in the regulation of amino

acid biosynthesis. This regulation is achieved by the binding of aminoacyl-tRNA to the suppressor binding site of amino acid biosynthetic enzyme genes (Eidlic and Neidhardt, 1965). Attenuation is another famous example of how aminoacyl-tRNA regulates the transcription and translation of genes for Trp and other amino acid biosynthesis (Bertrand *et al.*, 1976).

Another fundamentally different reaction involving aminoacyl-tRNA is catalyzed by aminoacyl-tRNA transferase. In these reactions the aminoacyl residue is transferred from tRNA to an acceptor molecule. The acceptor molecules can be phosphatidylglycerol, peptide and protein. Then the modified protein may function to regulate biosynthesis of specific enzymes (Soffer *et al.*, 1974).

More recently it was found that uncharged tRNA could bind to the leader sequence of its cognate synthetase gene to regulate the transcription of the gene (Grundy *et al.*, 1993; 1994). The interaction of the leader with the appropriate tRNA is necessary for antitermination. This antitermination increases the transcription and translation of the synthetase and in turn compensates for amino acid limitation. Free tRNA was also known to serve as primer for reverse transcriptase in RNA tumor virus. tRNA^{Trp} is the primer for avian virus reverse transcriptase (Waters *et al.*, 1975). tRNA^{Phe} is the primer for murine reverse transcriptase (Peters and Dahlberg, 1979).

General structure of tRNA

Most known tRNA sequences can be folded into the cloverleaf model of secondary structure (Figure 1.1A). Such a structure contains four loops and four stems as indicated. The size of the variable loop ranges from 13 to 21 bases in different

tRNA species. The anticodon is located in the anticodon loop and is the site which interacts with mRNA during protein biosynthesis. There are some exceptions for this cloverleaf model. Some mitochondrial tRNAs lack the entire D loop and/or D stem (DeBruign *et al.*, 1980).

Several crystal structures of tRNA have been solved. All of them have an L-shaped tertiary structure (Figure 1.1B). In the crystal structure of yeast tRNA^{Phe} (Kim *et al.*, 1974; Robertus *et al.*, 1974), the acceptor stem and the T stem form one continuous double helix. The D stem and the anticodon-stem form another double helix. Each helix is antiparallel and right handed. These two double helixes represent the two arms of the L. The two ends of the L contain the anticodon loop and the 3' CCA end. The distance between these two sites is about 75 Å.

The three dimensional structure of tRNA is stabilized by extensive base-base interactions. These interactions include base pairing in the helical regions and tertiary interactions and base stacking in the loop regions. In the case of yeast tRNA^{Phe}, only five bases out of 76 bases are not stacked. All other 71 bases (93%) are in stacking conformation. Base-backbone and backbone-backbone interactions also contribute to the stable tRNA structure. Such interactions involve 2' -OH groups.

The structure of the seven base anticodon loop is characterized by the stacking of five bases on the 3' side of the loop. There is a sharp U-turn from U33 to base 34. The anticodon loop conformation is stabilized by several intra-loop interactions and a bound Mg²⁺ ion.

Some bases are absolutely conserved or semiconserved in all tRNAs. Most of these bases are involved in tertiary interactions in yeast tRNA^{Phe}. These base pairs can be replaced with equivalent tertiary base pairs in other tRNAs with little alter-

ation of backbone structure. Thus the crystal structure of yeast tRNA^{Phe} represents the general structural features of all tRNAs.

Mg²⁺ binding to tRNA

Mg²⁺ has been known to stabilize the functional structure of tRNAs long before the determination of the crystal structure of yeast tRNA^{Phe} (Fresco *et al.*, 1966). Figure 1.2 shows the Mg²⁺ binding sites in the structure of yeast tRNA^{Phe}. There are two Mg²⁺ binding sites in the D-loop, one in the anticodon loop and one in the P10 loop/D loop formed by bases 8 to 12. These Mg²⁺ ions are coordinated to water and neighboring bases and the oxygens of phosphates. The bound Mg²⁺ ions in the corner of the L stabilize the tertiary interactions between the T and D loops. The other two Mg²⁺ ions stabilize the conformations of the P10 loop and the anticodon loop. There are likely to be additional Mg²⁺ ions bound to tRNA that can not be located in the crystal structure. These Mg²⁺ ions are not seen because they are less rigidly held in the crystal structure or their binding constant are low. The crystals used in this study (Kim *et al.*, 1974) contain two spermines per tRNA, and the positive charged spermine molecules may compete with Mg²⁺ for binding to tRNA.

It is of interest to compare the Mg²⁺ binding sites located by x-ray diffraction studies with the results of other studies. Methods sensitive to changes in tRNA conformation have provided evidence of general tRNA cation binding. These methods include light scattering, measurement of diffusion coefficients (Olson *et al.*, 1976), diffusion migration of native and denatured tRNA on gels (Lindahl *et al.*, 1966) and

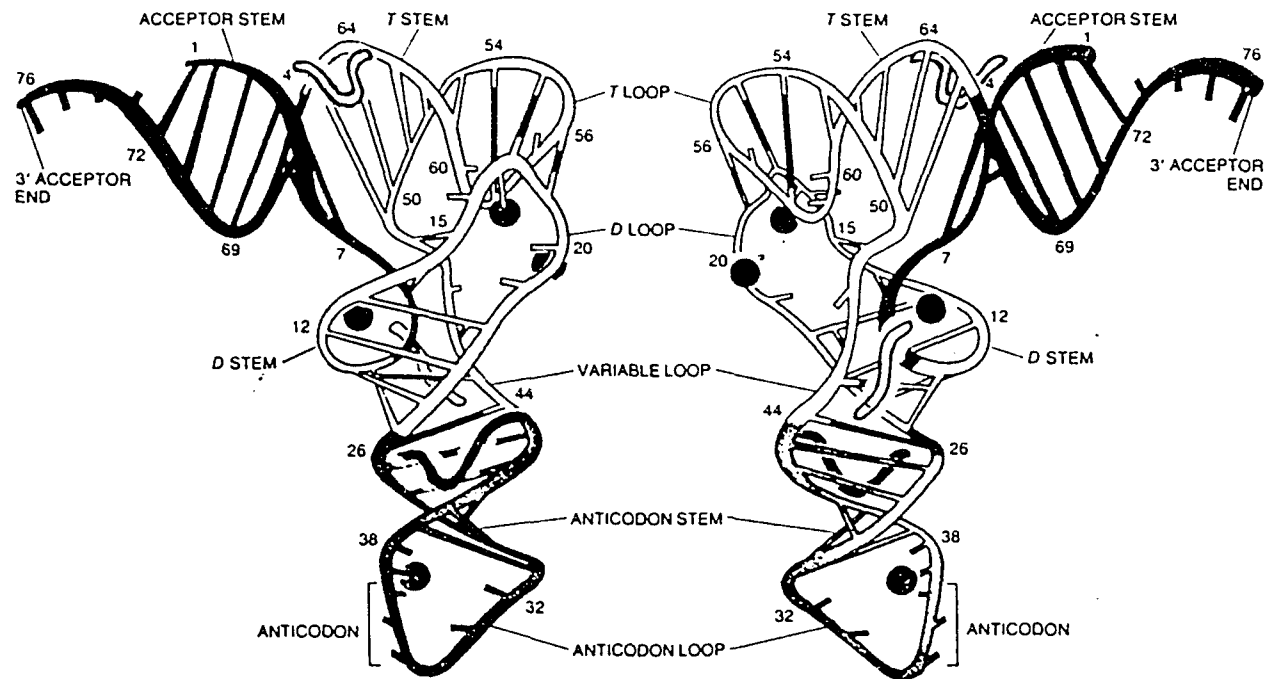


Figure 1.2: Mg^{2+} and spermine binding sites located in the x-ray crystal structure of yeast tRNA^{Phe}

changes in spectra of the fluorescent Y base and s^4U8 in yeast tRNA^{Phe} (Römer and Hach, 1975). All these methods showed the effects observed on tRNA are correlated with tRNA cation binding. Other methods include monitoring the changes of NMR signals (Stein and Crothers, 1976) and enzyme digestion patterns of tRNA (Chao and Kearns, 1977) have also been correlated with specific Mg^{2+} binding in tRNA.

Specific Mg^{2+} binding to tRNA has been probed by fluorescence measurement. The fluorescence of the Y base and s^4U8 are quenched by Eu^{3+} and by Mn^{2+} (Kayne and Cohn, 1974; Leroy *et al.*, 1977), indicating the binding of cations at the anticodon region and the P10 loop. Rhodes (1977) studied the initial stages of thermal unfolding of yeast tRNA^{Phe} in the presence and absence of Mg^{2+} . Two regions protected by Mg^{2+} from thermal unfolding have been found. One is within the P10 loop region, another is in the U59 region. These results correlated well with the existence of binding sites in these regions as seen in the crystal structure. It is clear that Mg^{2+} ions are required to facilitate the three dimensional folding of tRNA. Conformational changes in the molecule may be induced by altering the Mg^{2+} concentration. These conformational changes in tRNA may affect the interactions between tRNA and other molecules.

tRNA modifications

One of the characteristics of tRNA is the presence of a variety of post-transcriptionally modified nucleosides. Modifications occur at the base and/or at the 2' -OH groups. Some modified nucleosides like I, Ψ , s^4U are present in most tRNA, while some hypermodified nucleosides are present in only one or a few tRNA species.

The modified nucleosides in tRNA are believed to play important roles in tRNA function. Most bases involved in tertiary interactions are modified. Such bases are considered important in the stabilization of the tRNA conformation (Watanabe *et al.*, 1976). The compact structure of modified tRNA is more resistant to attack by RNase and nucleases (Derrick and Horowitz, 1993).

Most tRNAs contain a modified purine at position 37 which is adjacent to the 3' side of the anticodon. Often tRNAs that recognize codons starting with A or U contain hypermodified bases at position 37. Thus hypermodification may be necessary for stabilization of an AU base pair and thus enhance the fidelity of codon-anticodon interaction. The presence of modified nucleosides next to the anticodon is also shown to be important in ribosome binding of aminoacyl-tRNA. *E. coli* suppressor tRNA^{Tyr} containing A at position 37 is only slightly active in protein synthesis (Gefter and Ressel, 1969). Similar behavior has been observed with *E. coli* tRNA^{Ile} lacking t⁶A at position 37.

Modified nucleosides in the first position of the anticodon influence codon-anticodon interactions. For example, I at position 34 can pair with U, C and A in the third position of the codon; o⁵U recognizes A, G and U in the third position of the codon. Such interactions have been described by Crick as wobble base pairing (Crick, 1966).

There are 7 modified nucleosides found in native *E. coli* tRNA^{Val}. They are s⁴U at position 8, D at 17, cmo⁵U at 34, m⁶A at 37, m⁷G at 46, T at 54 and Ψ at 55 (Yaniv and Barrel, 1969).

Unmodified tRNA

Unmodified tRNA is synthesized by *in vitro* transcription of the tRNA gene by T7 RNA polymerase. In this method, the tRNA gene is directly linked to a T7 promoter. Bst NI digestion of the plasmid produces a template which will yield tRNA having the correct 3' CCA end. In the presence of excess GMP, 96% of the transcripts start with pG (Sampson and Uhlenbeck, 1988, Chu and Horowitz, 1989). Most of these synthetic tRNAs can be efficiently aminoacylated by their cognate synthetases. The implication is that the structure of the *in vitro* transcript is similar to that of native tRNA.

But the structural stability of *in vitro* transcribed tRNA is lower than that of the native tRNA molecule. The melting temperature (T_m) for unmodified tRNA is lower than that of native tRNA at all Mg^{2+} concentrations (Sampson and Uhlenbeck, 1988; Derrick and Horowitz, 1993). The structural differences become more pronounced at low Mg^{2+} concentrations. For example, large differences between ^{19}F NMR spectra of native FU-tRNA^{Val} and the *in vitro* transcript were seen in the absence of Mg^{2+} , however, in the presence of 15 mM Mg^{2+} , the two spectra were nearly identical (Chu and Horowitz, 1989). Despite the structural differences, most unmodified tRNAs are fully active in protein translation. Again excess Mg^{2+} ions are required for optimal activity.

1H NMR studies of tRNA

The determination of the crystal structure of yeast tRNA^{Phe} stimulated a variety of biophysical studies on the conformation and dynamics of tRNA in solution.

^1H NMR has been one of the most important tools for such studies. For tRNA each Watson-Crick base pair contains one imino proton. When the imino proton is protected from exchange by hydrogen bonding, it resonates in the low field region (11–15 ppm) of the ^1H NMR spectrum. Peaks in this region usually are resolved fairly well. Peaks can be assigned by standard sequential NOE techniques (Redfield, 1978). Once assigned these peaks become very useful structural markers in probing tRNA in solution. This approach has been used to study several native tRNAs. The low field imino proton spectra of *E. coli* tRNA^{Val}, yeast tRNA^{Phe} and several other tRNAs have been completely assigned (Johnston and Redfield, 1977; 1978; Hyde and Reid, 1985; Hare *et al.*, 1985; Amano and Kawakami, 1992).

The effects of Mg^{2+} , spermine and temperature on the conformation of *E. coli* tRNA^{Phe} have been investigated by ^1H NMR (Hyde and Reid, 1985). Two slowly exchangeable conformers were observed at low Mg^{2+} . Spermine affects tertiary interactions. The thermal unfolding of tRNA^{Phe} starts from the tertiary interactions followed by helical stems. The T stem and anticodon stem are the most stable structural elements in yeast tRNA^{Phe}.

Unmodified yeast tRNA^{Phe} was also examined by imino proton NMR (Hall *et al.*, 1989). In the presence of excess Mg^{2+} , the transcript has a very similar structure to that of native tRNA^{Phe}. But at low Mg^{2+} the transcript has a very different structure. Large conformational changes allow the possible formation of an extra GU base pair.

^{19}F NMR studies of tRNA

^{19}F nuclei can be incorporated into *E. coli* tRNA^{Val} and other tRNAs by growing *E. coli* in the presence of FU. To synthesize unmodified FU-tRNA, FUTP is used in the transcription mixture instead of UTP. These FU-tRNAs have been shown to be fully active in aminoacylation. Incorporation of FU into tRNA provides a new approach for probing the solution structure of FU-tRNAs. ^{19}F NMR spectra of *E. coli* FU-tRNA^{Val}, FU-tRNA^{fMet} and FU-tRNA^{mMet} have been reported (Horowitz *et al.*, 1977; Hills *et al.*, 1983; Hardin *et al.*, 1988). The spectra have a large chemical shift dispersion of about 10 ppm. Effects of ionic strength, temperature, pH and codon binding have been monitored by ^{19}F NMR.

In order to probe conformational changes in particular regions of tRNA, the individual ^{19}F peaks must be assigned. There are 14 ^{19}F probes in *E. coli* tRNA^{Val}. These ^{19}F resonances have been completely assigned by systematic base substitution (Chu *et al.*, 1992a, 1992b). Since then structures of many tRNA^{Val} mutants have been probed by ^{19}F NMR. The interaction of FU-tRNA^{Val} with VRS has been studied by ^{19}F NMR (Chu and Horowitz, 1991). Binding of VRS to FU-tRNA^{Val} induces chemical shift changes of several resonances. These peaks belong to FU residues in the anticodon loop and the inside of the L-shaped molecule. This observation is consistent with studies showing that the anticodon of *E. coli* tRNA^{Val} is involved in recognition by VRS (Schulman and Pelka, 1988; Pallanck and Schulman, 1991).

tRNA identity

The term tRNA identity has been used to designate the sites that govern tRNA aminoacylation specificity. Thus nucleotides not in contact with synthetase may act indirectly by properly positioning other nucleotides to interact with synthetase are also considered as identity elements (Normanly *et al.*, 1986; Schulman, 1991; Giegé *et al.*, 1993).

Early studies on tRNA identity relied on naturally occurring tRNA variants and on the chemical modification of tRNA. In some cases one synthetase can aminoacylate tRNAs with different anticodons. Mutations in the anticodon of *E. coli* tRNA^{Gln}, tRNA^{Ser} and tRNA^{Tyr} do not affect the aminoacylation specificity (Kaplan *et al.*, 1965; Weigert *et al.*, 1965). In other cases modification of the anticodon reduces aminoacylation or the resulting tRNA can be aminoacylated by other synthetase. The acceptor stem can also be a specificity determinant in certain tRNAs. tRNA^{Ala} with chemical modifications in the acceptor stem is inactive in aminoacylation (Schulman and Chambers, 1968). This early work suggested that tRNA identity elements can be located in every part of tRNA structure.

The development of recombinant DNA technology allowed synthesis of DNA coding for tRNAs having any desired mutation. These mutant tRNAs can be functionally analyzed *in vitro* or *in vivo*. The *in vivo* assay system uses tRNAs with CUA (amber) or UCA (opal) anticodons. The effect on aminoacylation specificity of nucleotide substitutions outside of the anticodon can be addressed by looking at the suppression efficiency and identifying the amino acid inserted at a UAG or UGA nonsense codon. Only 8 nucleotides changes are required to convert suppressor tRNA^{Ile}

to a tRNA^{Ser} (Normanly *et al.*, 1992).

An *in vivo* assay system for studying tRNA identity in those tRNAs that require the anticodon for synthetase recognition is to study the initiator tRNA^{fMet}. Initiation of protein synthesis depends on N-formylation of aminoacyl-tRNA, but it does not depend on the anticodon or amino acid. Thus recognition of the anticodon by synthetase can be tested by looking at the initiation efficiency of protein synthesis (Varshney *et al.*, 1991).

The *in vitro* assay uses unmodified tRNAs synthesized by T7 RNA polymerase. The kinetic parameters K_m , V_{max} for tRNA mutants can be determined. Part of the tRNA molecule can also be examined for its aminoacylation specificity. A minihelix containing only the acceptor stem and T-stem and loop of tRNA^{Ala} can be specifically aminoacylated by its cognate synthetase (Francklyn and Schimmel, 1989).

In general both *in vitro* and *in vivo* assay systems generate consistent results in determining tRNA identity elements, with few exceptions. Several factors may contribute to a lack of correlation. The *in vivo* system reflects the net outcome of 20 synthetases competing for overexpressed tRNA. Any step from aminoacylation to protein synthesis can contribute to the final observation. The *in vitro* system uses unmodified tRNA, thus the effects of nucleoside modifications cannot be considered.

The most comprehensive description of the molecular basis of tRNA identity is enhanced by several detailed x-ray structures of tRNA-synthetase complexes. For *E. coli* GlnRS-tRNA^{Gln} complex (Rould *et al.*, 1989, 1991), the enzyme interacts with tRNA^{Gln} from the 3' CCA end to the anticodon. The enzyme approaches

tRNA^{Gln} from the minor groove side of the acceptor stem. Binding of the enzyme opens up the first U1A72 base pair. This allows the 2-amino group of G73 to form a hydrogen bond with the phosphate group of A72. As a result the acceptor terminus forms a hair pin structure upon GlnRS binding. This structure explains why GlnRS discriminates against tRNAs with A73, C73 or U73, since they do not have a 2-amino group to form the hairpin structure. The enzyme also forms five specific binding pockets for C34, U35, G36, m²A37 and Ψ38 in the anticodon loop. The tight binding pocket for U35 explains why some suppressor tRNAs with U at position 35 can be aminoacylated by GlnRS.

AspRS binds to acceptor stem and anticodon of tRNA^{Asp} (Ruff *et al.*, 1991; Cavarelli *et al.*, 1993) . The enzyme approaches tRNA^{Asp} from the major groove side of the acceptor stem. Binding results in a kink in the anticodon stem. G10U25 is also in contact with the enzyme. Kinetic results showed that G73, G10U25 and the anticodon are important for aminoacylation.

The crystal structure of *Thermus thermophilus* seryl-tRNA synthetase complexed with tRNA^{Ser} revealed how the conserved base G20b from the D loop determines the orientation of the long variable arm. The enzyme specifically recognizes the shape of tRNA^{Ser} through backbone contacts, sequence specific interactions are secondary (Biou *et al.*, 1994)

Some modified bases have been shown to be essential for tRNA identity. An *E. coli* tRNA^{Ile} has a anticodon containing lysidine at position 34 (Muramatsu *et al.*, 1988). Without modification the tRNA has a CAU anticodon that is recognized by MetRS, but not by IleRS. Here the lysidine base blocks mischarging by another enzyme and enhances interaction with IleRS. In many other cases modified bases

assist the discrimination of tRNAs by synthetases.

Codon-anticodon interaction

Recognition of codons in mRNA by the appropriate tRNA is an essential step in protein translation. This step links the genetic code on mRNA to protein sequence. To understand the accuracy of this recognition process, a detailed knowledge of the structure and dynamics of the codon-anticodon complex is essential.

This subject has attracted extensive investigations by various methods. Interaction of codon-containing oligonucleotide UCC, UUCA and UUCAG with yeast tRNA^{Phe} (anticodon GAA) was studied by equilibrium dialysis (Eisinger *et al.*, 1971, 1973; Pongs *et al.*, 1973). Although based on the crystal structure of yeast tRNA^{Phe}, C32 and U33 are not available for binding to the oligoes, it was found that UUCA and UUCAG were bound more tightly to the anticodon region than UUC (Greerdes *et al.*, 1980a, 1980b). This implies that the anticodon loop conformation could change upon binding of the complementary oligonucleotides. Other studies have shown that the presence of modified bases adjacent to the anticodon also stabilizes the codon-anticodon complex (Grosjean *et al.*, 1976). Effects of UCA, UUCA, UUCAG binding to yeast tRNA^{Phe} have been studied by ¹H NMR (Greerdes *et al.*, 1980a, 1980b). Binding of UUC to the anticodon resulted in aggregation of yeast tRNA^{Phe}. Such an aggregation of tRNA molecules was not observed upon addition of UUCA or UUCAG. Four or five extra imino proton resonances were seen in the ¹H NMR spectrum of yeast tRNA^{Phe} upon binding of UUCA or UUCAG.

CHAPTER 2. MATERIALS AND METHODS

Materials

DNA restriction enzymes and modifying enzymes were purchased from New England Biolabs and Promega Corporation. The DNA sequencing kit was from United States Biochemical Corp. The site-directed mutagenesis kit used was from Amersham Inc. Inorganic pyrophosphatase was from Boehringer Mannheim. T7 RNA polymerase was prepared from *E. coli* BL21/pAR1219 (Grodberg and Dunn, 1988). VRS was purified (Chu and Horowitz, 1991) from an overproducing strain *E. coli* GRB2328, which was a gift from Dr. George L. Marchin of Kansas State University.

Native *E. coli* tRNA^{Val} was obtained from Subriden RNA or purified from *E. coli* BL21(DE3)/pVALT7 (see methods below). NTPs were from United States Biochemical Co. FUTP was from Sierra Bioresearch. ³H-valine and [α -³⁵S] dATP were from Amersham. DNA oligonucleotides were synthesized by the Nucleic Acid Facility of Iowa State University. Most chemicals were from Sigma or Fisher Chemical Corp. Biosafe NA scintillation fluor was obtained from Research Product International. Dialysis membranes were from BRL. Media for cell growth were from Difco Chemical Co. All other materials were of reagent grade or higher.

E. coli TG1 (K12, [lac-pro], SupE, thi, hsdD51/F' tra36, proA+B+, lacI^q, LacZ

M15), used as host for plasmid transformation, was from Amersham Inc. *E. coli* BL21(DE3) used for overexpression of native tRNA^{Val} was from NOVAgene. pUC119 and helper phage M13K07 were gifts of Dr. Alan Myers, Iowa State University.

Methods

Purification of oligonucleotide GUAA

The oligonucleotide GUAA (0.2 μ mole) was synthesized in a ABI synthesizer by the Nucleic Acid Facility at Iowa State University. The following purification protocol works well for 0.2–1 μ mole synthesis scale.

GUAA bound to CPG (controlled pore glass) was transferred into a glass vial and 2 ml of NH₄OH:ethanol=3:1 was added. Then the vial was capped tightly and incubated at 55 °C in a water bath for 24 hours to cleave the oligonucleotide from CPG. The sample was then cooled on ice for 15 min and transferred to a siliconized plastic tube and dried under a speed Vac.

The dried oligonucleotide was resuspended in 600 μ l of 1M TBAF in THF and incubated at room temperature for 24 hours. This step removes the protective groups from the oligonucleotide. Then the sample was dried and dissolved in 10 ml H₂O and desalted by a Sep-pak C18 plus cartridge. The cartridge was first activated with 10 ml CH₃CN and washed with 10 ml 0.1 M TEAA at pH 7.0. After loading the sample the cartridge was washed with 5 ml 0.1 M TEAA and the oligonucleotide was then eluted with CH₃CN:methanol:H₂O=7:7:6. 0.5-ml fractions were collected and the oligonucleotide-containing fractions were dried.

The desalted oligonucleotide was dissolved in 500 μ l H₂O and applied to a C18

HPLC column equilibrated with 0.1 M TEAA. The column was washed with 0.1 M TEAA for 10 min at a flow rate of 1 ml/min. Then a gradient was developed from 100% buffer A (0.1 M TEAA) to 50% buffer A and 50% buffer B (90% CH₃CN and 10% 0.1 M TEAA) in 60 min. The oligonucleotide was eluted at about 30 min.

The ¹H NMR spectrum (data not shown) of the oligonucleotide at this stage shows considerable contamination with TBAF, CH₃CN and other solvents used in the purification procedure. These solvents were removed by ethanol precipitation of the GUAA and repeated washing with ethanol. Then the oligonucleotide was dried and dissolved in D₂O. The ¹H NMR spectrum showing the region containing the resonances of aromatic protons and 1' sugar protons in D₂O is shown in Figure 2.1. Very little contamination with solvent is evident. Six resonances were seen in the aromatic region and five resonances occur in the 1' sugar proton region (one of the resonances in the 1' sugar proton region belongs to the C5H of U) as expected for GUAA.

***In vitro* transcription of tRNA^{Val} by T7 RNA polymerase**

The recombinant phagemid pVAL119-21 contains the cloned *E. coli* tRNA^{Val} gene joined directly to an upstream T7 promoter and a downstream Bst NI site (Chu and Horowitz, 1989). The plasmid was purified by CsCl density gradient ultracentrifugation (Maniatis *et al.*, 1983). Bst NI digested plasmid served as template for T7 RNA polymerase. The transcription reaction was carried out in 40 mM Tris-HCl (pH 8.1), 22 mM MgCl₂, 1 mM spermidine, 5 mM DTT, 4 mM each of ATP, CTP, GTP and UTP, 16 mM GTP, 80 μg of linearized DNA, 4 units of inorganic pyrophosphatase, 0.6 mg of T7 polymerase for 1 ml transcription mixture. To synthe-

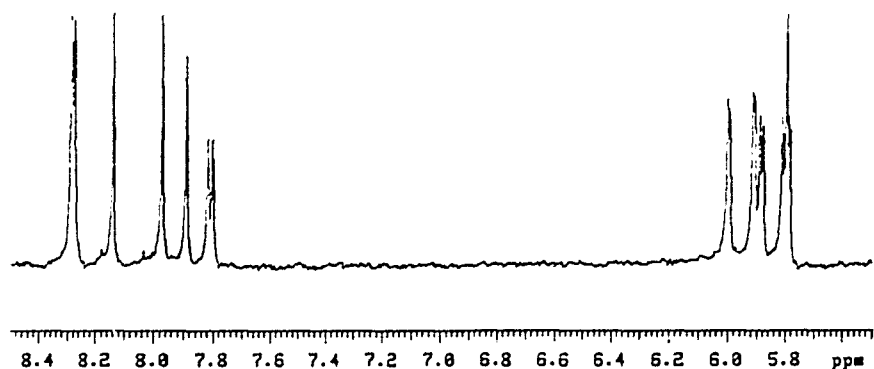


Figure 2.1: Aromatic and 1' sugar proton region of ^1H NMR spectrum of GUAA in D_2O at 6 °C

size FU-tRNA, FUTP was used instead of UTP in the transcription reaction. After incubation for 2 h at -12 °C, the reaction was stopped by extraction with 1:1 (v/v) phenol/chloroform/isoamylalcohol (25:24:1) followed by ethanol precipitation of the tRNA.

HPLC purification of transcribed tRNA

The transcribed tRNA was separated from the non-incorporated nucleotides and DNA fragments by HPLC on a Toyopearl DEAE-650S column (250x4.6 cm) (Chu and Horowitz, 1989). The column was equilibrated with 25 mM Tris-HCl, pH 7.4, 250 mM NaCl. The tRNA was eluted with a 40 min linear gradient from 350 to 600 mM NaCl in 25 mM Tris-HCl buffer at pH 7.4. The eluted tRNA was ethanol

precipitated.

tRNA from the DEAE column was further purified by HPLC on a Vydac C4 reverse phase column (250x4.6 cm). The column was developed with a linear gradient from 100% buffer A (1.0 M NH₄OAC, pH 6.5, 20 mM MgCl₂) to 50% buffer A and buffer B (10 mM NH₄OAC, pH 6.5, 20 mM MgCl₂ and 10% methanol). The eluted tRNA was ethanol precipitated and dried. tRNA concentration was measured at 260 nm using a value of 0.1% = 24A₂₆₀/ml. For aminoacylation kinetic experiments the tRNA concentration was determined by a plateau charging assay (see below).

Site-directed mutagenesis

tRNA^{Val} anticodon loop mutants were generated by oligonucleotide-directed mutagenesis of the cloned tRNA^{Val} gene by the method of Eckstein (Taylor *et al.*, 1985). Mutant clones were selected by dideoxy sequencing (Sanger *et al.*, 1980). For double mutants, a single stranded DNA with the first mutation was used as template for mutation at a second position.

Overexpression of native tRNA^{Val}

Cloning system design The idea was to use the T7 expression system to produce a large amount of native tRNA^{Val}. To do so, a host cell containing an IPTG-inducible T7 RNA polymerase gene and a vector containing a T7 promoter upstream of the tRNA gene are required. *E. coli* BL21(DE3) which has a T7 RNA polymerase gene in its chromosome that is controlled by a UV5 Lac promoter is a suitable host strain. It was transformed with pVAL119-21 which contains a T7

promoter at the upstream end of a tRNA^{Val} gene. On induction with IPTG, the tRNA^{Val} gene should be transcribed by T7 RNA polymerase. The transcript should be then processed to yield mature tRNA^{Val}. This was indeed the case. The level of tRNA^{Val} activity in extracts from BL21(DE3) containing pVAL119-21 was 20-fold higher than that in TG1 cells (without T7 RNA polymerase gene) containing pVAL119-21 (Figure 2.2). For this experiment, 1 ml culture of cells was taken at each time point. Cells were recovered by centrifugation and stored at -20 °C. Then the cells were resuspended in 150 μ l of TE buffer containing 15 mM MgCl₂. Crude tRNA was extracted once with 150 μ l of phenol:chloroform=1:1 and once with chloroform. The tRNA was ethanol precipitated, dried, and dissolved in 20 μ l H₂O. Two μ l was used for valine accepting activity assay.

The tRNA^{Val} yield was further increased by inserting a T7 terminator sequence downstream of the tRNA^{Val} gene. The T7 terminator should turn down the transcription of plasmid DNA sequences and increase the transcription of the tRNA gene. The terminator-containing fragment was excised from pET11a (NOVAgene) by Bam HI/Hind III digestion. The 288 bp fragment was purified by agarose gel electrophoresis. The pVAL119-21 was also digested with Bam HI/Hind III and the large fragment was purified by agarose gel electrophoresis. The Bam HI and Hind III sites in pVAL119-21 are just downstream of the tRNA^{Val} gene. Then the 288 bp fragment was ligated into the large fragment to generate the recombinant plasmid pVALT7. The ligation mixture was used to transform *E. coli* TG1. The recombinant plasmid was selected by screening for the presence of the desired Bst NI restriction pattern. The sequence was confirmed by DNA sequencing analysis. Plasmid DNA was isolated from the correct clone and used to transform *E. coli* BL21(DE3). This

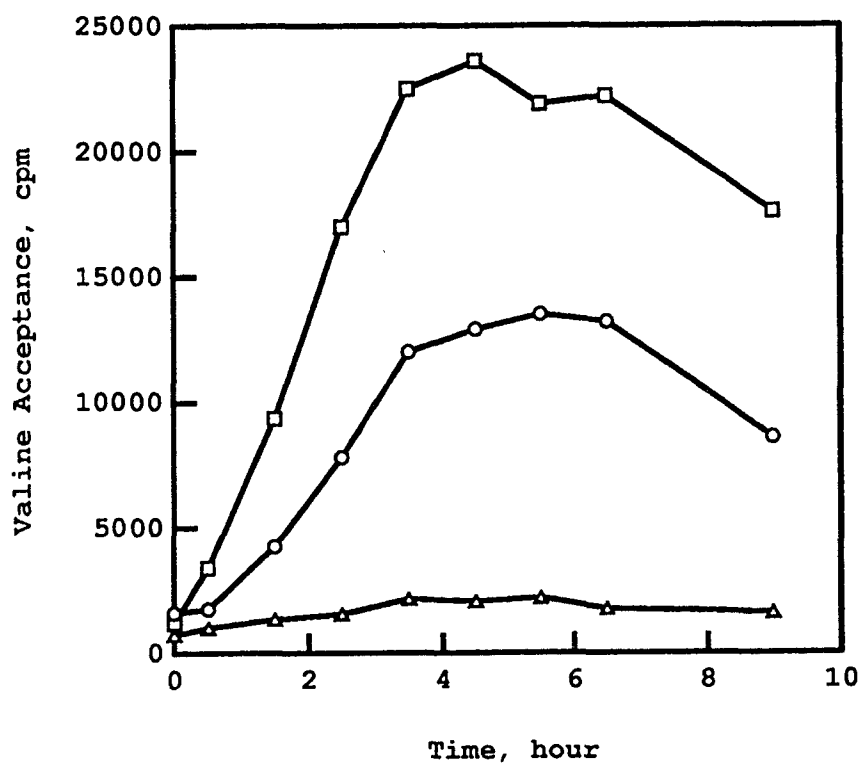


Figure 2.2: Expression of *E. coli* tRNA^{Val}. (Δ) TG1 cell transformed with pVALT7 without induction by IPTG. (\circ) BL21(DE3) containing pVAL119-21 with induction by 0.3 mM IPTG. (\square) BL21(DE3) containing pVALT7 with induction by 0.3 mM IPTG

construct almost doubled the yield of tRNA^{Val} compared with the system without the T7 terminator. The assay of tRNA^{Val} activity in the different expression system is shown in Figure 2.2. tRNA^{Val} activity reaches a maximum after 4–6 h induction.

Cell growth *E. coli* BL21(DE3) harboring pVALT7 was grown in LB media supplied with 50 µg/ml ampicillin at 37 °C. Typically 4 liter of media was inoculated with 400 ml overnight culture. When OD₆₀₀ reached 0.7 to 0.8, the cells were induced with 0.3 mM IPTG. The cells were allowed to grow at 37 °C for another 4 to 5 hours and were then collected by centrifugation.

Purification of expressed tRNA^{Val} 15–20 g cells were resuspended in 60 ml of 10 mM Tris-HCl, pH 7.5, 15 mM MgCl₂, and then extracted with an equal volume of phenol saturated with Tris-HCl, pH 7.5. After 30 min of stirring at room temperature, the aqueous phase was collected by centrifugation at 15,000 rpm for 15 min. This aqueous phase was extracted two times with chloroform, then 0.1 volume of 3M NaOAc (pH 5.4) and 0.4 volume of 2-propanol were added. After centrifugation at 15,000 rpm for 15 min, one third volume of 2-propanol was added to the supernatant to pellet the tRNA. The recovered crude tRNA was washed with ethanol, dried and dissolved in a minimal amount of 25 mM Tris-HCl, pH 7.4, 250 mM NaCl.

The crude tRNA was then chromatographed on a DEAE column, followed by C4 reverse-phase chromatography. Column conditions are the same as those used to purify *in vitro* transcribed tRNA. The tRNA^{Val}-containing pool from the C4 column (detected by aminoacylation assay) was further fractionated on a BD-cellulose column

(1.1x30 cm). The column was equilibrated with 20 mM NaOAc, pH 4.5, 0.4 M NaCl, 10 mM MgCl₂. Elution was performed with a linear gradient in the same buffer containing 0.4 M NaCl to 1 M NaCl. Fractions with valine-accepting activity were pooled and precipitated with ethanol.

Characterization of expressed tRNA^{Val} The purified native tRNA^{Val} shows a single band on 16% PAGE (data not shown). The valine accepting level is over 1400 pmole/A260. Figure 2.3 shows the imino ¹H NMR spectra of commercial (A) (Subriden) tRNA^{Val} and overexpressed tRNA^{Val} (B) recorded at 22 °C in the presence of 15 mM Mg²⁺. The two spectra are almost identical except for a slight shift of several peaks in the 12–12.5 ppm region. The imino protons from modified nucleosides, peak B (s⁴U), peak C (T54), peak K' (m⁷G46), peak U (Ψ55), in the expressed tRNA, all have identical chemical shifts to the corresponding peaks in the spectrum of commercial tRNA. This strongly suggests that the overexpressed tRNA is largely modified, at least at the positions involving tertiary interactions (s⁴U8, m⁷G46, T54, Ψ55).

Aminoacylation kinetics

Aminoacylation kinetic experiments were carried out at 37 °C in 65 μl reaction containing 100 mM HEPES, pH 7.5, 15 mM MgCl₂, 1 mM KCl, 7 mM ATP, 1 mM DTT, and 99 μM [³H] Valine. tRNA and VRS concentrations vary with different tRNA mutants. tRNA concentration was determined by a plateau charging assay. In this assay excess amounts of VRS were used. The reaction was monitored by assaying the level of valine acceptance. The reaction mixture was same as the aminoacylation

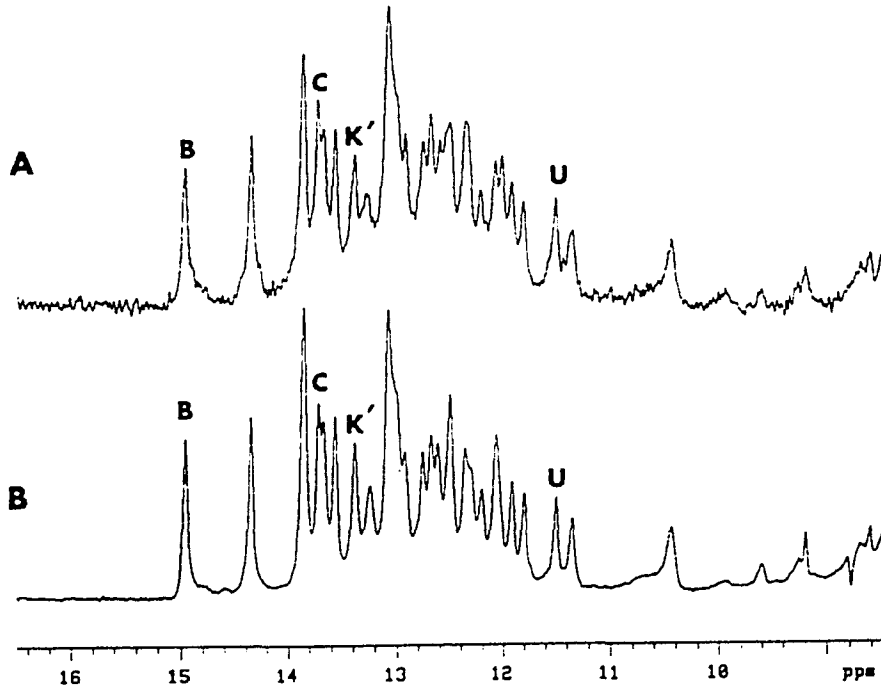


Figure 2.3: Imino ^1H NMR spectra of commercial (A) and overexpressed (B) *E. coli* tRNA^{Val} in buffer containing 10 mM phosphate, pH 7, 100 mM NaCl, 15 mM MgCl₂ at 22 °C

kinetic experiment. 10 μl were removed at 30-s intervals and spotted on Whatman 3 MM paper which was pre-soaked with 10% TCA. The paper was washed 3 times with cold 5% TCA and two times with cold 95% ethanol. Then the paper was dried and counted in Biosafe NA scintillation fluor. Initial velocities were obtained at five different concentrations of tRNA at a fixed synthetase concentration. K_m and V_{max} were determined by a linear-reciprocal plot of the data (Cleland, 1979).

¹H NMR spectroscopy

For ¹H NMR spectroscopy, 5–25 mg of tRNA was dissolved in buffer containing 10 mM sodium phosphate, pH 7.0, 15 mM MgCl₂, 100 mM NaCl and dialyzed against the same buffer. The sample volume was adjusted to 405 μl with the same buffer and 45 μl D₂O was added. The sample was renatured by heating at 85 °C for 5 min and cooling slowly to room temperature prior to spectrum collection. For Mg²⁺ titration experiment, the sample was prepared with no added Mg²⁺. Titration with Mg²⁺ was carried out by adding small aliquots of concentrated MgCl₂ solution (0.2–1 M) directly to the NMR tube. For pH titrations, small amounts of 0.5 M HCl were used to adjust the sample pH in a 1.5 ml microcentrifuge tube. The sample was then returned to the NMR tube. Less than 15 μl of 0.5 M HCl were needed to adjust the sample pH from 7.0 to 4.2. For GUAA titration, aliquots of dried GUAA were dissolved in the NMR sample to attain the desired GUAA concentration.

All ¹H NMR spectra were taken on a Varian Instruments Unity-500 NMR spectrometer operating at 500 MHz. The spectra were collected at 22 °C or at the indicated temperatures. Chemical shifts are given relative to the H₂O resonance at 4.80 ppm at 22 °C. Spectra taken at other temperatures were corrected for an upfield peak shift of 5 Hz/°C with increasing temperature.

1D ¹H NMR spectra were obtained with the H₂O resonance suppressed using the 1–1 spin-echo selective excitation pulse sequence (Sklenar and Bax, 1987). The sweep width was set at 18,000 Hz. 16,000 complex points were collected. The acquisition time was 0.444 seconds. The recycle delay was 2 seconds. Typically 500–2,000 scans were collected to give a good signal-to-noise ratio. The spectra were processed with

2 Hz line broadening.

For 1D NOE experiments the pulse sequence contains a 100 μ s presaturation pulse and a jump-return pulse to suppress the H₂O resonance (Plateau and Gaéron, 1982). Sweep width ranges from 10,000 to 12,000 Hz were used and 4096 complex points were collected for each experiment. The presaturation pulse was just the power to saturate the irradiated peak by \sim 90%. The control spectrum was taken with the presaturation pulse set off-resonance downfield at 8,500 Hz. Difference spectra were obtained by subtracting the spectrum of interest from the control spectrum. Typically, 3,000 to 4,000 scans were collected at each frequency offset.

The 2D NOESY spectrum of tRNA^{Val} was obtained using a jump-return pulse sequence as the read pulse (Driscoll, 1989). The sweep width was 12,000 Hz in each dimension. The mixing time was 0.15 seconds. The spectrum was recorded with 2048 complex points in t_2 and 412 complex points in t_1 . 192 scans were collected per t_1 experiment. The data were apodized with a 60° shifted sine bell in both dimensions.

2D NOESY spectra of free GUAA and GUAA in the presence of tRNA^{Val} were obtained in D₂O solution containing 10 mM phosphate, 100 mM NaCl, 15 mM MgCl₂ at 6 °C. The GUAA concentration was 2 mM, the tRNA concentration was 0.2 mM. The sweep width was 5,000 Hz in each dimension. The mixing time was 0.15 seconds. The spectrum was recorded with 2048 complex points in t_2 and 300 complex points in t_1 . 64 scans were collected per t_1 experiment.

The TOCSY spectrum of GUAA was obtained at 6 °C with a mixing time of 0.05 seconds. The sweep width was 5,000 Hz in each dimension. The presaturation time was 1 second. The recycle delay was 2 seconds. The spectrum was recorded with 2048 complex points in t_2 and 300 complex points in t_1 . 64 scans were collected

per t_1 experiment.

The ROESY spectrum of GUAA was obtained at 6 °C with a mixing time of 0.15 seconds. The sweep width was 5,000 Hz in each dimension. The presaturation time was 1 second. The recycle delay was 1.8 seconds. The spectrum was recorded with 2048 complex points in t_2 and 256 complex points in t_1 . 64 scans were collected per t_1 experiment.

^{19}F NMR spectroscopy

Samples of FU-tRNAs (2-5 mg) were dissolved in 300 μl of 1.11xNMR buffer (standard buffer): 55 mM sodium cacodylate, pH 6.0, 16.6 mM MgCl_2 , 110 mM NaCl and 1.1 mM EDTA. Then the sample was dialyzed against two 250 ml changes of the same buffer. Finally the sample volume was adjusted to 405 μl and 45 μl D_2O was added to serve as an internal lock. The sample was renatured by heating at 85 °C for 5 min and then cooling slowly to room temperature before recording the spectrum.

^{19}F NMR spectra were recorded on a Varian Instruments Unity-500 spectrometer operating at 470.268 MHz. Data were collected by using 8,000 complex points, no relaxation delay and a 30 ° excitation pulse. Typically 5,000 to 10,000 scans were collected at the indicated temperatures and processed with 15 Hz spectral line broadening. Chemical shifts are reported as ppm using free 5-Fluorouracil as standard. Downfield shifts were shown as positive numbers. Spectra taken at 35 °C and 47 °C were corrected for an upfield shift of 0.10 ppm and 0.19 ppm respectively.

1D NOE ^{19}F NMR spectra were obtained with 10 mg FU-tRNA sample in

standard buffer at the indicated temperature. The sweep width was 20,000 Hz. the recycle delay was 1.7 seconds. The control spectrum was taken with the presaturation pulse set off-resonance upfield at -36,639 Hz.

CHAPTER 3. RESULTS

Structure comparison between native and transcribed tRNA^{Val}

Native tRNA contains a large proportion of post-transcriptionally modified nucleosides. However, *in vitro* transcribed tRNAs which do not have modified nucleosides remain good substrates for their respective synthetases. Thus the structure of the *in vitro* transcript must be very similar to that of native tRNA. It is also known that unmodified tRNAs are less stable than native tRNA under the same conditions. *In vitro* transcribed tRNA is very useful for studying tRNA function and its interactions with various ligands; it is, therefore, important to understand the structural similarities and differences between modified and unmodified tRNAs.

NMR spectroscopy has been very useful in monitoring tRNA structure in solution. The hydrogen-bound imino protons on tRNA nucleobases resonate in a uniquely downfield region of the ^1H spectrum. By observing the exchange rate of these protons, tRNA dynamics can be studied. Earlier workers have studied several native tRNAs by imino ^1H NMR. More recently, Hall and her colleagues have conducted a similar study on *in vitro* transcribed tRNA^{Phe} (Hall, *et al.*, 1989). To compare the structures of modified and unmodified *E. coli* tRNA^{Val}, ^1H NMR studies were performed to assign the imino ^1H NMR spectrum of the *in vitro* transcript, to compare

its spectrum to that of native (modified) tRNA^{Val}, and to examine the temperature and Mg²⁺ and pH dependence of the ¹H NMR spectra.

Solution structure in excess Mg²⁺

Assignment of ¹H NMR spectrum of transcribed tRNA^{Val} The secondary structure and expected tertiary interactions of tRNA^{Val} based on the crystal structure of yeast tRNA^{Phe} (Kim *et al.*, 1974; Robertus *et al.*, 1974) are shown in Figure 3.1. Figure 3.2 shows the imino proton NMR spectra of native (a) and *in vitro* transcribed tRNA^{Val} (b) in buffer containing 10 mM sodium phosphate, pH 7.0, 15 mM MgCl₂, 100 mM NaCl. Peaks of the spectra are labeled alphabetically. The spectrum of the native tRNA is almost identical to the previous published spectrum (Hare *et al.*, 1985). Thus the assignments are readily transferred to the spectrum in Figure 3.2a. But the spectrum of unmodified tRNA^{Val} is much different from that of the native tRNA. These differences make it difficult to transfer the already assigned peaks in native tRNA^{Val} to assignment of the spectrum of transcribed tRNA^{Val}. Thus the ¹H NMR spectrum of unmodified tRNA^{Val} has to be assigned independently.

The imino ¹H NMR spectrum of the transcript was assigned by sequential NOE techniques. Because of the good resolution of the spectrum the assignment was relatively straight forward. The 2D NOESY map is shown in Figure 3.3. In this map the strongest NOE cross peak is between peaks S and V. Based on the proposed 3-dimensional structure of tRNA^{Val}, the best candidates for peaks S and V are the imino protons of the G50U64 wobble base pair in the T-stem. Wobble base pairs exhibit strong reciprocal NOEs, because the imino protons of G and U, being on the

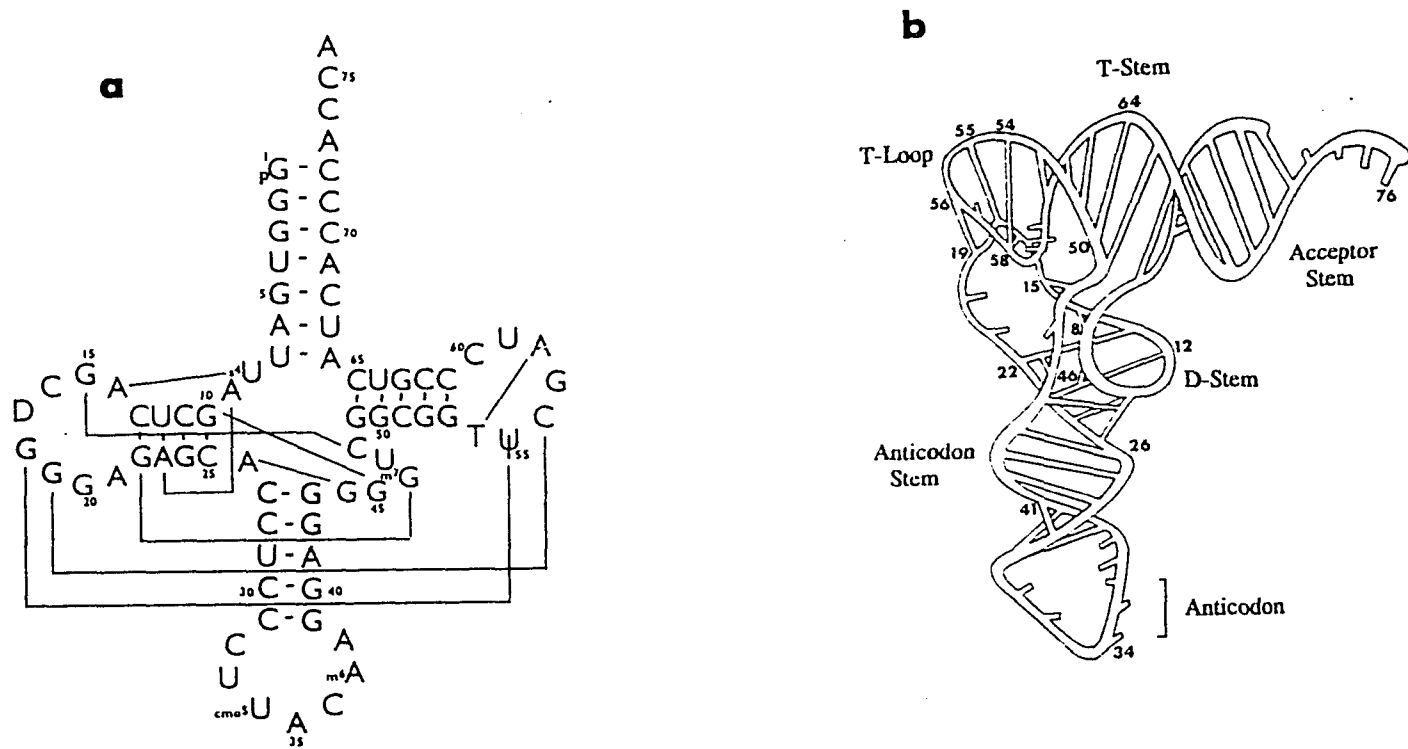


Figure 3.1: Model of the secondary structure (a) and tertiary (b) interactions of *E. coli* tRNA^{Val} based on the crystal structure of yeast tRNA^{Phe}. The positions of 7 modified nucleosides are indicated in the secondary structure

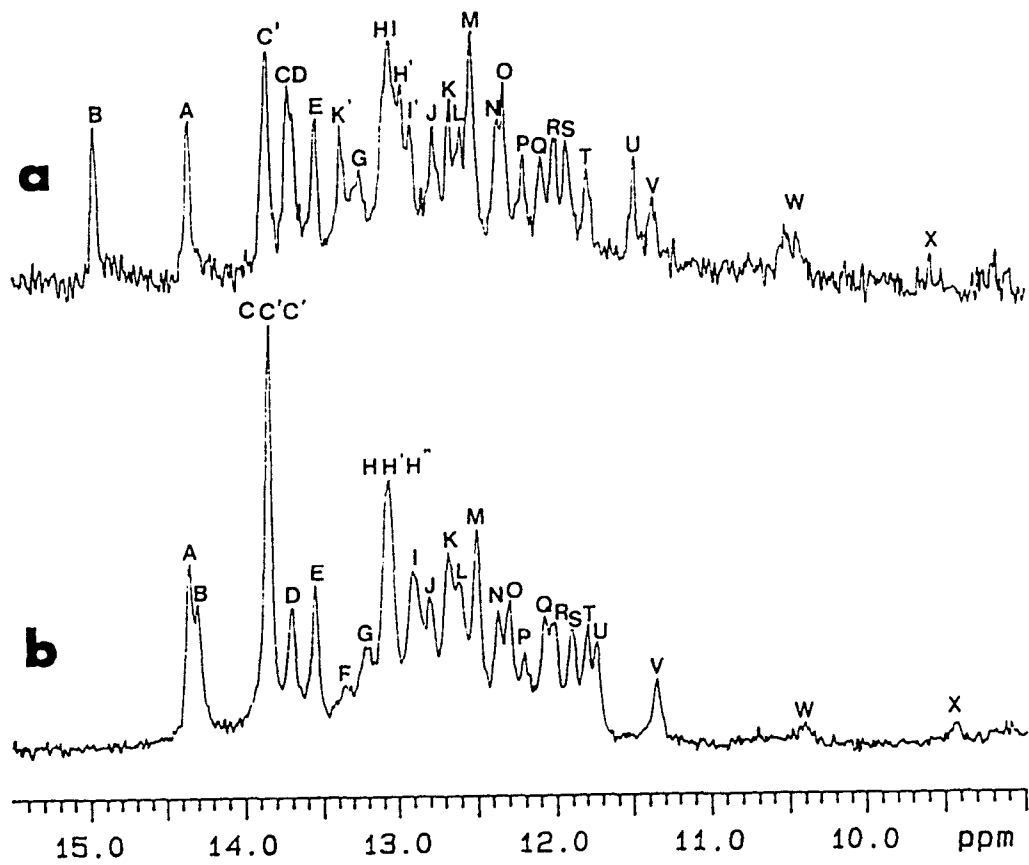


Figure 3.2: Imino ^1H NMR spectra of native (a) and *in vitro* transcribed tRNA^{Val} (b) in buffer (10% D₂O) containing 10 mM sodium phosphate, pH 7.0, 15 mM MgCl₂, 100 mM NaCl at 22 °C

same base pair, are very close to each other. Based on the fact that the imino proton of U resonates at lower field than that of G in a GU base pair (Griffey *et al.*, 1982), peak S was assigned to the imino proton of U64 and peak V to G50.

Assignment of the T stem begins with the already assigned GU base pair (peaks S and V). Peak V shows a NOE to peak Q. Both S and V show NOEs to peak J. Peak J shows a NOE to peak N and peak N to one of the resonances in peak H(H'). The NOE connectivities Q-V/S-J-N-H' assign the imino protons of the T stem, with peak Q corresponding to the imino protons of G49.

There are 5 Watson-Crick AU base pairs in tRNA^{Val}. These base pairs can be identified by the strong NOE between the imino proton of the uracil and the C2 proton of the adenine. The C2 proton of adenine has a narrow linewidth and is observed in 6.8–7.8 ppm chemical shift range. From the 2D NOESY map (data not shown) and one-dimensional NOE experiment (Figure 3.4), peaks A, C', C'', E and L were identified as Watson-Crick AU base pairs.

There are 3 Watson-Crick AU base pairs in the acceptor stem. NOE connectivities of seven resonances including 3 protons from AU base pairs should correspond to the acceptor stem. These assignment were made by following the NOE connectivities starting from peak L. In the 2D NOESY map (Figure 3.3) peak L shows a NOE only to peak A. Peak A shows a further NOE to peak T, and peak T to peak E. The NOE between peak T and peak E is very weak but can be seen in lower contours in the NOESY map (data not shown). It is also seen in the one-dimensional NOE experiment (Figure 3.4). Peak E has strong NOE to one of the resonances in peak H. This resonance in peak H has a NOE to one of the resonances in peak K. Peak K has a NOE to peak R, which has no other NOEs. The NOE connectivities

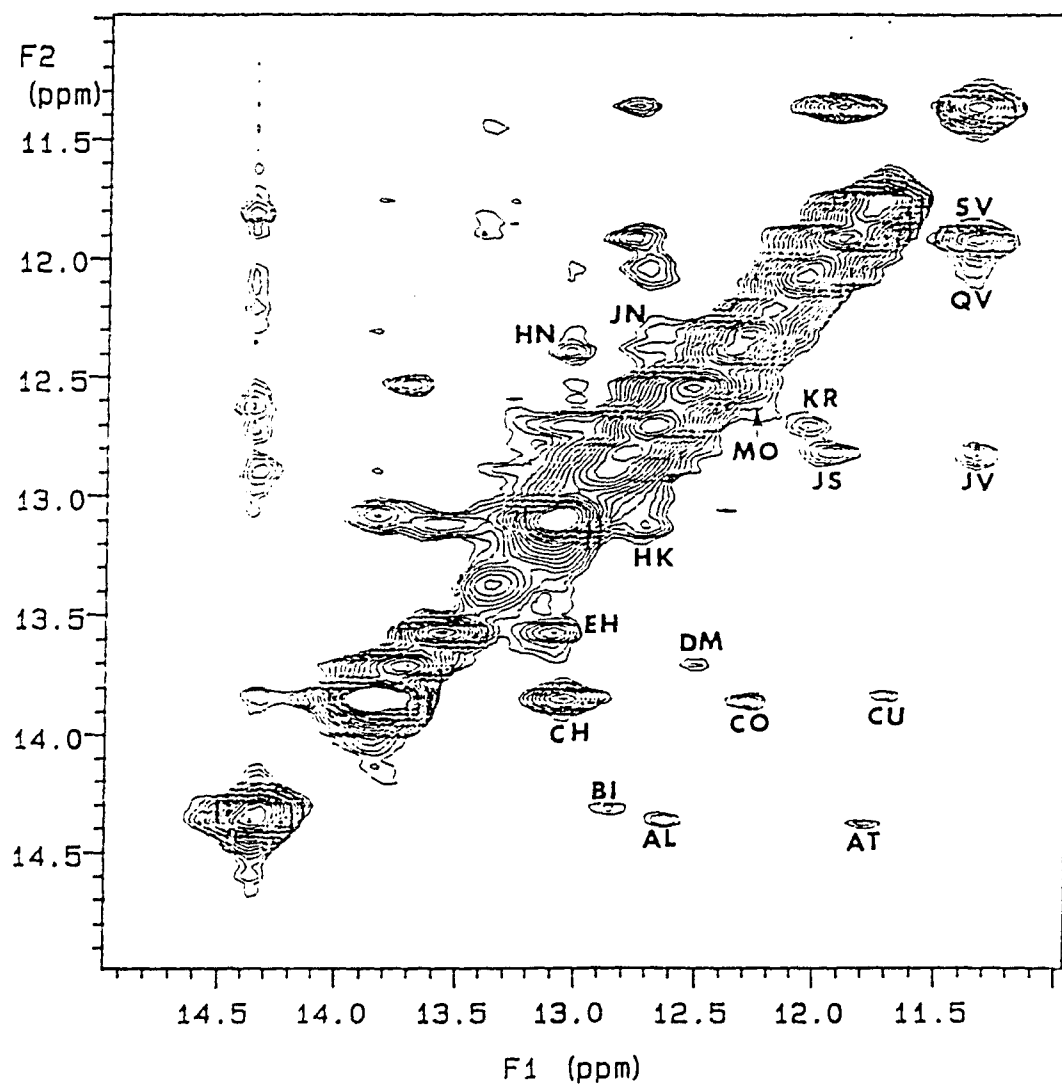


Figure 3.3: Imino proton region of two-dimensional NOESY NMR spectrum of the *in vitro* transcript in buffer containing 10 mM sodium phosphate, pH 7.0, 15 mM MgCl₂, 100 mM NaCl at 22 °C. The cross peaks are labeled with the letters of the parent peaks

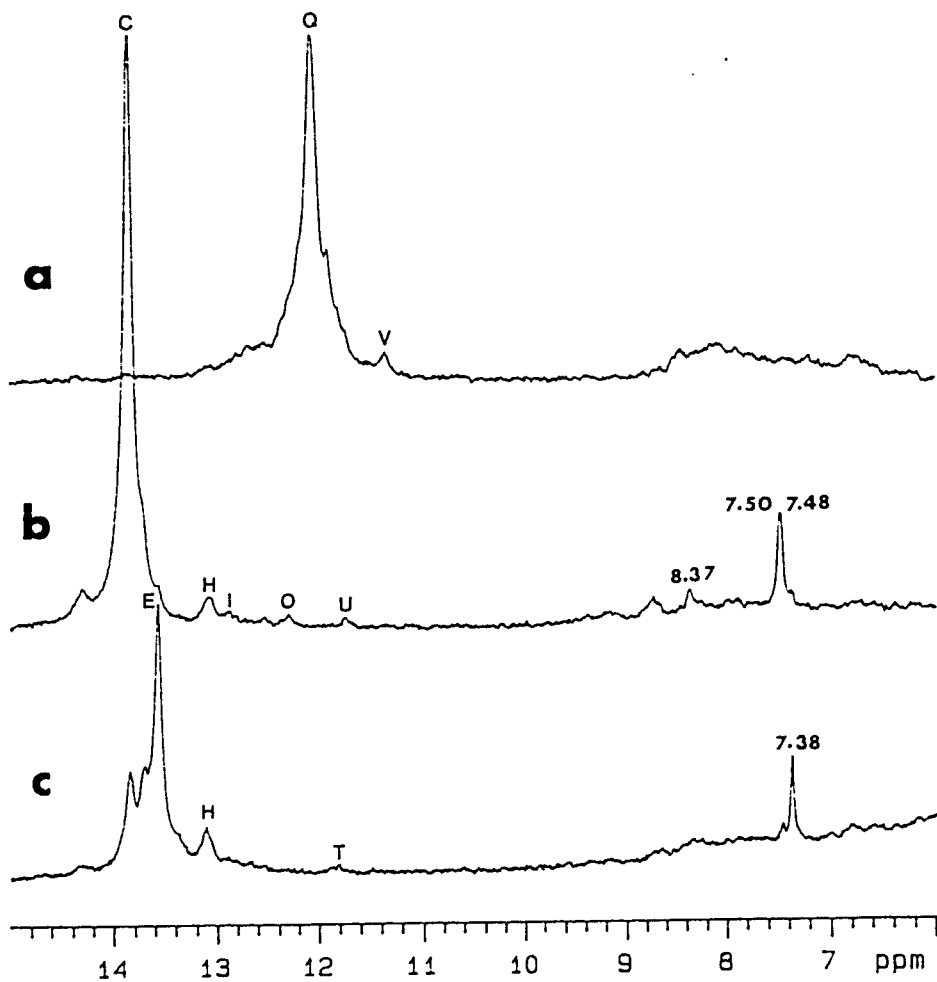


Figure 3.4: Downfield region of ^1H NMR one-dimensional difference NOE spectra of the unmodified tRNA at the same solution conditions and temperature as in Figure 3.2. The NOE partners of each saturated peak are indicated. (a) peak Q has been saturated. (b) peak C has been saturated. (c) peak E has been saturated. (d) peak P has been saturated. (e) peak X has been saturated. (f) peak M has been saturated

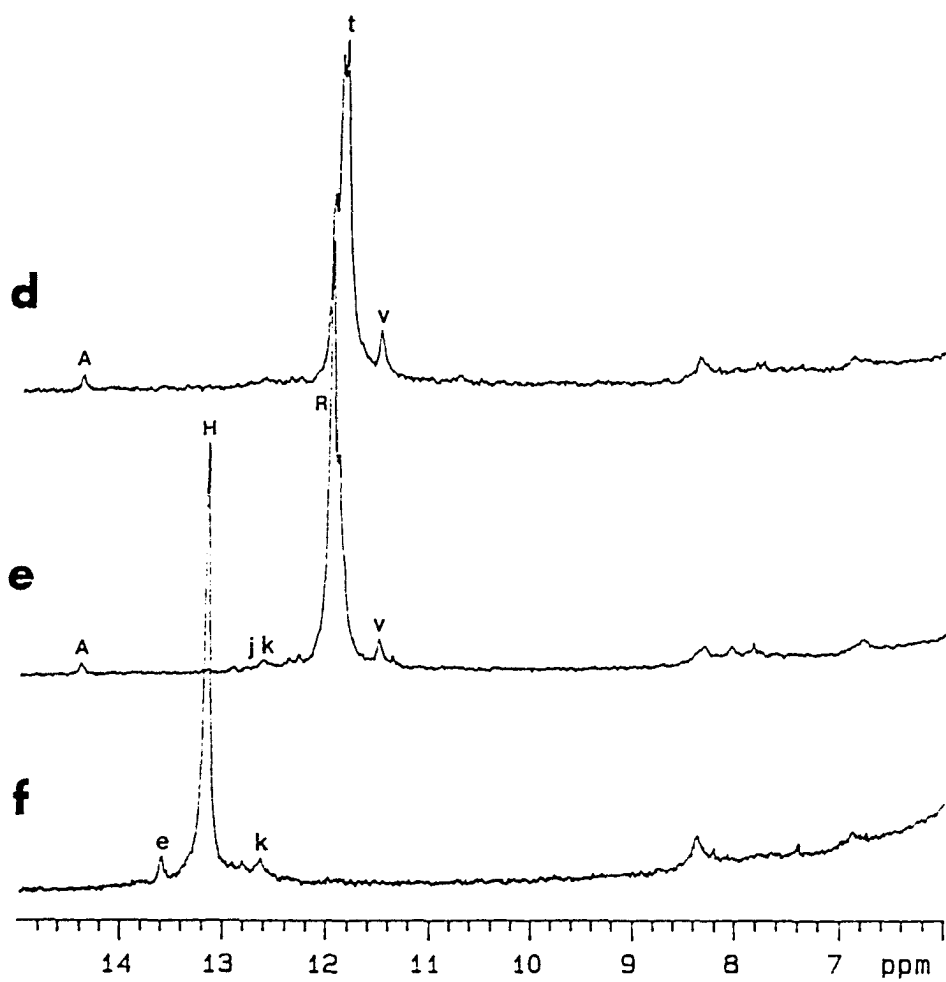


Figure 3.4 (Continued)

L-A-T-E-H-K-R match the imino protons from the acceptor stem. Peaks L, A and E correspond to the 3 AU Watson-Crick base pairs, with peak L corresponding to the imino proton of U7 and peak R to G1.

The other two resonances from AU Watson-Crick base pairs, peaks C' and C'', belong to the D stem and the anticodon stem. Peak C' has a NOE to peak O. Peak O has a NOE to peak M. The very strong cross peak between peak C and H probably correspond to double NOE from C' to H''. A possible NOE between H'' and G is partially obscured by the diagonal in the NOESY map (Figure 3.3). The NOE connectivities M-O-C'-H''-G with the Watson-Crick AU base pair resonance C' in the middle, assign these 5 peaks to the anticodon stem (see Figure 3.1A). The orientation of the anticodon stem assignment was prevented by the sequence symmetry of the stem. This problem was solved as described in the following section.

Assignment of the D stem starts from the remaining AU base pair resonance, C''. C'' has a weak NOE to peak I (Figure 3.4b). There is a NOE between peak D and peak M'. The cross peak from C'' to peak D is obscured by the diagonal in the 2D NOESY map (Figure 3.3), but when the data were reprocessed with apodization to enhance resolution, off diagonal intensity between peaks C and D was evident. NOE connectivities M'-D-C''-I assign these 4 peaks to the D-stem with peak M' corresponding to the G22 imino proton.

In the T loop, U54 forms a reverse Hoogsteen base pair with A58. Peak C is assigned to the U54 imino proton because of its NOE to peak H' (G53). There is a network of NOEs among peaks C, U and X (Figure 3.3 and Figure 3.4). Based on the crystal structure of yeast tRNA^{Phe}, peaks U and X must belong to hydrogen-bonded protons of G18 and U55. The amino proton of G18 forms a hydrogen bond

with O2 of U55. The imino proton of U55 forms a hydrogen bond with oxygen of the phosphate backbone. Peak X has a chemical shift, 9.45 ppm, which is outside the imino proton range. Thus peak X is assigned to the G18 amino proton and peak U is assigned to the U55 imino proton.

From the crystal structure of yeast tRNA^{Phe}, U8 forms a normal Hoogsteen base pair with A14. This base pair is stacked on the end of the D stem. A weak NOE can be seen between peak B and peak I (G22). Thus peak B is assigned to the U8 imino proton. G15 forms a reverse Watson-Crick base pair with C48. This base is stacked on the U8A14 base pair. The very weak NOE from peak P to peak B (Figure 3.4e) suggests peak P is the resonance from the G15 imino proton.

In yeast tRNA^{Phe}, A44 and G26 form a purine-purine base pair. It is expected that G44 and A26 will form a similar base pair in *E. coli* tRNA^{Val}. In such GA base pairs the C2 proton of A is close to the G imino proton and a strong NOE between them is expected. Peak F has a NOE to a sharp peak at 7.0 ppm, thus peak F is assigned to the G44 imino proton.

G46 forms a base triplet with G22C13. The structure places the G46 imino proton close to the G22 C8 proton (Figure 3.1). There is an NOE from K' to a peak at 7.90 ppm which could correspond to the G22 C8 proton. Therefore, K' is assigned to the G46 imino proton.

Orientation of the anticodon stem The orientation of the anticodon stem assignments was solved by examining the imino ¹H spectrum of tRNA^{Val} mutant 30U40A (Figure 3.5). Changing the C30G40 base pair to U30A40 is expected to shift the resonance of the U30 imino proton well downfield. In addition peaks of

base pairs adjacent to U30A40 should also shift. Comparison of the spectrum of U30A40 with that of wild type tRNA^{Val}, shows that extra intensity arises in the peak C region, which must correspond to the U30 imino proton resonance. Peak O in the spectrum of wild type tRNA^{Val} has disappeared. Thus peak O must be from G40. One of the two resonances in peak M, which has been assigned to the imino proton of either G39 or G43, shifts upfield to the position of peak O in the spectrum of U30A40. The splitting of peak C and the shift of peak M indicates that peaks C' and M are from base pairs adjacent to 30U40A. Therefore peak M was assigned to imino proton of G39, thus establishing the orientation of the anticodon stem assignments. Assignments of the spectrum of the 30U40A variant were confirmed by one-dimensional NOE experiments (data not shown).

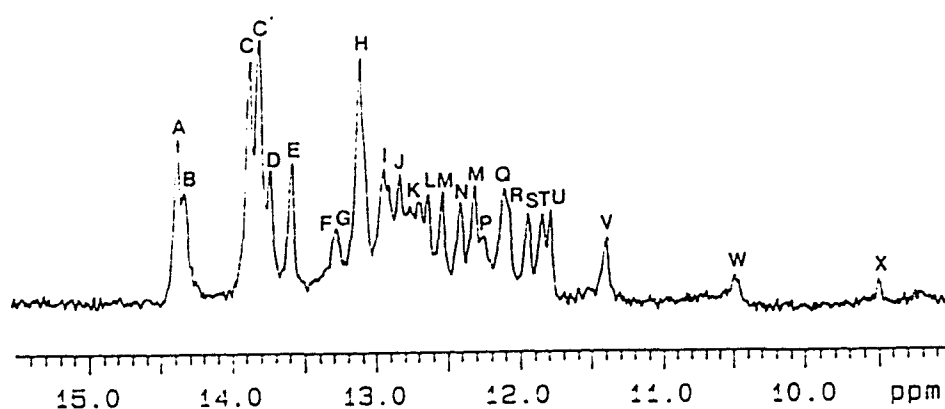


Figure 3.5: Imino ^1H NMR spectrum of tRNA^{Val} variant U30A40 obtained in the same solution conditions and temperature as in Figure 3.2

Summary of imino proton resonance assignments The assignment of the imino proton NMR spectrum of *E. coli* tRNA^{Val} in excess Mg²⁺ is summarized in Table 3.1. The NOE partners for each peak were also listed in the table. The partners include imino protons and aromatic protons. Assignment is to the U or G imino proton of a base pair except for peak X, which is the G18 amino proton. Peak S is assigned to the U64 imino proton and peak V to the G50 imino proton. Peak K' is assigned to the G46 imino proton. Peak U is assigned to the U55 imino proton. In AU Watson-Crick base pairs, the aromatic NOE partner is assigned to the adenine C2 proton. In AU Hoogsteen base pairs (peak B and C), the aromatic NOE partner is the C8 proton of adenine. In the AG purine-purine base pair (peak F), the aromatic NOE partner is the adenine C2 proton. And in the G22G46 tertiary interaction (peak K'), the aromatic NOE partner is the G22 C8 proton.

In vitro transcribed tRNA is very useful in studying tRNA function and its interactions with various ligands, so it is important to understand the structural similarities and differences between modified and unmodified tRNAs. The newly assigned imino proton spectrum of *in vitro* transcribed *E. coli* tRNA^{Val} allows this comparison to be made conveniently. Figure 3.6 compares the chemical shifts of assigned peaks in the imino proton spectrum of the unmodified *in vitro* transcript with those of native (modified) tRNA^{Val} (Hare *et al.*, 1985). Large chemical shift differences can be seen for peaks B, C, K', U and X. All these peaks belong to imino protons on modified bases or to an amino proton on a base that is paired to a modified base. Peak B corresponds to 4-thiouridine at position 8 in native tRNA; peak C to ribothymidine at position 54; peak K' to 7-methylguanosine at position 46; peak U to pseudouridine at position 55. Peak X is the resonance of the G18 amino

Table 3.1: Imino proton assignments in *E. coli* tRNA^{Val}

peak	position	Assignment	NOE partners	
			imino	aromatic
A	14.36	A6U67	L, T	7.63
B	14.31	U8A14	I, P	7.77
C	13.85	U54A58	H, U	8.37
C'	13.85	U29A41	H'', O	7.50
C''	13.85	U12A23	I, D	7.48
D	13.71	C11G24	M, H''	
E	13.56	U4A69	T, H	7.38
F	13.36	A26G44		7.00
G	13.21	C27G43	H''	
H	13.08	G3C70	E, K	
H'	13.08	G53C61	C, N	
H''	13.08	C28G42	C'', G	
I	12.92	C13G22	B, C''	
I'	12.92	G19C56		
J	12.81	C51G63	S, V, N	
K	12.69	G2C71	H, R	
K'	12.69	G22G46		7.90
L	12.62	U7A66	A	7.21
M	12.51	C31G39	O	
M'	12.51	G10C25	D	
N	12.38	G52C62	H', J	
O	12.31	C30G40	M, C''	
P	12.22	G15C48	B	
Q	12.08	G49C65	V	
R	12.03	G1C72	K	
S	11.92	G50U64	J, V	
T	11.81	G5C68	A, E	
U	11.76	G18U55	C, X	
V	11.37	G50U64	J, S, Q	
X	9.45	G18U55	U, C, H'	

proton which is hydrogen bonded to T55 in native tRNA. Such large chemical shifts are expected because base modifications perturb the electronic environments of these imino protons.

All other chemical shift differences are less than 0.1 ppm. Thus the results show that the structure of modified and unmodified *E. coli* tRNA^{Val} are remarkably similar in excess Mg²⁺ concentration. Any differences are localized to the vicinity of the modified bases. *In vitro* transcribed tRNA is, therefore, a suitable model system for biochemical and biophysical studies under conditions of high Mg²⁺ concentration.

Thermal stability comparison of modified and unmodified tRNA in excess Mg²⁺ concentration Although the structure of the *in vitro* transcript is similar to that of native tRNA, evidence indicated that lack of base modifications results in a less stable tRNA molecule. The melting temperature (*T*_m) of *in vitro* transcribed *E. coli* tRNA^{Val} is lower than that of native tRNA^{Val} under the same conditions (Derrick and Horowitz, 1993). Peak assignments for both modified and unmodified *E. coli* tRNA^{Val} allows a comparison of their thermal stability to be made by ¹H NMR.

Figure 3.7 and Figure 3.8 show the ¹H NMR spectra of modified and unmodified tRNA, respectively, at different temperatures. For the unmodified tRNA most tertiary peaks (C, U, I', F, X) are lost from the spectrum by 60 °C. The tertiary peaks K' (G46) and P, however, remain visible at 60 °C. Peak B (U8) is very broad at this temperature. Peak L has disappeared. Resonances of all other AU Watson-Crick base pairs are broadened.

Compared to the transcript, native tRNA^{Val} is much more stable. At 60 °C,

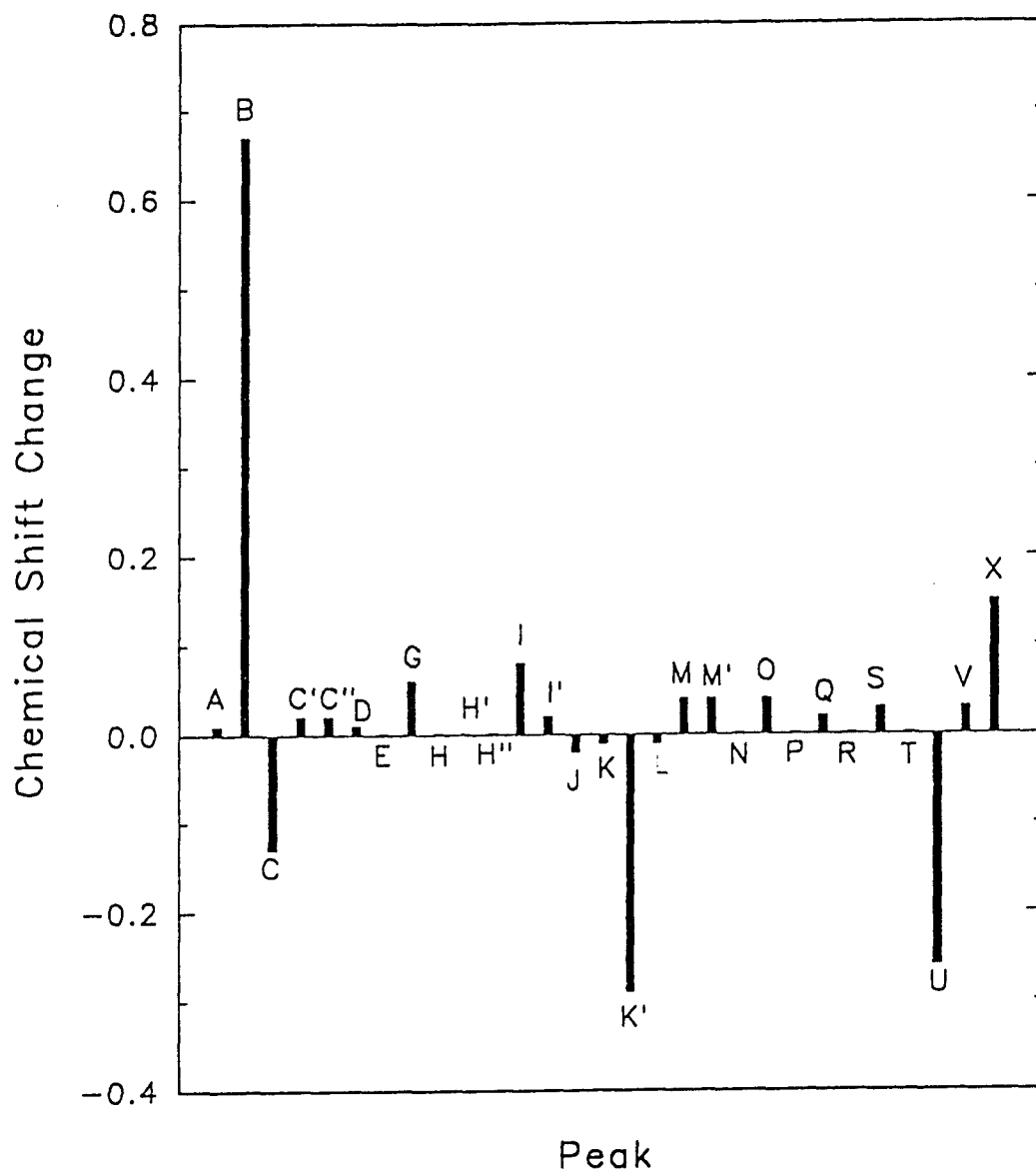


Figure 3.6: Difference in chemical shift of assigned peaks in the imino proton spectra of unmodified and modified *E. coli* tRNA^{Val}. A positive value of the chemical shift difference indicates an upfield shift of the resonance in unmodified tRNA

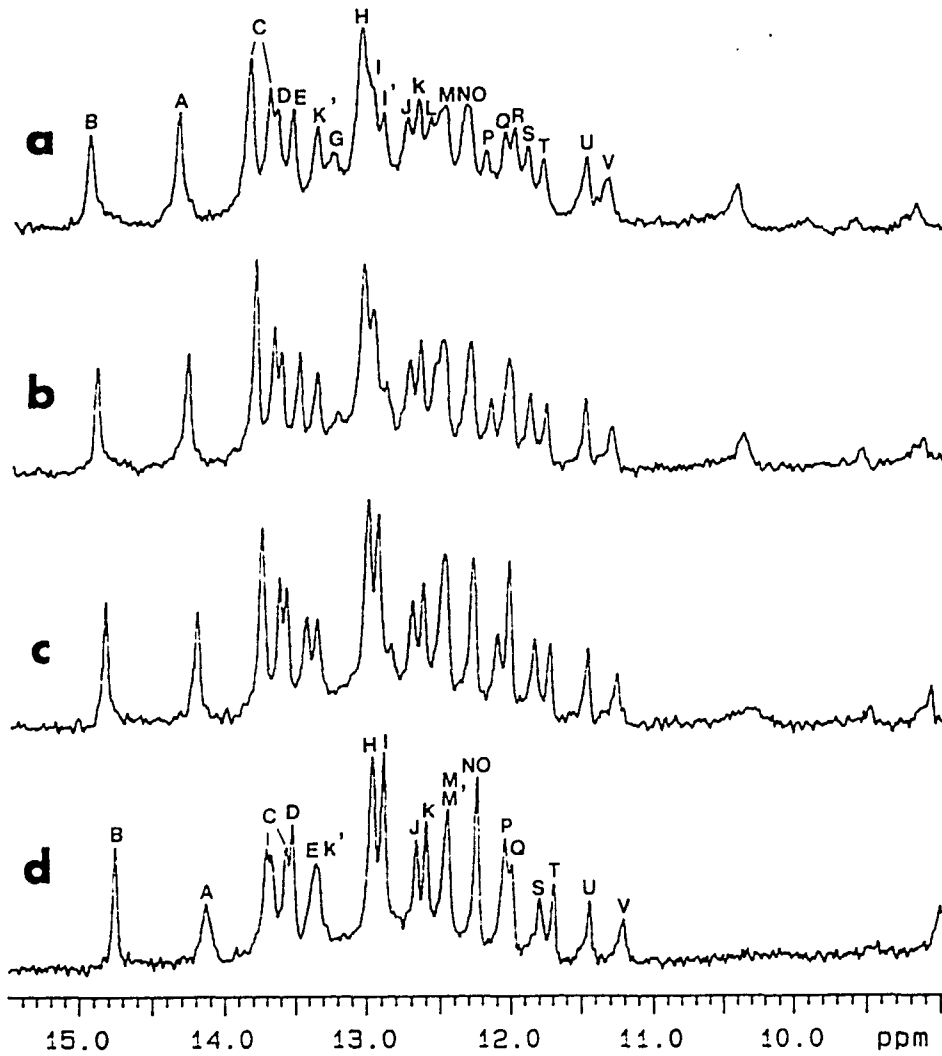


Figure 3.7: ^1H NMR spectra of native *E. coli* tRNA^{Val} obtained at different temperatures. The solution conditions were as in Figure 3.2. (a) 22 °C. (b) 35 °C. (c) 47 °C. (d) 60 °C

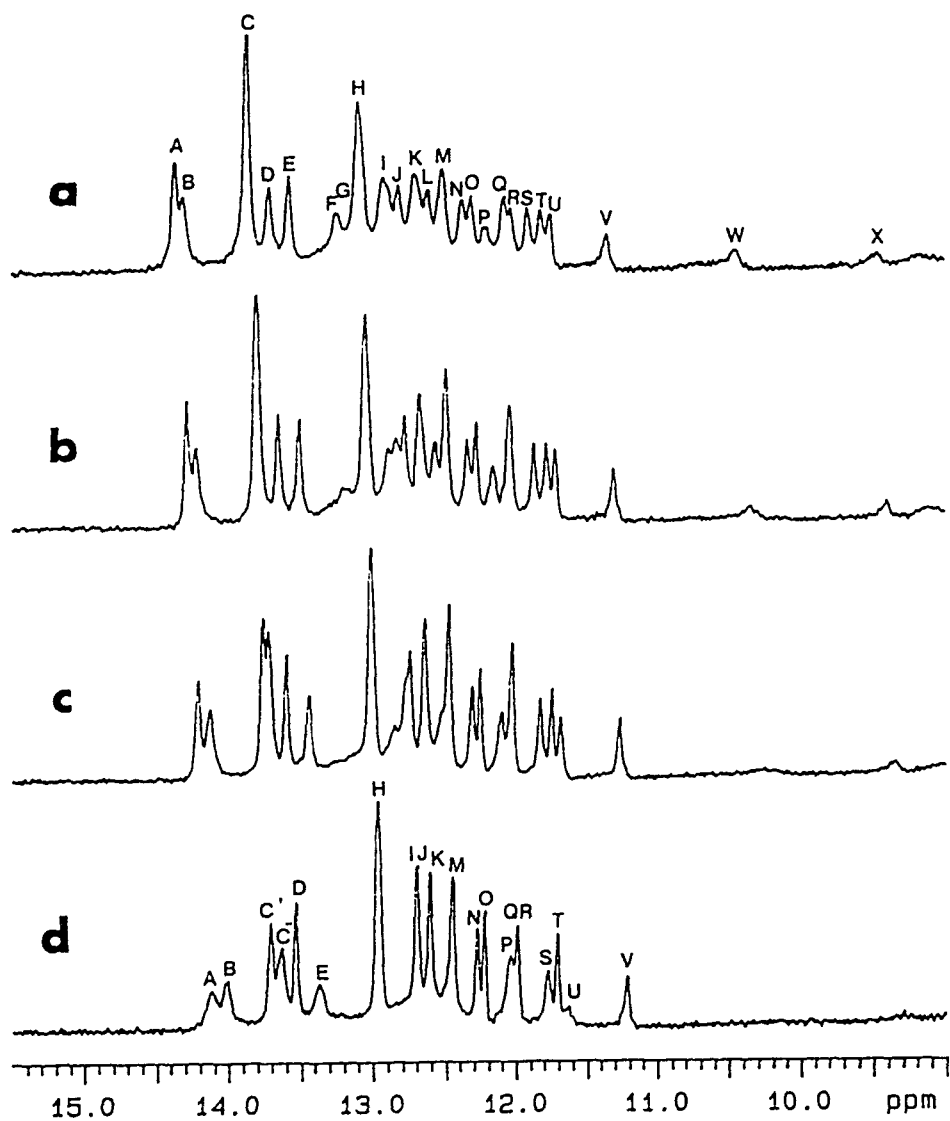


Figure 3.8: ^1H NMR spectra of unmodified *E. coli* tRNA^{Val} obtained at different temperatures. The solution conditions were as in Figure 3.2. (a) 8 °C. (b) 22 °C. (c) 47 °C. (d) 60 °C

most tertiary peaks, except peaks I' (G19) and F (G44) remain present. Other lost peaks are L(U7) and G (G43), which are at the ends of the acceptor and anticodon stems, respectively. Identity of peaks in spectra at higher temperatures were confirmed by one-dimensional NOE experiments. Clearly, base modifications stabilize tRNA tertiary interactions.

Structure of unmodified tRNA^{Val} at low Mg²⁺ concentration

Mg²⁺ is an essential element for tRNA function. Although unmodified tRNA^{Val} has a very similar structure to the modified tRNA in excess Mg²⁺, when Mg²⁺ is removed, the imino proton spectrum of unmodified tRNA is very different from that of modified tRNA (Figure 3.2). This and a previous ¹⁹F NMR study of *in vitro* transcribed 5-fluorouracil substituted *E. coli* tRNA^{Val} show the structure of unmodified tRNA^{Val} is disrupted at low Mg²⁺.

Imino proton NMR studies (Hall *et al.*, 1989) on the structure of *in vitro* transcribed yeast tRNA^{Phe} showed substantial conformational change as a function of Mg²⁺ concentration. They presented data for the formation of an extra GU base pair at low Mg²⁺, but further details of the conformational changes are unknown. Now with the complete assignment of the imino ¹H NMR spectrum of *E. coli* tRNA^{Val}, the conformational changes as a function of Mg²⁺ concentration can be described better.

Unmodified tRNA^{Val} exists in two conformations at low Mg²⁺ The imino ¹H NMR spectra of native and *in vitro* transcribed *E. coli* tRNA^{Val} in the absence of added Mg²⁺ are shown in Figure 3.9. The spectrum of the *in vitro*

transcript has fewer peaks than that observed in excess Mg^{2+} (Figure 3.2b). Many of the imino protons have become solvent exchangeable under these conditions. The remaining peaks were assigned by one-dimensional NOE methods and NMR studies at a variety of Mg^{2+} concentrations.

^1H NMR spectra of *in vitro* transcribed tRNA^{Val} were recorded at 13 Mg^{2+} concentrations in the range 0.5 to 40 mole Mg^{2+} per tRNA. Some of the spectra are shown in Figure 3.10. The Mg^{2+} titration results are summarized in Figure 3.11. When the ratio is 40, the spectrum is almost identical to that observed in excess Mg^{2+} . It is easier to follow the Mg^{2+} titration from high to low Mg^{2+} concentration. As the Mg^{2+} concentration decreases, some peaks lose intensity and disappear. These peaks are B (U8), C (U54), C'' (U12), D (G24), F (G44), G (G43), I (G22), I' (G19), K' (G46), L (U7), M' (G10), P (G15), U (U55), and X (G18 amino). Several peaks lose intensity and are replaced by peaks that grow in intensity with decreasing Mg^{2+} concentration. These are: C' (U29), E (U4), H' (G53), H'' (G42), J (G63), M (G39), O (G40), Q (G49), T (G5), and V (G50). The new peaks are designated by lower case letters matching the corresponding peaks at higher Mg^{2+} concentrations. Peaks that show little change are A (U67), H (G3), K (G2), N (G52), O (G40), R (G1), and S (U64).

At many intermediate Mg^{2+} concentrations, there are two peaks corresponding to one proton resonance. This indicates that *in vitro* transcribed tRNA exists in two conformational states corresponding to tRNA with and without bound Mg^{2+} . Peaks e and E, t and T, v and V etc. are examples of these different structures. Based on the chemical shift difference of a pair of peaks and their linewidths, the conformational exchange rate is estimated to be less than 4 s^{-1} .

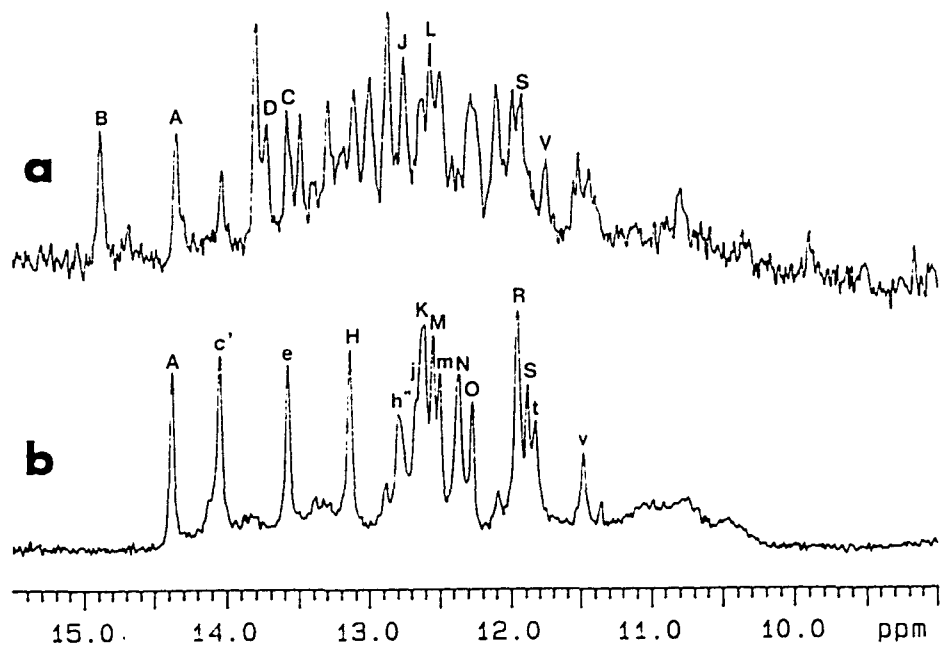


Figure 3.9: Expanded region of the ^1H NMR spectra of tRNA in H_2O (10% D_2O) with 10 mM sodium phosphate in the absence of added Mg^{2+} at 22 $^\circ\text{C}$. (a) Native *E. coli* tRNA^{Val}. (b) *E. coli* tRNA^{Val} transcribed *in vitro*

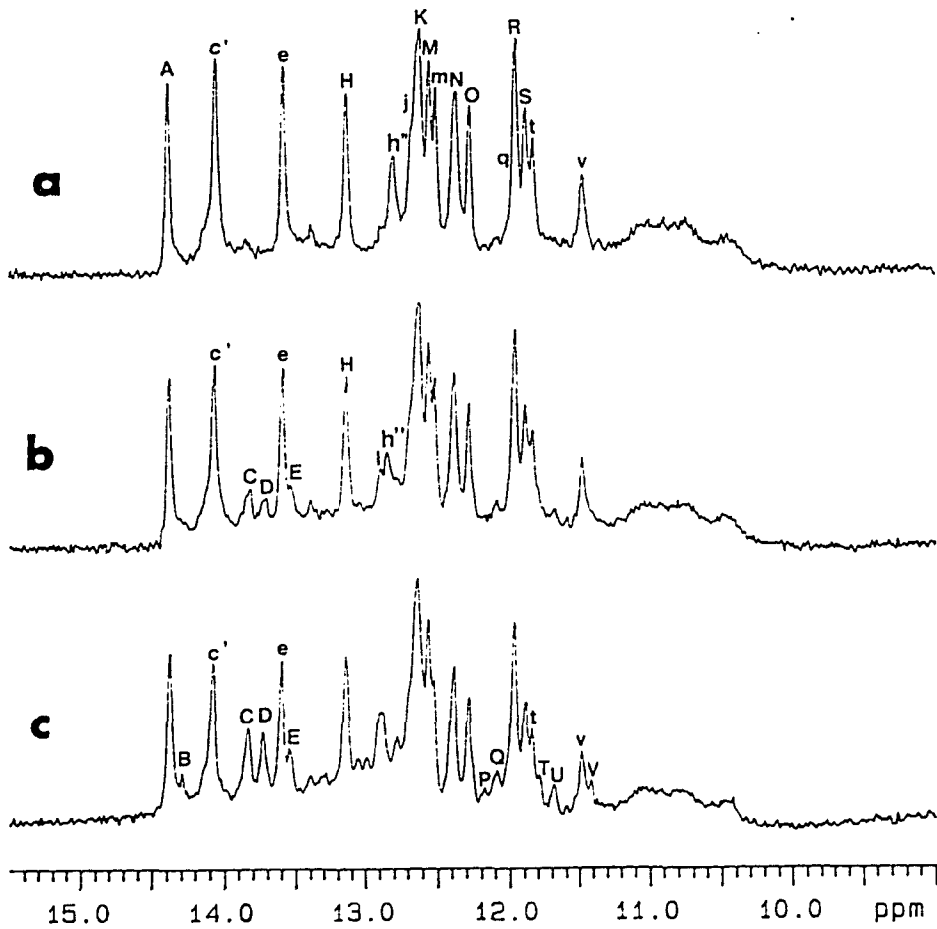


Figure 3.10: Mg^{2+} titration of unmodified *E. coli* tRNA^{Val}. Downfield region of the ^1H NMR spectra of the *in vitro* transcript at 22 °C. The solution conditions were as in Figure 3.2 except Mg^{2+} was added to attain the indicated $\text{Mg}^{2+}/\text{tRNA}$ ratio, γ . (a) $\gamma = 1$. (b) $\gamma = 4$. (c) $\gamma = 6$. (d) $\gamma = 10$. (e) $\gamma = 18$. (f) $\gamma = 40$

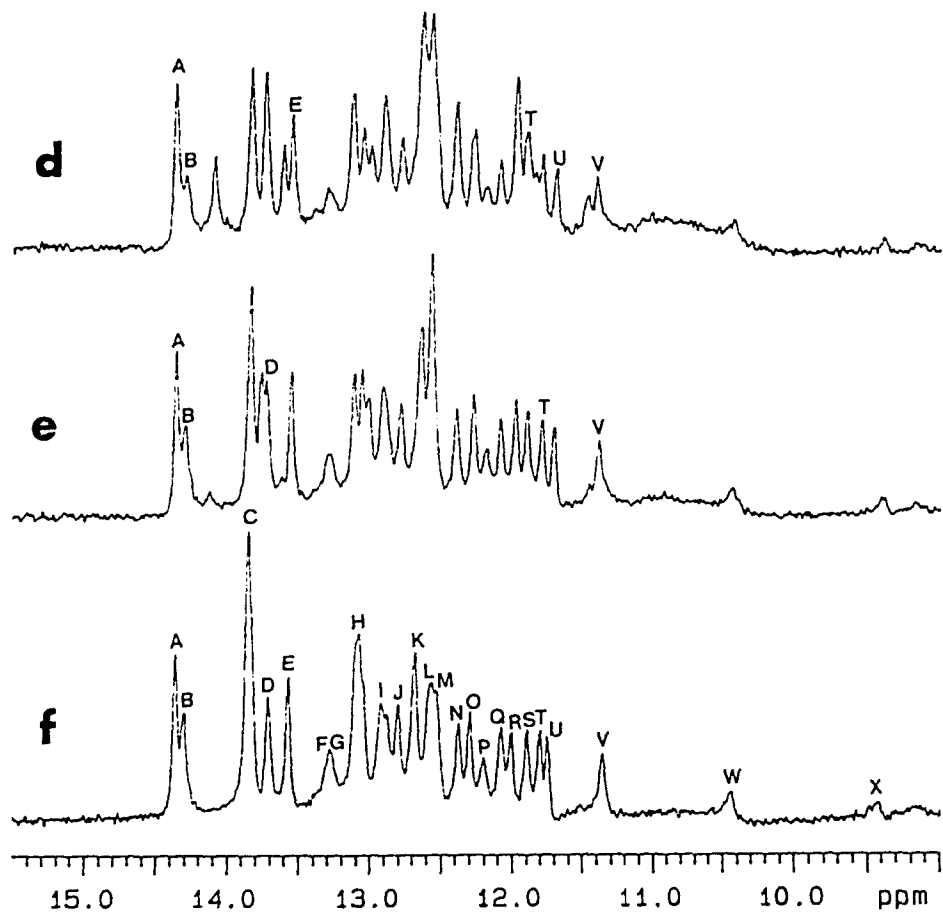


Figure 3.10 (Continued)

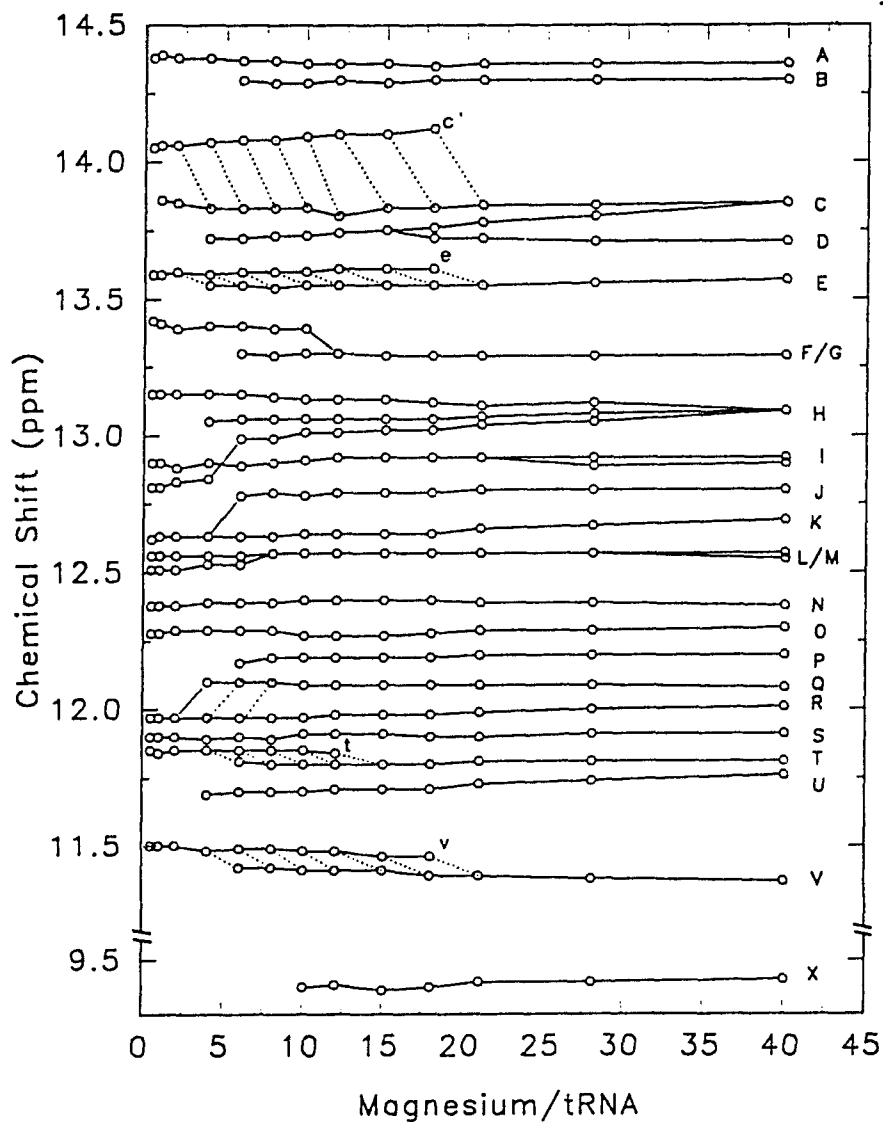


Figure 3.11: Plot of the chemical shift of the downfield ^1H NMR peaks as a function of the $\text{Mg}^{2+}/\text{tRNA}$ ratio. A dotted line joining two points indicates that there two resonances attributable to a particular proton, corresponding to two conformations (with and without bound Mg^{2+}) of tRNA. The disappearance of a solid line at a particular $\text{Mg}^{2+}/\text{tRNA}$ ratio indicates the disappearance of a peak

One-dimensional NOE experiments at low Mg^{2+} Since the 1H NMR spectrum at low Mg^{2+} is so different from that at excess Mg^{2+} , the assignments were confirmed by 1D NOE experiments. Some spectra are shown in Figure 3.12. When peak A is irradiated, a strong NOE to a sharp peak at 7.84 ppm can be seen. This confirms that peak A corresponds to an imino proton in an AU Watson-Crick base pair as expected from the previous assignment of peak A at high Mg^{2+} concentrations to U67. In addition, peak A has NOEs to peak S (U64), peak v (G50) and a weak NOE to peak q (G49). The NOEs from peak A (U67) to peak L (U7) and peak T (G5) at excess Mg^{2+} are lost. When peak v is irradiated, strong NOEs to peak A and peak S are seen. Peak v also has NOEs to peak j (G63) and possibly to peak q (G49). The aromatic peaks at 7.84 and 7.78 ppm are due to power spillover. Upon irradiation of peak c' (U29), there are NOEs to peak h'', peak o and two aromatic peaks at 7.78 ppm and 7.51 ppm. This confirms peak c' is U29 and h'' is G42 and peak o is G40. The peak at 7.51 ppm is from the C2 proton of A41. Peak c' has a shoulder at 22 °C, this shoulder becomes a peak at 10 °C (Figure 3.10a). When this peak is irradiated at 10 °C, intensity of the aromatic peak at 7.78 ppm increases, while intensity of the peak at 7.51 ppm decreases. Therefore, the unknown peak corresponds to a Watson-Crick AU base pair, possibly U12 (peak c'') or U7 (peak l). But at low Mg^{2+} no resonances or NOEs attributable to D-stem imino protons are observed, making assignment of this peak to c'' (U12) unlikely. The NOEs from peak A (U67) to peak v (G50) and peak S (U64) indicate that the base pair A6U67 is stacked on base pair G50U64. This structural change explains the aromatic NOEs observed in Figure 3.12b. G50 is so close to U67 and U7 that spillover from U67 and U7 results in the appearance of aromatic peaks at 7.84 and

7.78 ppm.

Assignments of other peaks at low Mg^{2+} have been confirmed by one-dimensional experiments. These are shown in Figure 3.10a. Upper case letters represent the peaks observed at high Mg^{2+} concentrations; lower case letters represent the corresponding peaks observed at low Mg^{2+} concentrations. Assignment of the spectrum at low Mg^{2+} revealed that the D stem is disrupted and the tertiary interactions have disappeared. Disruption of T and D loop interactions allows the strong interaction between base pairs G50U64 in the T stem and U6A67 in the acceptor stem to occur.

Thermal stability of unmodified tRNA at low Mg^{2+} Figure 3.13 shows the spectra of unmodified tRNA^{Val} obtained at 4 different temperatures. As the temperature rises, the acceptor stem is disrupted except for the A6U67 base pair (peak A). At 60 °C (Figure 3.13d) the A6U67 Base pair and T stem are still largely intact. The A6U67 base pair interacts strongly with the G50U64 wobble base pair at low Mg^{2+} and this interaction forms a thermally stable structural core. Other resonances remaining at 60 °C are from the anticodon stem. The unusually stable peak A was confirmed as a Watson-Crick AU base pair by 1D NOE methods. When peak A is irradiated at 53 °C, a NOE to a sharp peak at 8.16 ppm corresponding to the C2 proton of A6 is observed (data not shown).

At 8 °C (Figure 3.13a), a new peak, l, appears. This peak has been assigned to the U7 imino proton as described earlier.

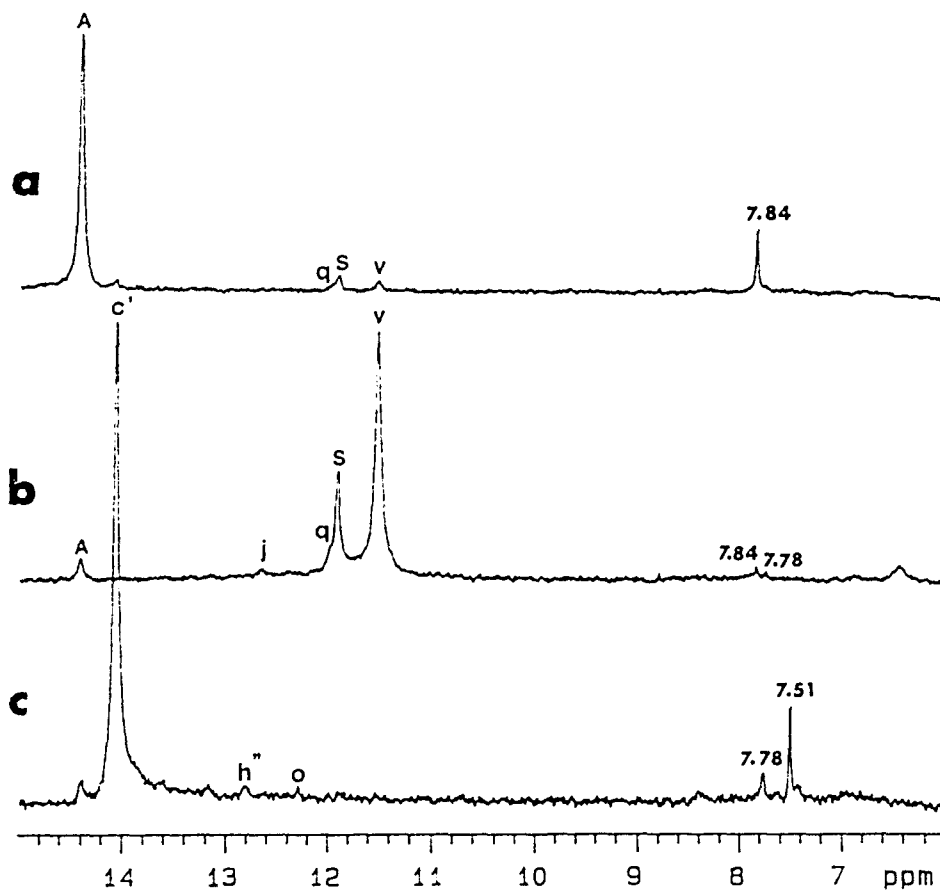


Figure 3.12: Downfield region of ^1H NMR one-dimensional difference NOE spectra of the unmodified tRNA at the same solution conditions and temperature as in Figure 3.9. The NOE partners of each saturated peak are indicated. Other apparent NOEs that have not been labeled are believed to be artifacts of power spillover or incomplete cancellation, or else could not be unequivocally assigned. (a) Peak A has been saturated. (b) Peak v has been saturated. (c) Peak c' has been saturated

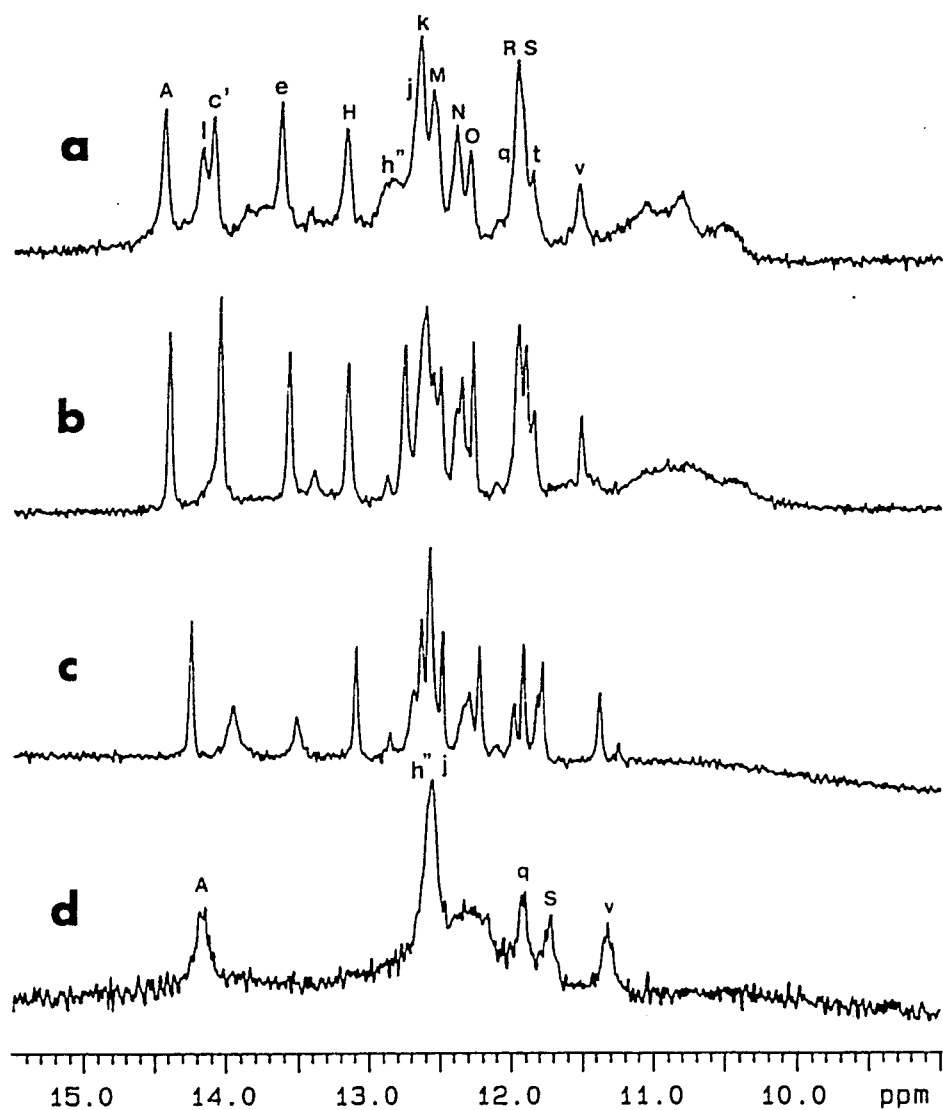


Figure 3.13: Expanded region of ^1H NMR spectra of unmodified *E. coli* tRNA^{Val} obtained at different temperatures. The solution conditions were as in Figure 3.9. (a) 8 °C. (b) 22 °C. (c) 47 °C. (d) 60 °C. The labeled peaks are assigned as follows: A (U67), h'' (G42), j (G63), Q (G49), S (U64), v (G50)

pH effect on native and *in vitro* transcribed tRNA^{Val}

The comparison of modified and unmodified tRNA^{Val} clearly shows the role of nucleoside modifications in stabilizing tRNA structure. But all these experiments were carried out at neutral pH. Control of pH, like Mg²⁺ and temperature and many other environmental factors, is essential for viability. To stay alive, the cell must have some mechanism to protect itself from damage at low pH. Do nucleoside modifications play any role in this? In this section pH effects on the structure of modified and unmodified *E. coli* tRNA^{Val} were probed by ¹H NMR. With assignments of spectra of modified and unmodified *E. coli* tRNA^{Val} completed, the tRNA conformation can be readily probed by looking at spectral changes as a function of pH.

pH effect on unmodified tRNA^{Val} Figure 3.14 shows the spectra of unmodified tRNA^{Val} recorded at different pHs in the absence of Mg²⁺. The spectrum obtained at pH 7.0 (Figure 3.14E), is very similar to previous spectra taken at the same condition (Figure 3.9). Some peaks start to shift or broaden at pH 5.1 (Figure 3.14D). Peak A decreases in intensity, while extra intensity shows up at 14.8 ppm and 13.8 ppm. Resonance intensity also increases at 11.1 ppm, which is where resonances of nonbase-paired amino protons are expected. At pH 4.7 (Figure 3.14C), peak A (U67) has almost completely disappeared, whereas intensity at 14.8 ppm increases further. Large changes in the spectrum occur at pH 4.5 (Figure 3.14B). Four peaks appear in the extremely low field region, from 15–18 ppm, which are labeled as 1, 2, 3 and 4. Such peaks are never observed in the imino ¹H NMR spectra of unmodified tRNA^{Val} at pH 7.0. Following the pH titration series, peak v (G50), peak c' (U29) and peak e (U4) can still be seen. The existence of these resonances

indicates that the T stem, the anticodon stem and the acceptor stem are at least partly intact at low pH. Other resonances cannot be assigned unequivocally.

The appearance of peaks at 15–18 ppm is unusual. These peaks were characterized further (see below). It is of interest to know if these peaks also appear at low pH in excess Mg^{2+} . The spectrum of unmodified tRNA^{Val} was obtained at pH 4.2 in the presence of 15 mM Mg^{2+} (data not shown). The spectrum at pH 4.2 is similar to that at pH 7.0 except for the shift of a few resonances; no peaks appear below 15 ppm in spectra recorded in 15 mM Mg^{2+} .

pH effect on native tRNA^{Val} Native tRNA^{Val} contains modified bases. The pH dependence of the ^1H NMR spectrum of native tRNA^{Val} was examined in the presence and absence of Mg^{2+} . In the presence of 15 mM Mg^{2+} , the spectrum at pH 4.2 is almost identical to that at pH 7.0 (data not shown), indicating that the native tRNA^{Val} is very stable at this condition. Figure 3.15 shows the spectra of native tRNA^{Val} recorded at different pHs in the absence of Mg^{2+} . The spectrum obtained at pH 4.6 (Figure 3.15b) is quite similar to that at pH 7.0 (Figure 3.15c). When the pH is lowered to 4.2, all peaks are broadened, but no sharp resonances are seen in the 15 ppm to 18 ppm region. The appearance of broad peaks at low pH is probably due to aggregation of the sample or to the occurrence of many conformations in slow exchange.

Analysis of the extremely low field peaks in the spectrum of unmodified tRNA^{Val} at low pH The ^1H NMR spectra of unmodified tRNA^{Val} at low Mg^{2+} and low pH show several peaks in the 15–18 ppm region. The appearance

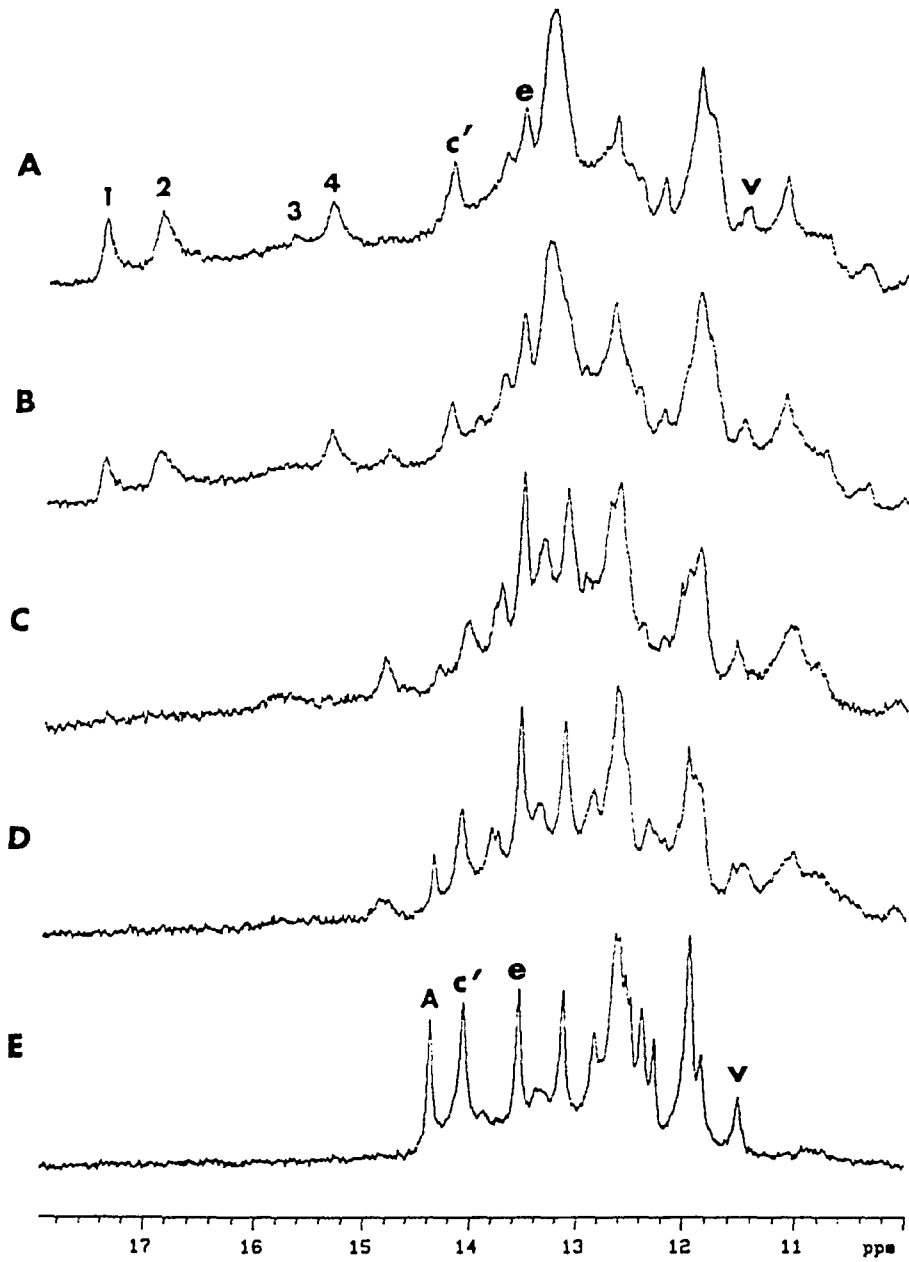


Figure 3.14: pH titration of unmodified tRNA^{Val} in the absence of Mg²⁺. (A) pH 4.2. (B) pH 4.5. (C) pH 4.7. (D) pH 5.1. (E) pH 7.0

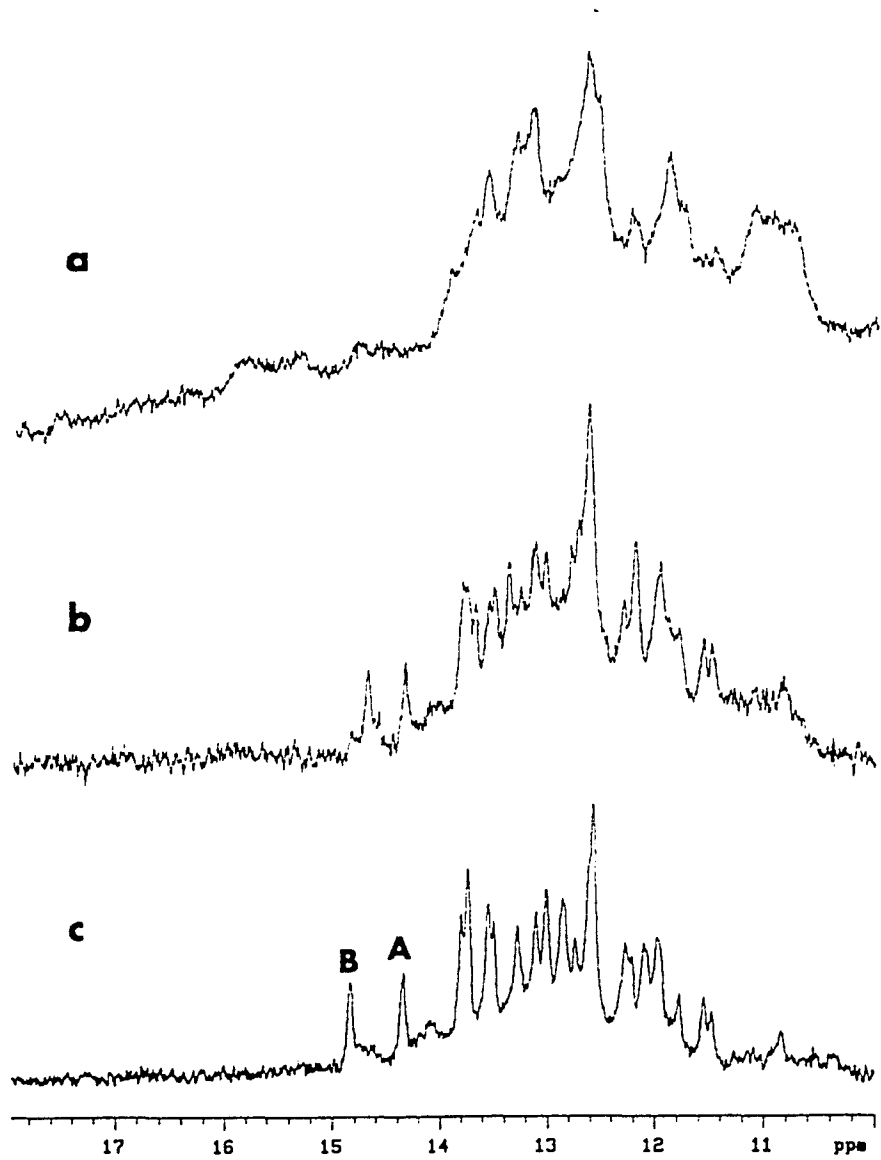


Figure 3.15: pH titration of native tRNA^{Val} shown by the downfield region of the ^1H NMR spectra in the absence of Mg^{2+} at 22 °C. (a) pH 4.2. (b) pH 4.6. (c) pH 7.0

of these peaks is accompanied by large changes in the imino proton region of the spectra. NMR studies of DNA showed that peaks in the extreme lowfield region are due to base-paired protonated A or C residues (Gehring *et al.*, 1993; Ahmed *et al.*, 1994). Considering that the pK_a of adenosine is 3.52 and the pK_a of cytidine is 4.17 (Saenger, 1984), the appearance of protonated bases at pH 4.7 indicates that A or C is in a special local environment in tRNA, which changes the pK_a value of A and C.

There are four peaks below 15 ppm in the spectrum of unmodified tRNA^{Val} at 22 °C at pH 4.2 (Figure 3.14A). When the temperature is dropped to 10 °C, the intensity of peak 3 increases (Figure 3.16B). To assign these resonances, 1D NOE experiments were performed at 10 °C.

Peaks 2, 3 and 4 show some very weak NOEs to unassigned peaks around 8–12 ppm but no sharp NOEs to the region around 7–8 ppm (data not shown). Thus none of these peaks correspond to the imino protons of U in AU Watson-Crick base pairs or from protonated A residues. When peak 1 is irradiated, two sharp NOEs of equal intensity are observed at 7.63 ppm and at 7.45 ppm (Figure 3.16A). Sharp peaks at 7–8 ppm are usually from the C2 proton of A. Of possible base pairs formed by A+ (AA+, GA+, CA+, UA+) only AA+ fits the requirement that the protonated N1H of A is equidistant from two C2 protons of A. The proposed structure of the base pair AA+ is shown in Figure 3.17. The geometry is such that the proton on N1 of A+ is equidistant from its own C2H and that of its base pair partner. Which two As in tRNA^{Val} are involved in this AA+ base pair is not known at this point.

From the pH titration series, peak 4 increases in intensity while the intensity of peak A (A6U67) decreases as the pH is lowered (Figure 3.14). Thus the appearance of peak 4 is probably related to the structural change in the A6U67 base pair. This

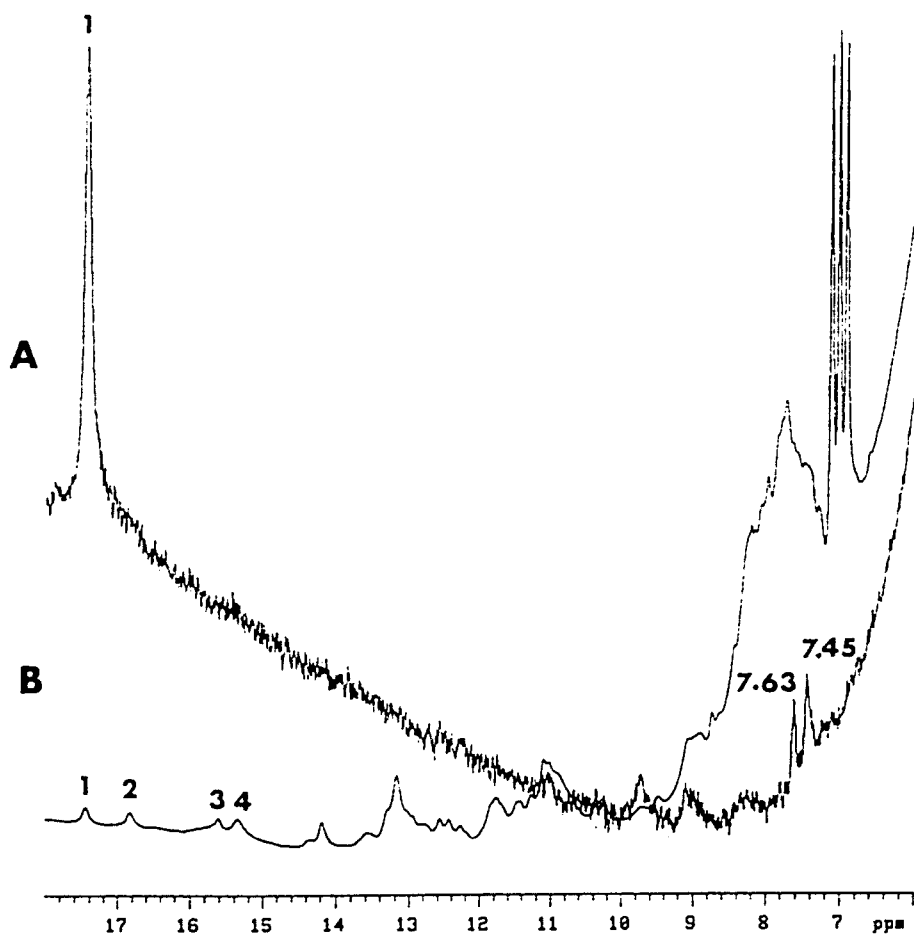


Figure 3.16: Analysis of the extremely low field peaks in the ^1H NMR spectrum of unmodified tRNA^{Val} at 10°C . (A) One-dimensional difference spectrum when peak 1 has been saturated. (B) The control spectrum of unmodified tRNA^{Val} obtained at low Mg^{2+} , pH 4.2 and at 10°C

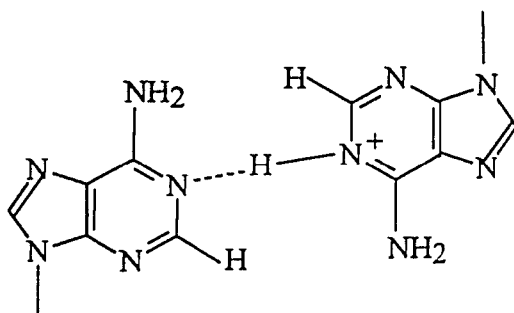


Figure 3.17: Proposed structure of AA⁺ base pair

conclusion is supported by evidence from the ^1H NMR spectrum of the tRNA^{Val} mutant G6C67, in which the A6U67 base pair is replaced by G6C67. Peak 4 has disappeared from the low pH spectrum of the G6C67 mutant tRNA^{Val} (data not shown). In addition peak 3 has also disappeared. Thus the environment of the imino proton corresponding to peak 3 is disturbed by the substitution of G6C67 for A6U67 and the proton is no longer protected from solvent exchange. But the identity of peaks 3 and 4 could not be assigned. Peaks 1 and 2 were unchanged in the spectrum of mutant G6C67, indicating that the environment of protons corresponding to peaks 1 and 2 are not disturbed by this base pair replacement.

It is known that the D stem and tertiary interactions of tRNA^{Val} disappear in the absence of Mg^{2+} (Figure 3.9). A triple mutant of tRNA^{Val} with mutations in the D stem, C9C12G23, was tested for the effects of low pH on the ^1H NMR spectrum. Surprisingly, the downfield peaks appear in the spectrum of this tRNA^{Val} variant. The intensity of peak 4 increases at 10 °C but the intensity of peaks 2 and 3 increase at 22 °C (data not shown). This result indicates the low field peaks are not related to the C9C12G23 tertiary interaction in tRNA^{Val}.

Since the spectrum of unmodified tRNA^{Val} is not well resolved at low pH and low Mg²⁺ concentration, it is difficult to assign resonances. However, by following the titration series and by 1D NOE experiments, base pairs could be observed in the anticodon stem (peak c' (U29)), T stem (peak v (G50)) and the acceptor stem (peak e (U4)).

Recognition of the anticodon loop of *E. coli* tRNA^{Val} by VRS

Anticodon variants

The anticodon bases, U34, A35 and C36 were independently replaced by other nucleotides. Aminoacylation kinetics of each mutant were measured at 37 °C and the kinetic parameters for aminoacylation of these mutant tRNAs were listed in Table 3.2. Mutants of A35 are inactive and those of C36 are about 1000-fold less active than wild type tRNA^{Val}, confirming the results of others (Pallanck and Schulman, 1991). Mutants at position 34 remain good substrates for VRS. These data confirm that the anticodon is an important site of VRS recognition.

Anticodon loop deletion and position-shift mutants

Knowing that A35 and C36 are strong recognition sites of VRS, deletion mutants were prepared having only the three anticodon bases U34A35C36 in the loop; mutants with the anticodon shifted one nucleotide toward the 3' side or 5' side of the anticodon loop were also constructed. Aminoacylation kinetic analysis shows that shifting the anticodon to the 5' side (mutant U33A34C35) or deleting all but the anticodon bases yields tRNA^{Val} mutants that have no detectable activity (data not

Table 3.2: Aminoacylation kinetics of anticodon variants

tRNA ^{Val} Variant	Km μM	Vmax $\mu\text{mole}/\text{min}/\text{mg}$	Vmax/Km	Relative Vmax/Km
Native	1.4 ± 0.2	4.5 ± 0.5	3.2	0.89
Wild Type	1.4 ± 0.2	5.0 ± 0.4	3.6	1.0
U34→G34	1.9 ± 0.3	4.3 ± 0.4	2.2	0.61
U34→C34	1.7 ± 0.2	3.9 ± 0.3	2.3	0.64
A35→G35	nm ^a	nm	2.7×10^{-5}	7.5×10^{-6}
A35→C35	nd ^b	nd		
A35→U35	nd	nd		
C36→A36	9.7 ± 1.5	0.20 ± 0.1	0.021	5.8×10^{-3}
C36→U36	45.9 ± 6.9	0.14 ± 0.1	0.031	8.6×10^{-4}
C36→G36	46.2 ± 9.2	0.22 ± 0.1	0.0048	1.3×10^{-3}

^aNot measurable.

^bNot detectable.

shown). Figure 3.18 shows the time course of aminoacylation of mutant U35A36C37, which has anticodon shifted one position to the 3' side. The results show that this tRNA^{Val} mutant is active, although much less so than wild type tRNA^{Val}. Its charging level almost reaches that of the wild type tRNA^{Val} within one hour. This result is surprising because the original anticodon (U34A35C36) is totally destroyed in this mutant. Thus the new anticodon (U35A36C37) must be recognized by VRS. To confirm that VRS recognizes the new anticodon, C37 in the mutant tRNA^{Val} U35A36C37 was converted to 37A. This mutation destroys the new anticodon and the resulting tRNA (U35A36) has no detectable aminoacylation activity (Figure 3.18).

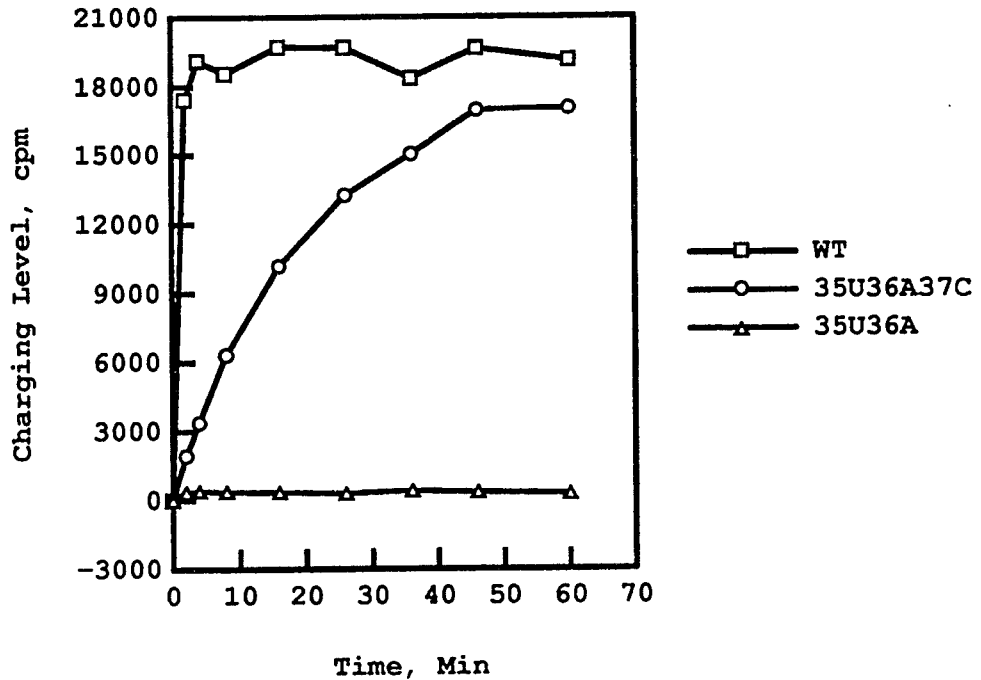


Figure 3.18: Time course of aminoacylation of wild type and mutant tRNA^{Val}. The tRNA concentration is 2 μ M

Anticodon contributes to the binding of tRNA^{Val} to VRS

To see if the inactivation of anticodon mutants is due to loss of the ability to bind to VRS, mutant G35 was tested for its ability to inhibit the aminoacylation of wild type tRNA^{Val} by VRS. The results show that mutant G35 has no detectable effect on VRS activity at concentration up to 6 μ M (Figure 3.19). However, a truncated tRNA^{Val} lacking the 3' ACCA sequence, which is missing the minor recognition base A73 but retains the wild type anticodon loop sequence is an inhibitor of aminoacy-

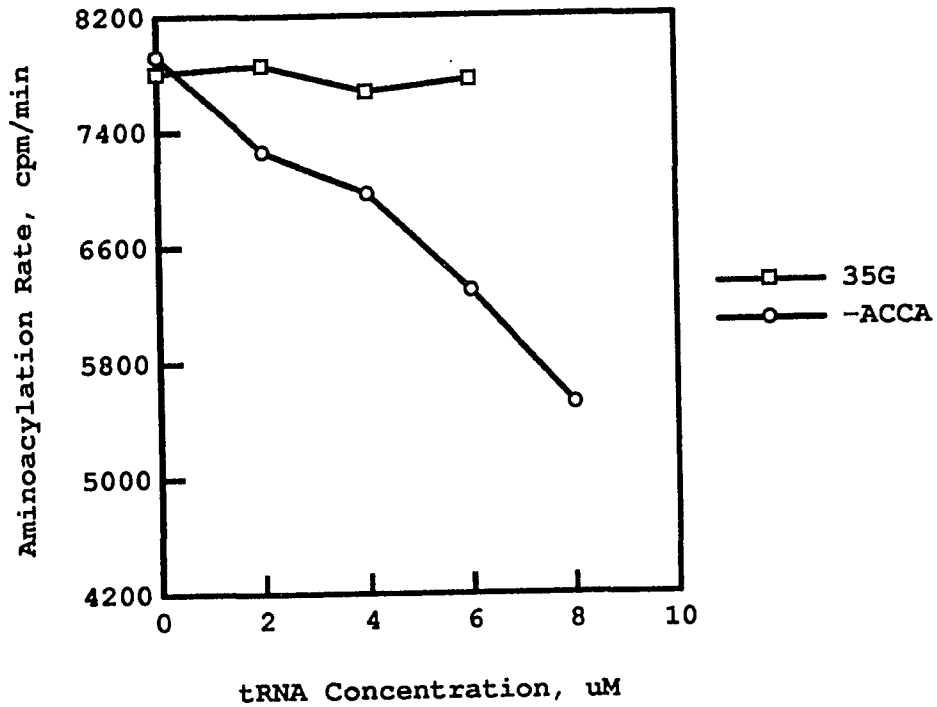


Figure 3.19: Inhibition of aminoacylation of wild type $tRNA^{Val}$ by $tRNA^{Val}$ mutants G35 and -ACCA

lation reaction (Figure 3.19). This suggests that specific aminoacylation of *E. coli* $tRNA^{Val}$ by VRS is achieved by binding of the anticodon loop of $tRNA^{Val}$.

Other mutants in the anticodon loop

The aminoacylation activity of $tRNA^{Val}$ variants with base changes for C32, U33, A37, A38 were also examined. The kinetic parameters for aminoacylation of these mutants are summarized in Table 3.3. Substitution of C32, U33 and A37 yields

tRNA variants that remain good substrates for VRS. The effect of replacing of 38A differs. Mutant C38 has slightly reduced activity; Mutant U38 has half of the V_m/K_m (specificity constant) value of wild type tRNA^{Val} due to a 3-fold reduction in K_m and a 5-fold reduction in V_m . Replacement of A38 with G38 lowers the specificity constant (V_m/K_m) 12-fold. This is due to an increase in K_m and decrease in V_m . Considering that position 32 is C, an extra base pair may form between G38 and C32, extending the anticodon stem. If an extra base pair is formed, a large conformational change in the anticodon loop is expected, which in turn may cause the recognition sites A35 and C36 to be improperly positioned for productive interaction with VRS.

Table 3.3: Aminoacylation Kinetics of nonanticodon variants

tRNA ^{Val} Variant	K_m μM	V_{max} $\mu\text{mole}/\text{min}/\text{mg}$	V_{max}/K_m	Relative V_{max}/K_m
Native	1.4 ± 0.2	4.5 ± 0.5	3.2	0.89
Wild Type	1.4 ± 0.2	5.0 ± 0.4	3.6	1.0
C32→U32	1.4 ± 0.2	4.0 ± 0.8	2.9	0.81
C32→G32	0.7 ± 0.0	3.6 ± 0.4	5.2	1.4
C32→A32	0.7 ± 0.2	4.5 ± 0.4	6.5	1.8
U33→C33	1.3 ± 0.2	4.8 ± 0.3	3.7	1.03
U33→G33	1.6 ± 0.1	5.7 ± 0.4	3.6	1.0
A37→U37	1.1 ± 0.1	4.5 ± 0.3	4.1	1.1
A37→G37	1.0 ± 0.2	5.6 ± 0.1	5.7	1.6
A38→G38	4.7 ± 0.2	1.4 ± 0.2	0.3	0.083
A38→U38	0.5 ± 0.1	0.9 ± 0.1	1.8	0.50
A38→C38	1.4 ± 0.2	4.2 ± 0.4	3.0	0.83
A38→G38+C32→G32	0.2 ± 0.0	2.7 ± 0.1	12.3	3.4
A38→G38+C32→A32	0.2 ± 0.0	1.9 ± 0.1	9.5	2.6
A38→G38+C32→U32	0.8 ± 0.1	5.5 ± 0.1	6.7	1.9
A38→C38+C32→G32	2.6 ± 0.4	6.6 ± 1.2	2.5	0.7
A38→C38+C32→A32	0.6 ± 0.0	4.3 ± 0.0	7.4	2.1
A38→U38+C32→G32	0.3 ± 0.1	2.5 ± 0.6	8.6	2.4
A38→U38+C32→A32	1.2 ± 0.1	5.6 ± 0.3	4.7	1.3

Effect of positions 32 and 38 on anticodon loop structure

Aminoacylation activity of tRNA^{Val} variants at positions 32 and 38

The anticodon is the major identity site of *E. coli* tRNA^{Val} (Table 3.2). The observation that mutant tRNA^{Val} G38 has only 8% of the wild type activity suggests that bases outside the anticodon may also play roles in aminoacylation. Additional experiments were carried out to explore the reasons for the lower activity of mutant G38. Changing C32 in mutant G38 to the noncomplementary bases G32, A32, or U32, produces double mutants that are more active than G38 (Table 3.3). Kinetic data for double mutants at positions 32 and 38 show that mutants with purines at position 32 generally have a lower K_m , provided that the base is not complementary to that at position 38. As a result, these mutants have specificity constants (V_m/K_m) greater than 1. These data indicate the interactions between base 32 and base 38 could affect the binding of tRNA^{Val} to VRS. The anticodon loop may have a very different conformation with different bases at positions 32 and 38. In the next sections, the interactions between position 32 and position 38 were studied by ¹H and ¹⁹F NMR.

Evidence for conformational changes in tRNA^{Val} mutant G38

Aminoacylation kinetic analysis showed that the tRNA^{Val} variant G38 is only 8% as active as wild type tRNA^{Val} (Table 3.3). Considering that C is located at position 32, it is possible G38 forms a base pair with C32. Base pair formation will alter the anticodon loop conformation and reduce the activity of the G38 variant. The first indication of a conformational change in mutant G38 was that it migrates more slowly than wild type tRNA^{Val} on 16% denaturing PAGE (Figure 3.20). The



Figure 3.20: Comparison of gel mobility of wild type tRNA^{Val} and mutant G38

difference in migration rate is an indication of a difference in molecular conformation. Of all 16 combinations of mutations at positions 32 and 38, mutant G38 is the only one that migrates slower than the wild type tRNA (data not shown for other mutants). Furthermore, this behavior was not changed with different treatments of the G38 sample. Heating the tRNA at 80 °C for 10 min in the presence or absence of Mg²⁺ before loading on the gel does not change its gel mobility. These results indicate that mutant G38 has a very stable and different conformation from wild type tRNA^{Val}.

¹⁹F NMR study of FU substituted tRNA^{Val} variant G38 also showed conformational changes in this mutant. Figure 3.21 shows the ¹⁹F NMR spectra of the FU-G38 variant and wild type FU-tRNA^{Val} recorded at 22 °C. The peak at 4.65

ppm (containing resonances FU33 and FU47) in the spectrum of wild type tRNA splits into two peaks in the spectrum of the G38 variant. Of these two peaks, one stayed in the original position, the other shifted to the down field in the spectrum. The peak at 4.20 ppm has very similar chemical shift position to that of FU34 in the spectrum of wild type tRNA^{Val}, thus this 4.20 ppm peak is probably FU34. Therefore the shifted resonance at 4.98 ppm is assigned to FU33. However, it is possible that base pair formation (see below) between C32 and G38 distorts the anticodon loop conformation sufficiently that the assignments should be reversed.

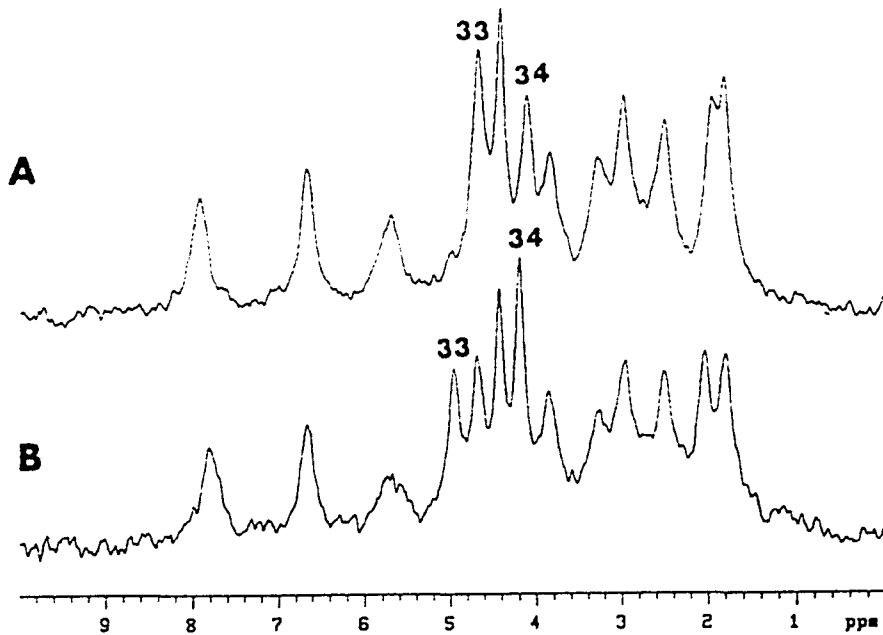


Figure 3.21: ¹⁹F NMR spectra of wild type FU-tRNA^{Val} (A) and FU-G38 variant (B) obtained in standard buffer at 22 °C

Possible formation of an extra base pair between C32 and G38

If C32 and G38 form an extra base pair at the bottom of the anticodon stem in tRNA^{Val} variant G38, the imino proton from G38 should be protected from solvent exchange and should be observed in the imino ¹H NMR spectrum of tRNA^{Val} G38 variant. Figure 3.22 shows the imino ¹H NMR spectra of G38 and wild type tRNA^{Val}. The difference spectrum (Figure 3.22C) clearly shows that there is extra intensity at 12.6 ppm in the spectrum of the mutant tRNA. Resonances in this region of the spectrum are expected from imino protons of a CG base pair. This extra intensity may correspond to the imino proton of G38 possibly base paired to C32. Besides this extra intensity in the spectrum of mutant G38, several other peaks shift. The shifted peaks are labeled in the difference spectrum, they are peak A (U67), C' (U29), E (U4), L (U7), O (G40), V (G50). Position changes of these peaks indicate conformational changes in the anticodon stem, the acceptor stem and the T stem of tRNA^{Val} as a result of the A38→G38 substitution.

tRNA^{Val} mutant C37G38 shows the same gel mobility as mutant G38 (data not shown). The imino proton NMR spectrum of mutant C37G38 shows extra intensity at 12.7 ppm (data not shown). These results suggest that this mutant has a structure similar to that of mutant G38. However, the resolution of the spectrum is not good enough to resolve peaks G38 and G39.

Native tRNA^{Val} mutant G38 overexpressed in and isolated from *E. coli* cells also migrates more slowly than native tRNA^{Val} on denaturing PAGE (data not shown). Figure 3.23 shows the the spectra of native tRNA^{Val} and overexpressed tRNA^{Val} mutant G38 recorded in the presence of 15 mM Mg²⁺ at 22 °C. The spectrum of

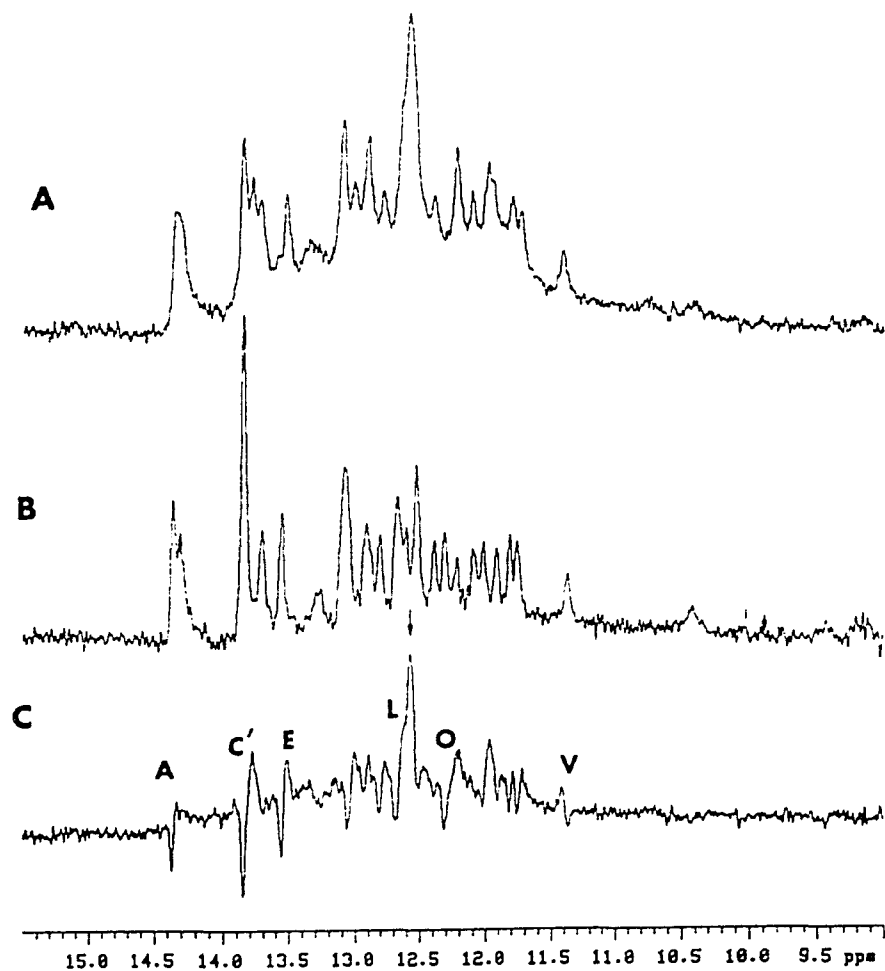


Figure 3.22: Imino ^1H NMR spectra of tRNA^{Val} mutant G38 (A), wild type tRNA^{Val} (B) and the difference spectrum (C) obtained by subtracting B from A. Spectra were recorded in 15 mM Mg^{2+} at 22 °C. The position of extra intensity in the difference spectrum is indicated by an arrow

the mutant shows extra intensity at 12.5 ppm. This is clearly seen in the difference spectrum obtained by subtracting the spectrum of the native tRNA from that of the mutant tRNA. Thus the imino proton of G38 is likely to reside in this peak. But the resolution is not good enough to resolve peaks G38 and G39.

Besides the extra intensity in the spectrum of native overexpressed mutant G38, many other peaks also shift. These shifted peaks, A (U67), B (s⁴US), C' (U29), C (T54), K' (m⁶G46), S (U64), V (G50), are distributed in the anticodon stem, the acceptor stem, and the T stem, indicating conformational changes in these regions of the tRNA. This result is consistent with the result obtained from the spectrum of *in vitro* transcribed mutant G38 (Figure 3.22).

Effects on tRNA^{Val} structure of substitution of A38 with G38

The above analysis of conformational changes in tRNA^{Val} mutant G38 were all from experiments carried out in the presence of 15 mM Mg²⁺. Chemical shift changes were observed not only for imino protons of the anticodon stem but also for imino protons of the acceptor stem and the T stem (Figures 3.22 and 3.23). These long range structural changes were further analyzed in the absence of Mg²⁺. In Figure 3.24, the spectrum of tRNA^{Val} variant G38 recorded in the absence of Mg²⁺ is compared with the already assigned spectrum of wild type tRNA^{Val} obtained in the same conditions (Figure 3.10a).

The two spectra are substantially different. As observed in 15 mM Mg²⁺, there is extra intensity at 12.6 ppm in the spectrum of the mutant tRNA possibly due to formation of an additional base pair between C32 and G38. Other changes were seen in the low field region of the spectrum. The spectrum is difficult to assign by simple

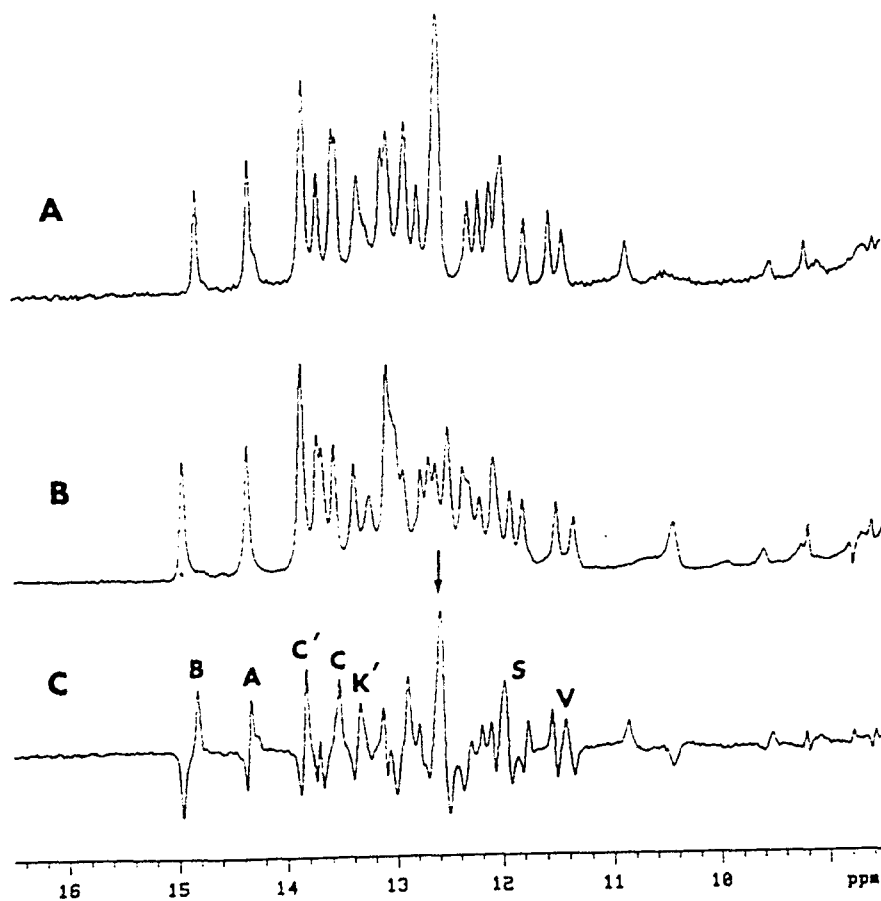


Figure 3.23: Imino ^1H NMR spectra of overexpressed tRNA^{Val} mutant G38 (A) and native tRNA^{Val} (B) and the difference spectrum (C) obtained by subtracting B from A. Spectra were recorded in 15 mM Mg^{2+} at 22 °C. The position of extra intensity in the difference spectrum is indicated by an arrow

comparison with that of wild type tRNA^{Val}, but some assignments were made by 1D NOE experiments (data not shown). The assignments are shown in Figure 3.24A. The peak at 13.6 ppm (*C'*) shows NOEs to peak *h''* (G42) and peak O (G40), and a sharp peak at 7.56 ppm, which is probably the C2 proton of A41, indicating the resonance at 13.6 ppm corresponds to the imino proton of U29. The peak at 14.08 ppm (*c'*) also shows weak NOEs to peak *h''* (G42) and the peak at 7.56 ppm, indicating that both the resonances at 13.6 ppm (*C'*) and 14.08 ppm (*c'*) correspond to the imino proton of U29. Thus the anticodon stem of mutant tRNA^{Val} G38 exists in two conformational states that are in slow exchange at low Mg²⁺ concentration. The peak at 13.6 ppm, has a similar chemical shift position to that of peak *C'* (U29) in the spectrum of tRNA^{Val} mutant G38 in excess Mg²⁺ (Figure 3.22), and presumably corresponds to the conformation of the anticodon stem in the G38 mutant tRNA^{Val} resembling that present in native tRNA^{Val}. The peak at 14.08 ppm then corresponds to a low Mg²⁺-form of the anticodon stem of the G38 mutant of tRNA^{Val}.

It is also noted that peak l (U7) in the spectrum of tRNA^{Val} mutant G38 in the absence of added Mg²⁺, resonates at 13.4 ppm at 22 °C, which is very different from the position of this peak in the spectrum of wild type tRNA^{Val} recorded under the same conditions. In the spectrum of wild type tRNA^{Val}, peak l is a shoulder on peak *c'* at 14.10 ppm (Figure 3.24B). Observation of a resonance corresponding to U7 in the spectrum of mutant G38 suggests that the environment of U7 at the junction of the acceptor and T stems is only partially disturbed at low Mg²⁺ in this mutant tRNA. As in the wild type tRNA^{Val} spectrum, no evidence for the presence of D stem and tertiary interactions is observed in the spectrum of mutant G38 at low Mg²⁺.

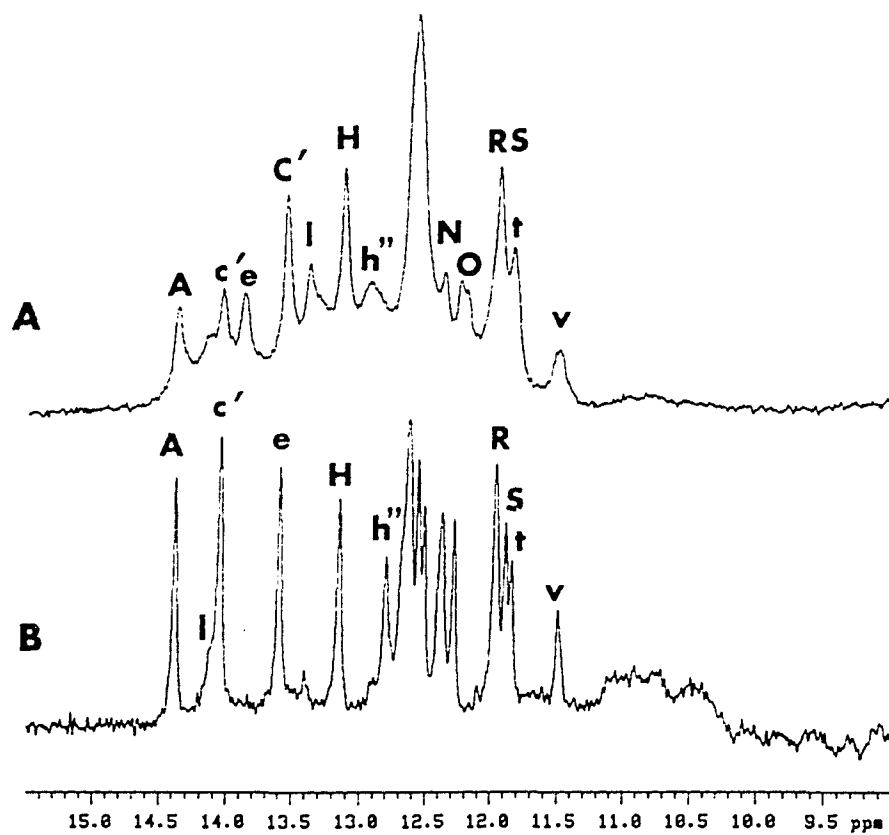


Figure 3.24: Imino ^1H NMR spectra of tRNA^{Val} mutant G38 (A) and wild type tRNA^{Val} (B) obtained in the absence of Mg^{2+} at 22 °C

A stable structural core has been identified in wild type *E. coli* tRNA^{Val} at low Mg²⁺ concentrations which is stable at 60 °C (Figure 3.13d). When the ¹H NMR spectrum of mutant G38 is recorded at 60 °C, this stable structural core is not observed (Figure 3.25). At 60 °C, peak v (G50) and S (U64) have disappeared from the spectrum of the G38 mutant, but both remain visible in the spectrum of the wild type tRNA (compare Figure 3.25A and B); peak A (U67) is also largely gone from the spectrum of the G38 mutant. On the other hand, peak e (U4) remains visible and peak H (G3) retains full intensity in the spectrum of the mutant tRNA but both are absent from the spectrum of wild type tRNA^{Val}. These results indicate that the acceptor stem of the G38 mutant remains intact at 60 °C at low Mg²⁺ concentrations. The most stable base pairs in the tRNA^{Val} variant G38 are in the anticodon stem and the acceptor stem, rather than in the T stem and the associated A6U67 base pair as, in the wild type tRNA^{Val} (Figure 3.12).

¹⁹F NMR studies of dynamics of the anticodon loop

There is a pyrimidine at position 32 in most tRNAs (Figure 1.1), whereas A, U or C are found at position 38; very few tRNAs have G at position 38. The x-ray crystal structure of yeast tRNA^{Phe} shows that C32 is stacked on A31 and U33 on the 5' side of the anticodon loop. Base 38 is stacked on the 3' side of the anticodon loop. Positions 32 and 38 occupy unique positions in the tRNA, at the top of the anticodon loop. It is of interest to know their interaction and the effect of their interaction on anticodon loop conformation. ¹⁹F NMR is a powerful tool to monitor changes in anticodon loop conformation by looking for shifts of peaks FU33, FU34 in the ¹⁹F NMR spectra. Seven mutant tRNAs which contain FU at position 32

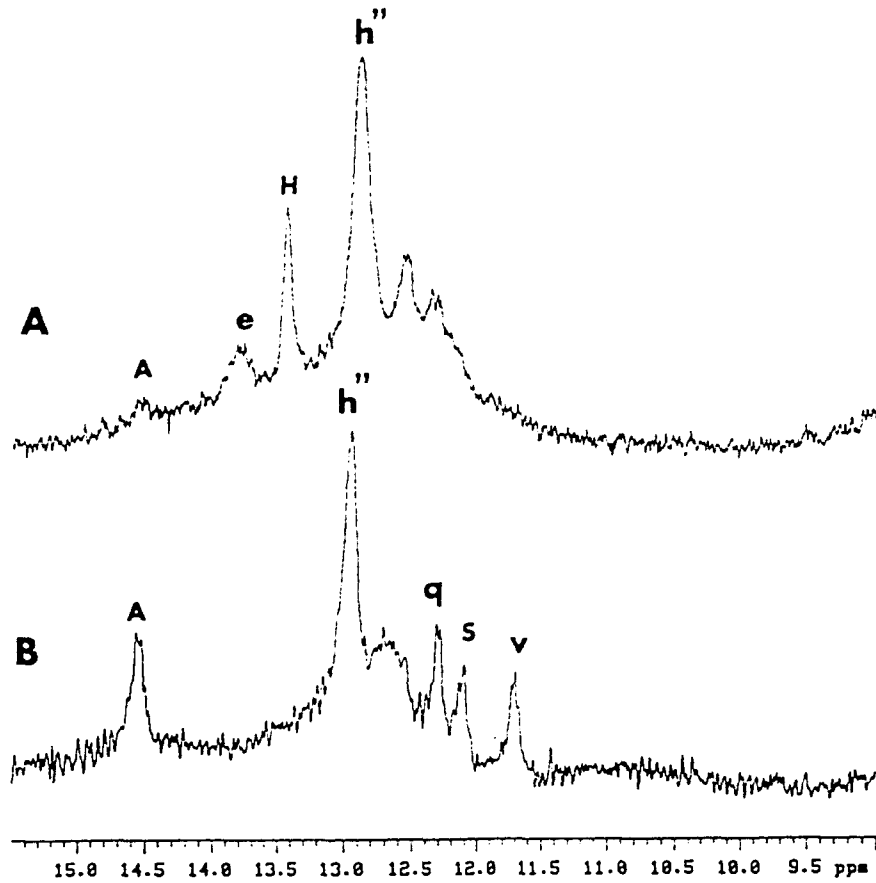


Figure 3.25: Imino ¹H NMR spectra of tRNA^{Val} mutant G38 (A) and wild type (B) obtained in the absence of Mg²⁺ at 60 °C

or 38 or both were prepared. ^{19}F NMR spectra of these mutants were recorded in standard buffer at 22 °C, 35 °C and 47 °C. Chemical shift positions of FU32, FU33, FU34 and FU38 in the spectra of mutant tRNAs were compared with those of FU33 and FU34 in wild type FU-tRNA^{Val}. Figure 3.26 shows the spectrum of wild type FU-tRNA^{Val} obtained at 22 °C, 35 °C and 47 °C. The spectrum has been completely assigned (Chu *et al.*, 1992a; 1992b).

Mutant U32 Figure 3.27 shows the spectra of ^{19}F NMR spectra of FU-tRNA^{Val} mutant U32 obtained at 22 °C, 35 °C and 47 °C. Assignment of the spectrum is straightforward. In the spectrum recorded at 22 °C (Figure 3.27C), a broad peak at 3.58 ppm, indicated by an arrow, is observed. This peak becomes sharper at 35 °C and 47 °C and is assigned to FU32. In addition peak FU33 is shifted upfield to overlap FU34 in the ^{19}F NMR spectrum of the U32 mutant of FU-tRNA^{Val}.

FU32 becomes sharper with rising temperature. This indicates that FU32 is in a thermally dynamic environment. The low intensity of FU32 at 22 °C may be an indication that this ^{19}F nucleus is in a fast exchanging environment. Considering that position 38 is an A in the FU32 mutant, it is possible that FU32 forms a base pair with A38 at 22 °C and the base pair is in fast exchange between the open and closed states. At higher temperatures the base pair may stay open most of the time, thus the peak is sharp and represents FU32 in the unpaired state.

Mutant U32G38 Figure 3.28 shows the ^{19}F NMR spectra of FU-tRNA^{Val} mutant U32G38 at 22 °C, 35 °C and 47 °C. Compared to the spectrum of wild type

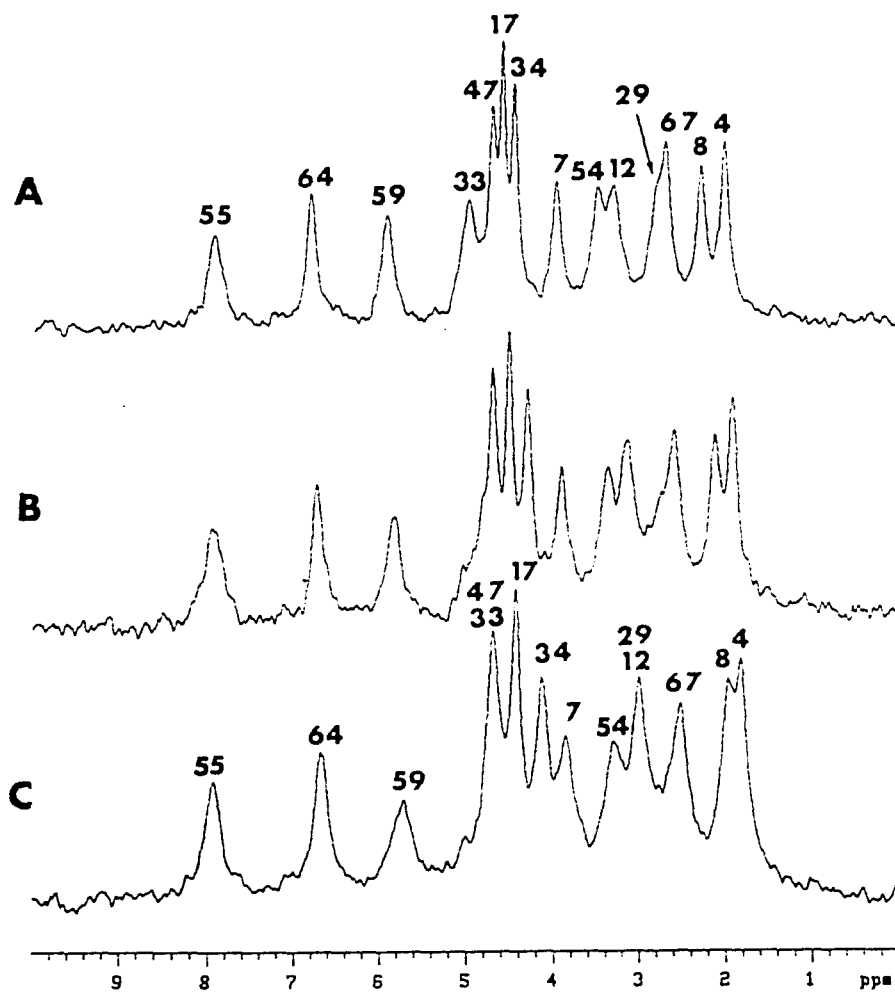


Figure 3.26: ^{19}F NMR spectra of wild type FU-tRNA^{Val} obtained in standard buffer at different temperatures. (A) 47 °C. (B) 35 °C. (C) 22 °C

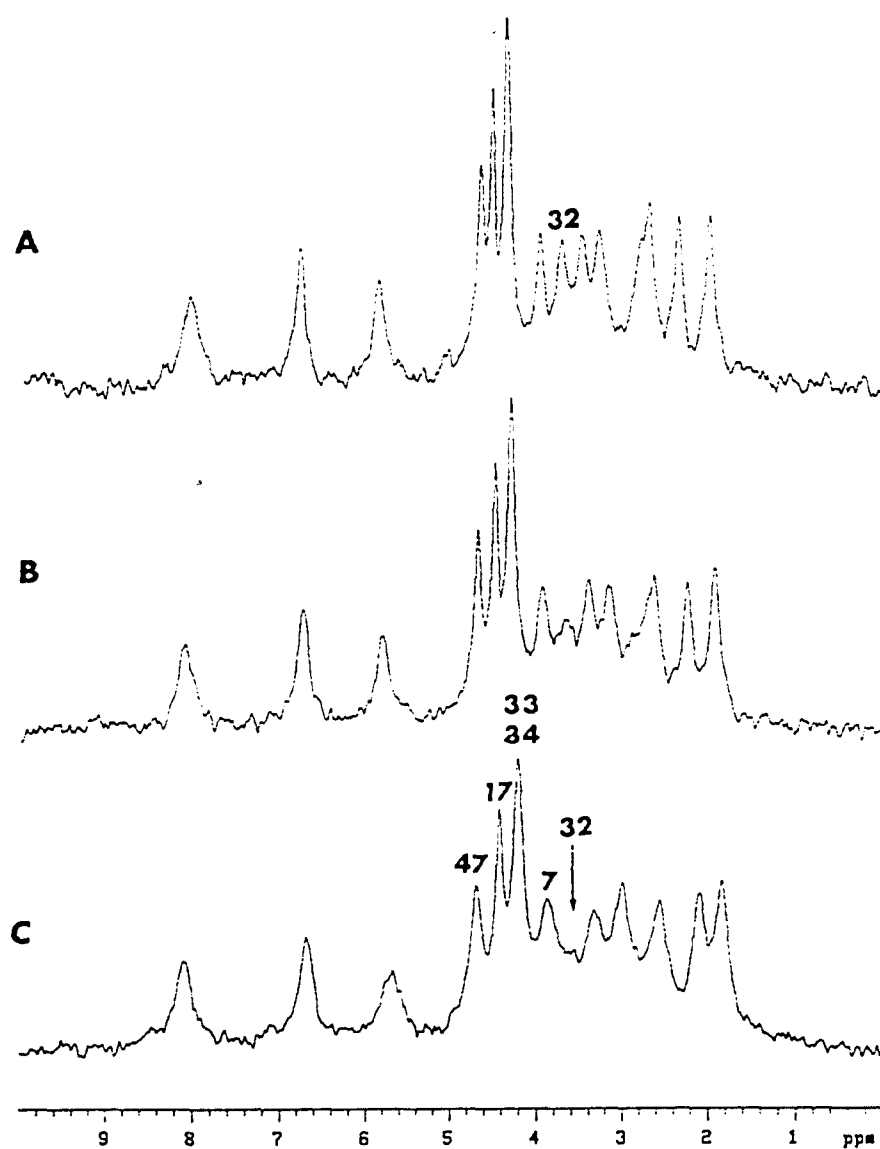


Figure 3.27: ^{19}F NMR spectra of FU-tRNA^{Val} mutant U32 obtained in standard buffer at different temperatures. (A) 47 °C. (B) 35 °C. (C) 22 °C

FU-tRNA^{Val} at 22 °C, there is an extra peak at 7.11 ppm. In the ¹⁹F NMR spectra of FU substituted tRNAs, the FUs of GU wobble base pairs resonate in the lowfield region (Chu and Horowitz, 1989). Since position 38 is a G, it is possible that FU32 will form a base pair with G38. Thus it is reasonable to assign this 7.11 ppm peak to FU32.

The candidates for FU33 and FU34 are the resonances at 4.19 ppm and 3.86 ppm in the spectrum of the mutant tRNA. The peak at 4.19 ppm has the same chemical shift position as FU34 in the spectrum of wild type FU-tRNA^{Val}, and it can be assigned to FU34. Thus the resonance at 3.86 ppm is assigned to FU33. However, the conformational changes caused by mutations at positions 32 and 38 may cause unpredictable environments for FUs in the anticodon loop. Thus the assignments for these FU peaks are tentative. Temperature dependence of the spectra shows large upfield chemical shift changes for FU32 compared to FU33 and FU34.

Mutant U38 Figure 3.29 shows the ¹⁹F NMR spectra of FU-tRNA^{Val} mutant 38U at 22 °C, 35 °C and 47 °C. Comparison with the spectra of wild type FU-tRNA^{Val} recorded at 22 °C shows an extra peak at 5.14 ppm in the spectrum of the mutant tRNA. Furthermore, FU33 has shifted from its position in the spectrum of wild type FU-tRNA^{Val}. The peak at 4.18 ppm has similar chemical shift position to FU34 in the spectrum of wild type FU-tRNA^{Val}, thus this resonance is assigned to FU34. The peak at 5.14 ppm is likely to be FU38 because a similar peak was found in the spectrum of mutant U38U32 in which FU38 is not expected to interact with FU32. This resonance is not sensitive to temperature (Figures 3.29). Therefore, the peak at 4.43 ppm can be assigned to FU33 which overlaps FU17. Again, conformational

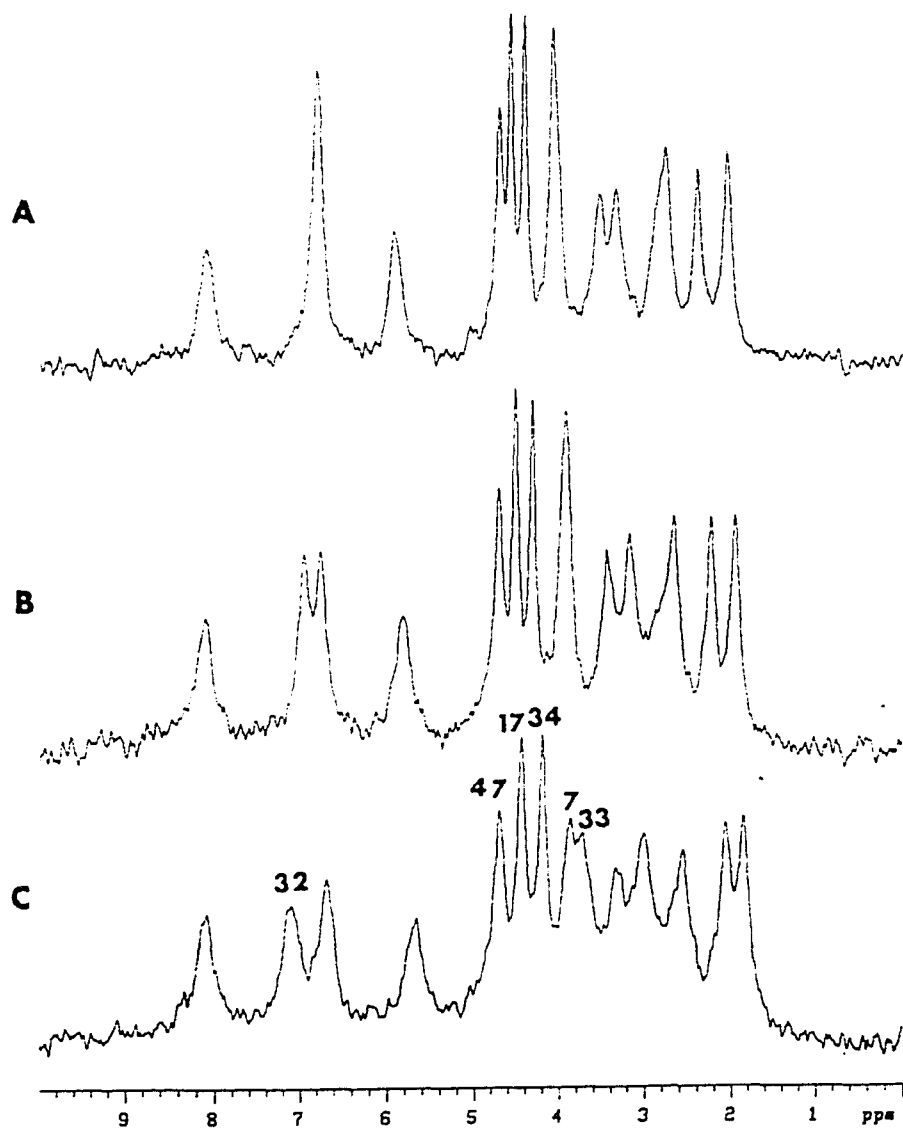


Figure 3.28: ^{19}F NMR spectra of mutant FU-tRNA^{Val} U32G38 obtained in standard buffer at different temperatures. (A) 47 °C. (B) 35 °C. (C) 22 °C

changes in the anticodon loop may cause unusual changes for FU peaks from the loop, thus these assignments are only tentative.

Mutant U38G32 Figure 3.30 shows the ^{19}F NMR spectra of FU-tRNA^{Val} mutant U38G32 at 22 °C, 35 °C and 47 °C. Compared to the spectra of wild type FU-tRNA^{Val}, an extra peak is seen at 5.17 ppm which does not shift with temperature. Similar peak was seen in the spectra of the FU-tRNA^{Val} mutant U38 (Figures 3.29). Although there is a potential for an interaction between FU38 and G32, no low field peak can be seen in the spectrum of this mutant. Therefore, interaction of FU38 and G32 is unlikely and this peak is thus assigned to FU38. The resonance at 4.29 ppm is close to the position for FU34 in the spectra of wild type FU-tRNA^{Val} and other mutants and is assigned to FU34. Compared to the spectrum of wild type FU-tRNA^{Val} (Figure 3.26), intensity is lost from the peak at 4.7 ppm (FU33) and additional intensity is seen at 3.82 ppm. This 3.82 ppm peak is assigned to FU33.

It is interesting to compare this mutant with mutant U32G38. They both have the potential to form a GU base pair between the base at position 32 and that at 38. In the spectrum of the U32G38 mutant, FU32 is observed far downfield, at 7.11 ppm, as expected for a FU in a GU wobble base pair (Chu and Horowitz, 1989) (Figure 3.28). Clearly peak FU38 in the spectrum of the U38G32 mutant is not shifted to downfield, suggesting that FU38 does not form a base pair with G32 in this mutant tRNA.

Mutant U38A32 Figure 3.31 shows the ^{19}F NMR spectra of FU-tRNA^{Val} mutant U38A32 at 22 °C, 35 °C and 47 °C. FU34 is almost unaffected in the spec-

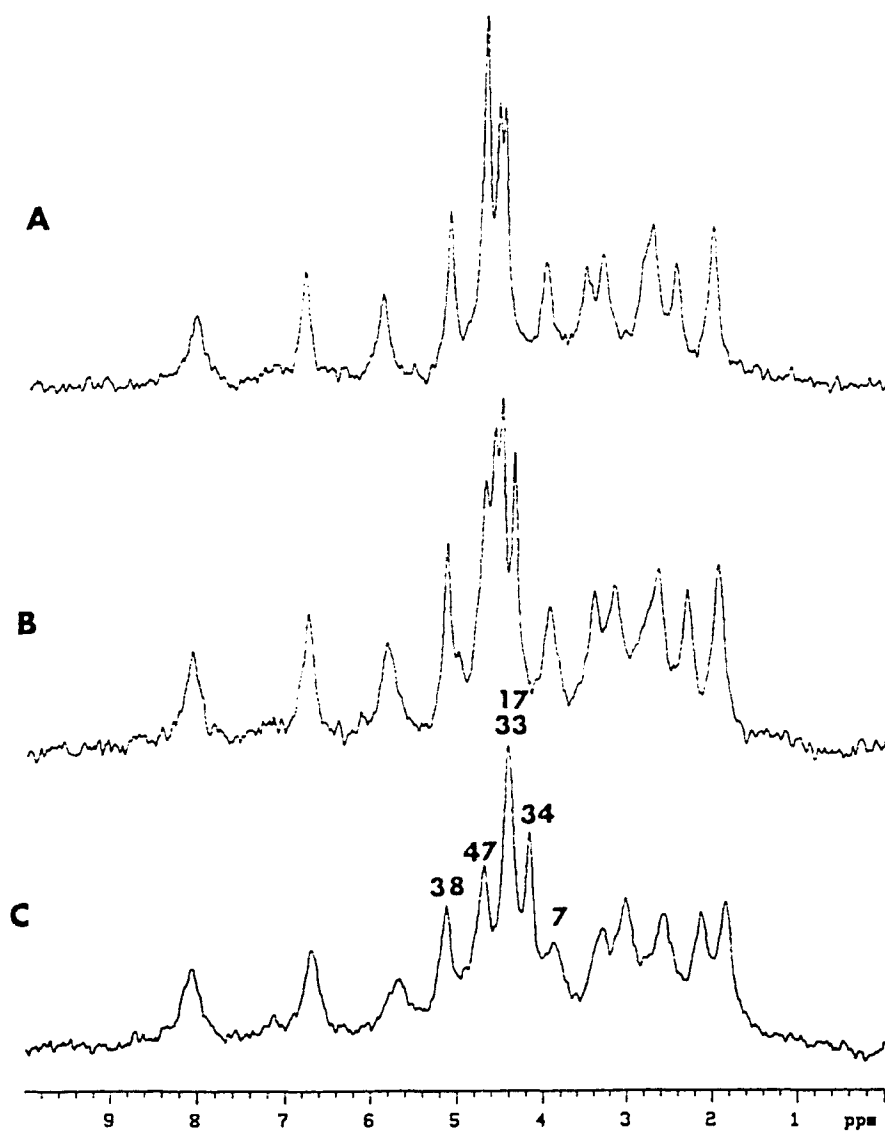


Figure 3.29: ^{19}F NMR spectra of FU-tRNA^{Val} mutant U38 obtained in standard buffer at different temperatures. (A) 47 °C. (B) 35 °C. (C) 22 °C

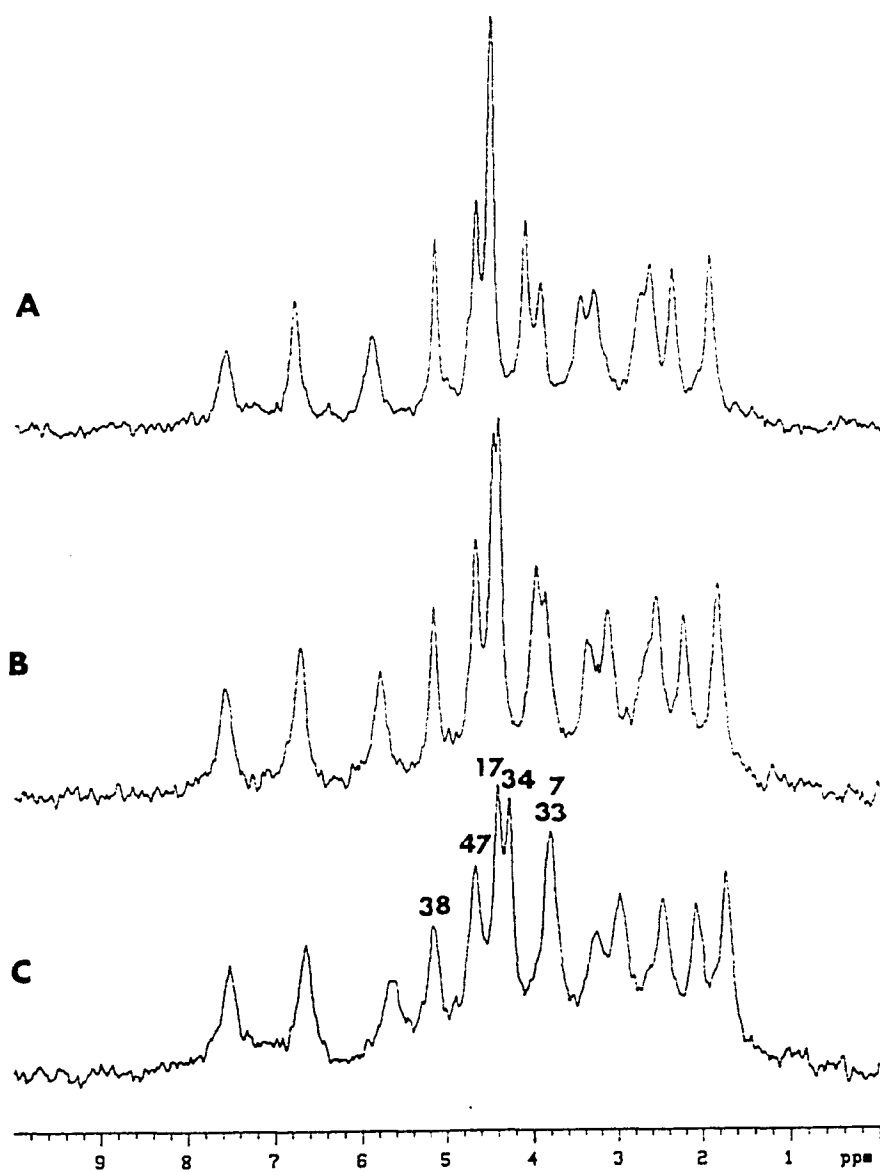


Figure 3.30: ^{19}F NMR spectra of FU-tRNA^{Val} mutant U38G32 obtained in standard buffer at different temperatures. (A) 47 °C. (B) 35 °C. (C) 22 °C

trum of this mutant. Extra intensity is observed at 5.72 ppm and 3.28 ppm at 22 °C, and intensity is lost at 4.7 ppm (FU33). There is a potential for a base pair formation between U38 and A32. In fact, imino ^1H NMR study (data not shown) of this mutant showed extra intensity in the AU base pair region and there is slightly shift of peak C' (U29) from the anticodon stem. Thus assign the peak at 3.28 ppm to FU38 is consistent with an AU base pair formation. Also this resonance shifts to upfield with increasing temperature, possibly because of disruption of base pairing at higher temperature. The peak at 5.72 ppm can therefore be assigned to FU33.

Mutant U32U38 Figure 3.32 shows the ^{19}F NMR spectra of FU-tRNA^{Val} mutant U32U38 at 22 °C, 35 °C and 47 °C. There are two extra FUs in this mutant tRNA; four of the seven bases in the anticodon loop are FUs. Careful comparison of the spectra of the mutant tRNA with that of wild type FU-tRNA^{Val} reveals four resonances (22 °C) at 5.57 ppm, 4.89 ppm, 4.33 ppm and 3.81 ppm (Figure 3.32), that can be assigned to these four FUs. The signal at 3.57 ppm can be assigned to FU38 because it is found in the chemical shift region of FU38 in other mutants of FU-tRNA^{Val} with FU at position 38. The peak at 4.33 ppm is presumably FU34, which is close to FU34 in the spectrum of wild type FU-tRNA^{Val}. FU32 and FU33 is hard to be distinguished, but considering the peak at 4.89 ppm is close to position FU33 in the spectrum of wild type FU-tRNA^{Val}, it can be assigned to FU33. Thus the peak at 3.81 ppm is assigned to FU32.

Mutant U32C38 The ^{19}F NMR spectra of mutant FU-tRNA^{Val} U32C38 at 22 °C, 35 °C, 47 °C are shown in Figure 3.33. Compared to the spectrum of wild type FU-tRNA^{Val} at 22 °C, resonances seen at 6.66 ppm, 3.96 ppm and 3.00 ppm

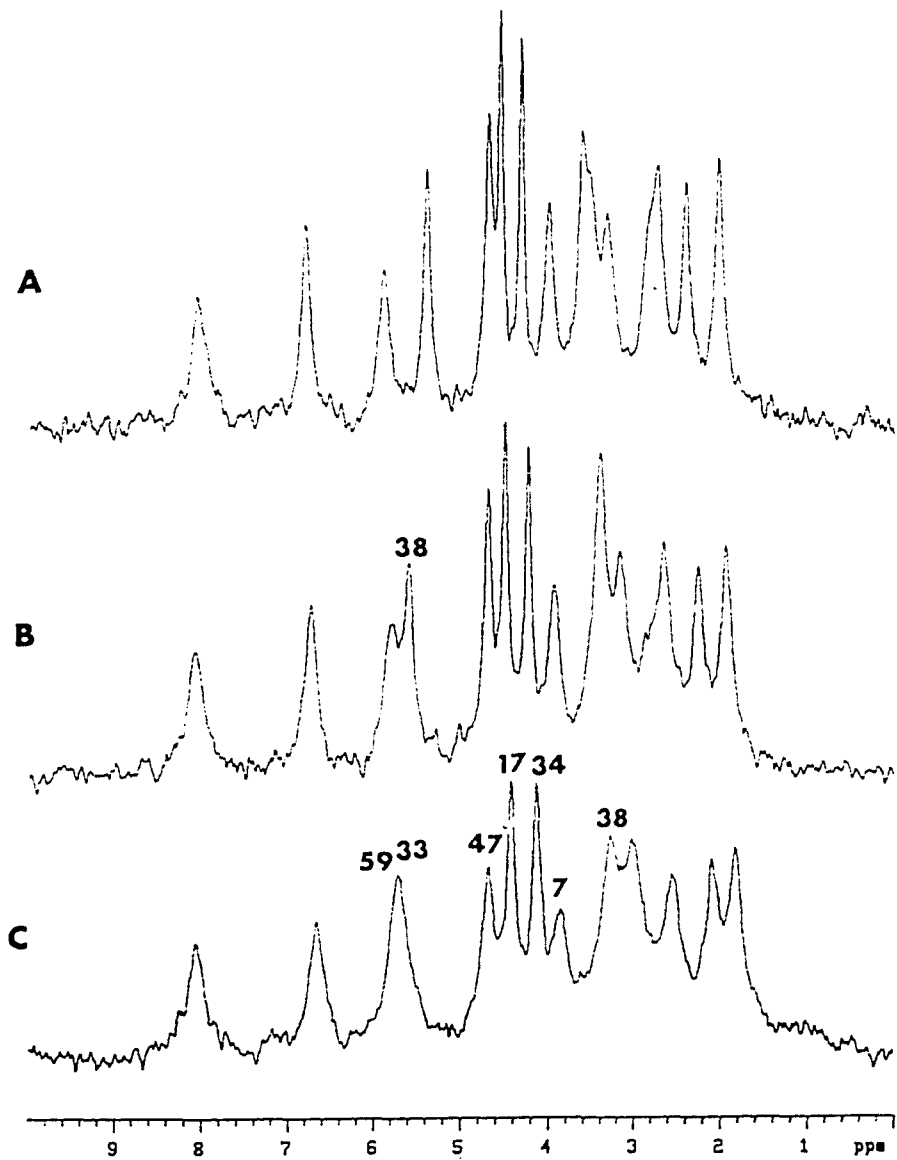


Figure 3.31: ^{19}F NMR spectra of FU-tRNA^{Val} mutant U38A32 obtained in standard buffer at different temperatures. (A) 47 °C. (B) 35 °C. (C) 22 °C

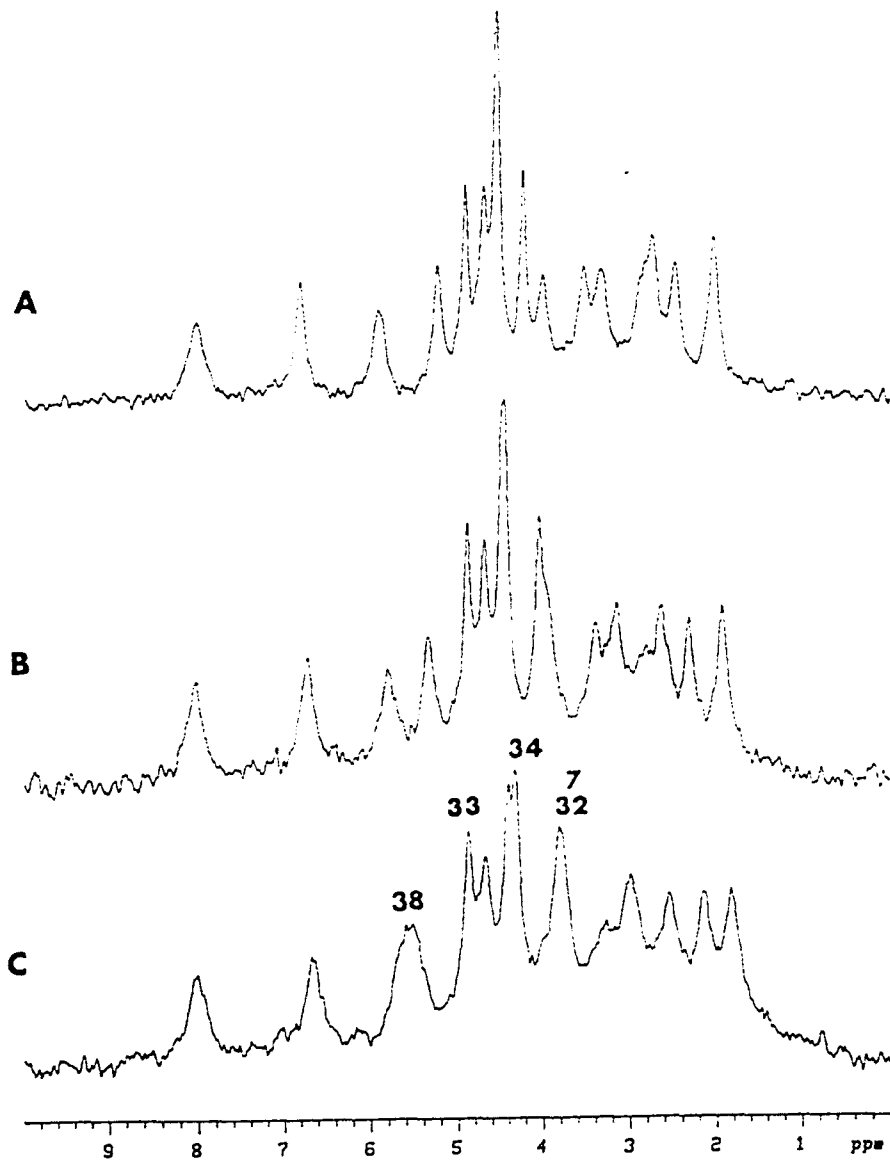


Figure 3.32: ^{19}F NMR spectra of FU-tRNA^{Val} mutant U32U38 obtained in standard buffer at different temperatures. (A) 47 °C. (B) 35 °C. (C) 22 °C

do not match known peaks in the spectrum of wild type FU-tRNA^{Val} and could be assigned to the three FUs in the anticodon loop. The loss of intensity at 4.70 ppm, which includes the resonances of FU33 and FU47 in the spectrum of wild type FU-tRNA^{Val}, indicates that FU33 has shifted to another position. Because two of these three resonances are not in the middle of the spectrum, the two associated ¹⁹F nuclei are in an environment that is different from a single stranded region. Thus the anticodon loop of this mutant must have an unusual conformation.

To help assign the resonances for the FUs in the anticodon loop, 1D NOE experiments were carried out at 8 °C (data not shown). At this low temperature the peak at 6.66 ppm shifts to 6.90 ppm, the peak 3.0 ppm shifts to 2.50 ppm. 1D NOE experiments showed that these two peaks have reciprocal NOEs, indicating they are either from FU32 and FU33 or from FU33 and FU34. No NOEs were observed from the resonance at 3.96 ppm (22 °C). Considering that FU33 is on the 5' side and FU34 in the 3' side of the anticodon loop, the two FU residues are quite far apart in the tRNA structure and a NOE from FU33 to FU34 is not expected. On the other hand, FU32 and FU33 are stacked on the 5' side of the anticodon loop, and a NOE between these two ¹⁹F nuclei is expected. Therefore, these two resonances belong to FU32 and FU33 and the peak at 3.96 ppm can be assigned to FU34. Which of the peaks at 6.66 ppm and 3.00 ppm is FU32 and FU33 is difficult to determine. However in the spectrum of FU-tRNA^{Val} mutant U32U38 (Figure 3.32), FU32 resonates upfield of FU7 and the peak corresponding to FU33 resonates downfield of FU47 in wild type FU-tRNA^{Val}. The chemical shift positions of these resonances is very sensitive to temperature. With increasing temperature they shift toward the middle of the spectrum. It seems reasonable, therefore, to assign FU32 in FU-tRNA^{Val}

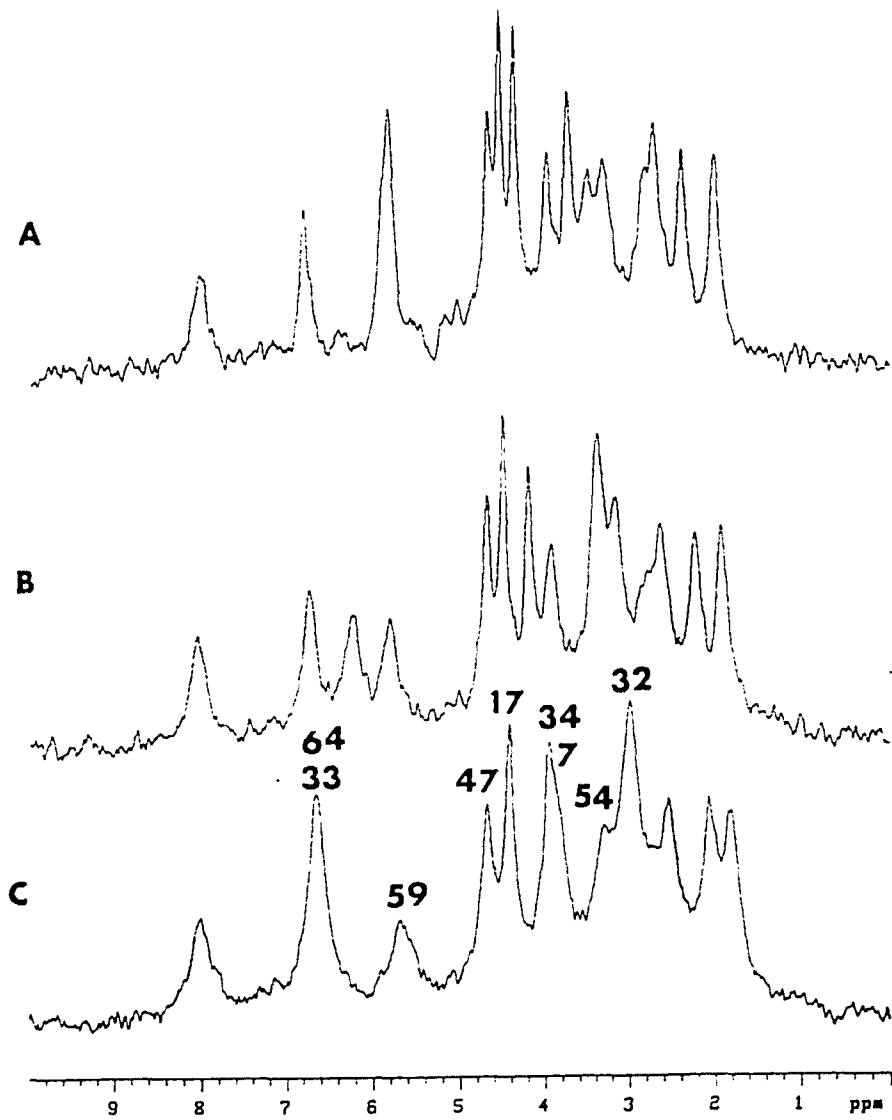


Figure 3.33: ^{19}F NMR spectra of FU-tRNA^{Val} mutant U32C38 obtained in standard buffer at different temperatures. (A) 47 °C. (B) 35 °C. (C) 22 °C

mutant U32C38 to the peak at 3.00 ppm and FU33 to that at 6.66 ppm. The reason for the downfield shift of FU33 or FU32 in tRNA^{Val} mutant U32C38 is not as yet understood.

Codon-anticodon interactions studied by ¹H NMR

Interaction of tRNA with mRNA is an essential step in protein biosynthesis. The anticodon of tRNA recognizes the codon in mRNA by base pairing. This recognition must be very specific for the accuracy of protein synthesis. A detailed understanding of the the structure and dynamics of the mRNA-tRNA complex is very important. This section describes the results of ¹H NMR studies of *E. coli* tRNA^{Val} codon-anticodon interactions.

GUAA binding to tRNA^{Val}: imino ¹H NMR study

E. coli tRNA^{Val} has the anticodon triplet UAC. U34 is modified to cmo⁵U in the native tRNA. A codon-containing tetranucleotide GUAA with its 3' A complementary to base U33 in tRNA^{Val} was used in this study. Previous studies showed that GUAA binds only to the anticodon loop of native FU-tRNA^{Val} (Gollnick *et al.*, 1987). The assignment of the imino ¹H NMR spectrum of native *E. coli* tRNA^{Val} (Hare *et al.*, 1985) made it possible to monitor the effects of codon binding on tRNA conformation. Conformational changes or disruption of tRNA secondary or tertiary structure upon codon binding can be observed easily by following the changes of the imino ¹H NMR spectrum. If the complex is stable enough, the imino protons involved in base pairing between codon and anticodon should be observed.

Figure 3.34 shows the imino ^1H NMR spectra of native *E. coli* tRNA^{Val} after addition of different molar ratios of GUAA to the tRNA. No significant changes were seen in the spectra obtained as the molar ratio of GUAA to tRNA was increased to 3. Thus no structural changes in tRNA^{Val} upon GUAA binding could be detected by imino ^1H NMR. Since no extra imino proton resonances were observed in the presence of GUAA, the tetranucleotide is in fast exchange between the bound and free state. The linewidth does not change with increasing GUAA, thus GUAA binding to tRNA^{Val} does not cause aggregation of the tRNA molecules.

Structure of GUAA upon binding to tRNA^{Val}

Another approach to the study of the codon-anticodon complex is to compare the structure of GUAA when it is free and bound to tRNA^{Val}. This can be done by transfer NOE experiments, a method widely used in determining ligand conformation in macromolecular complexes (Clore *et al.*, 1984; Gronenborn and Clore, 1990). Transfer NOE is a method for studying the conformation of small ligands bound to macromolecules in an exchanging system. It involves the transfer of information about the cross relaxation between two bound ligand protons from the bound state to the free state via chemical exchange. In the case of GUAA with a molecular weight about 1,000, its correlation time, τ_c , is very short. Thus $\omega\tau_c$ is close to 1 (where ω is the Larmor frequency) and NOEs between protons in free GUAA are close to zero. When GUAA binds to tRNA, the molecular weight of the complex is about 27,000 and this increases the correlation time, τ_c , and therefore, the value of $\omega\tau_c$. Thus NOEs between protons of bound GUAA can be detected by transfer NOE experiments. By determining a sufficient number of interproton distances from the

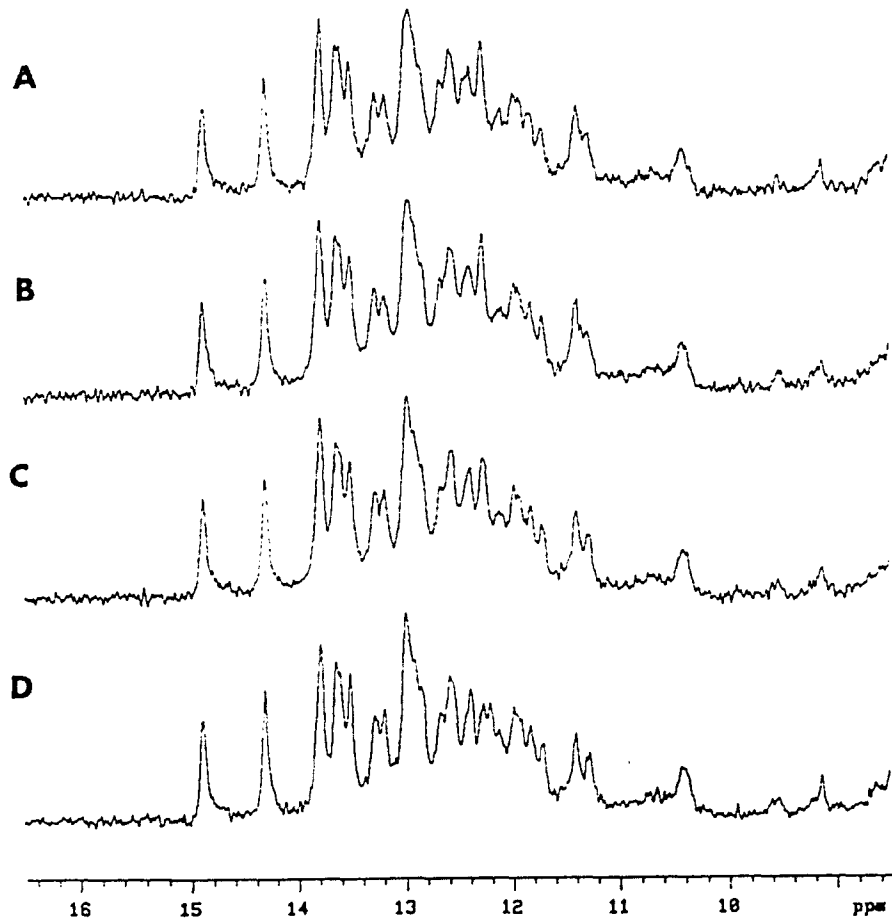


Figure 3.34: Imino ^1H NMR spectra of GUAA binding to native tRNA^{Val} in the presence of 15 mM Mg^{2+} . The molar ratio of GUAA to tRNA is 3 (A), 2 (B), 1 (C) and 0 (D)

intensities of NOE cross peaks, the structure of GUAA in the bound state can be solved. Then the structure of the codon-anticodon complex can be better described.

Free GUAA In order to determine the structure of GUAA, its ^1H NMR spectrum must first be assigned. Figure 3.35 shows a portion of the NOESY map of GUAA measured at 6 °C in D_2O containing 10 mM phosphate, 100 mM NaCl and 15 mM MgCl_2 . As expected very few NOEs can be seen in the NOESY map of free GUAA. Only a few NOE cross peaks from the aromatic protons (7–8.5 ppm) to the sugar protons (3–6 ppm) can be seen. Because of the low sensitivity of the NOESY map, it was not analyzed in detail, but served as a control for comparison with other spectra (see below).

The problem of low sensitivity was overcome by performing a ROESY experiment. In ROESY, the transient NOEs are observed in the rotating frame (Bax and Davis, 1985; Rance, 1987; Kessler *et al.*, 1987). These NOEs (ROEs) show up as negative values compared to the diagonal peaks. ROESY experiments are particularly useful in detecting NOEs between protons in low molecular weight ligands like GUAA. In this case the laboratory-frame NOE is close to zero for a small molecule like GUAA, because $\omega\tau_c$ is close to 1 (where ω is the Larmor frequency). While the rotating-frame NOE is always positive and observed under spin-locked conditions. The ROE cross peak intensities match the normal NOE cross peak intensities. Figure 3.36 shows the same portion of a ROESY spectrum of free GUAA shown in the NOESY spectrum described above (see Figure 3.35). It shows the cross peaks from the aromatic protons to the sugar protons and from the 1' sugar proton to other sugar protons. Compared to the NOESY map, many more ROE cross peaks can be

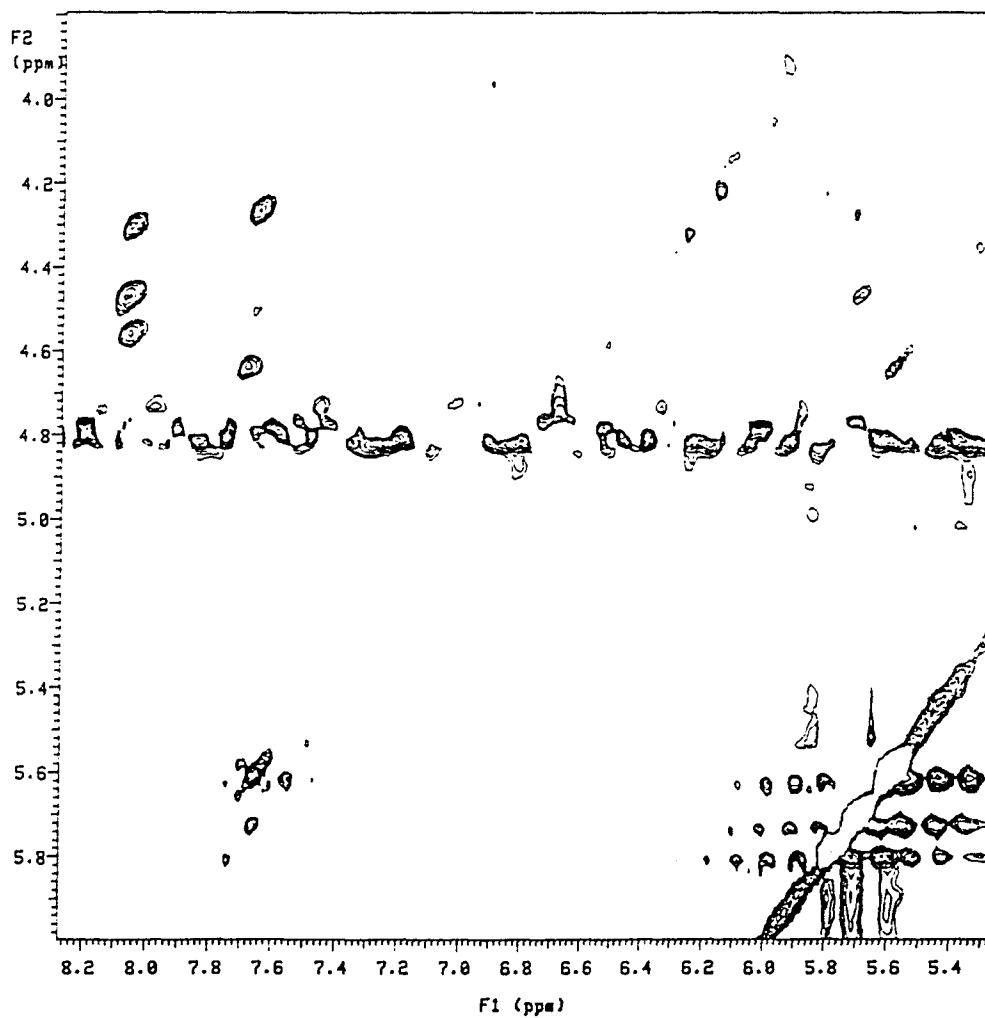


Figure 3.35: Portion of two-dimensional NOESY spectrum of GUA measured at 6°C in D₂O containing 10 mM phosphate, 100 mM NaCl and 15 mM MgCl₂, showing NOE cross peaks from aromatic protons to sugar protons

observed.

Assignment of the spectrum starts from the ROE cross peaks between aromatic protons and the 1' sugar protons. The aromatic proton resonances are at 7–8.5 ppm, while the 1' sugar protons and the C5H of U resonate at 5–6 ppm (Brown *et al.*, 1994; Peterson *et al.*, 1994). There is a very strong cross peak between the aromatic peak at 7.66 ppm and a peak at 5.60 ppm. The best candidates for these two protons are C6H and C5H on adjacent carbons of U2 in GUAA. Thus the peak at 7.66 ppm is assigned to the C6H of U2 and the peak at 5.60 ppm to the C5H of U2.

GUAA is assumed to exist in an A-type right-handed helical form as shown in Figure 3.37. In such a structure the aromatic peak can have NOEs to its own sugar proton resonances or to those of the nucleotide on its 5' side. Thus a ROE from a C5H, C6H or C8H aromatic proton to a sugar proton indicates that the sugar proton resonance is from either the same nucleotide unit or the proton of the 5' adjacent one. Conversely a sugar proton will exhibit a ROE to an aromatic proton of its own nucleotide or to one on the 3' adjacent unit. Such cross peaks link the aromatic protons to their own sugar protons or to the sugar protons of the nucleotide on their 5' side.

There are ROE cross peaks from 7.66 ppm (C6H of U2) to 1' sugar proton peaks at 5.72 ppm and 5.58 ppm (Figure 3.36). Since the resonance at 5.58 ppm also has a ROE to an aromatic peak at 7.69 ppm, the resonances at 5.58 ppm and 7.69 ppm can only belong to nucleotide G1. Thus the peak at 7.69 ppm was assigned to C8H of G1 and the peak at 5.58 ppm was assigned to the 1' sugar proton of G1. Therefore the 5.72 ppm peak is assigned to the 1' proton of U2.

ROEs are observed from aromatic peaks at 8.09 ppm, 8.06 ppm and 7.69 ppm

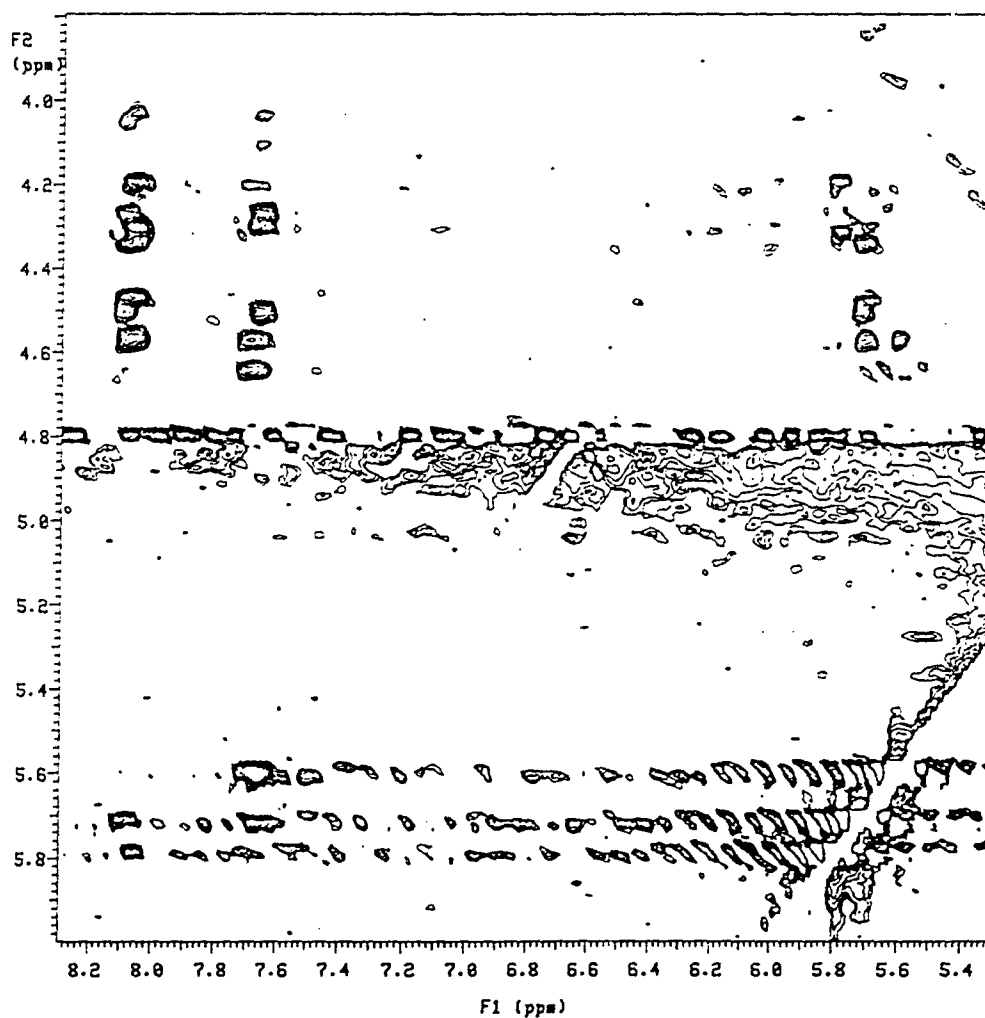


Figure 3.36: Portion of two-dimensional ROESY spectrum of GUAA measured at 6 °C in D₂O containing 10 mM phosphate, 100 mM NaCl and 15 mM MgCl₂, showing NOE cross peaks from the aromatic protons to the sugar protons and 1' of sugar proton to other sugar protons

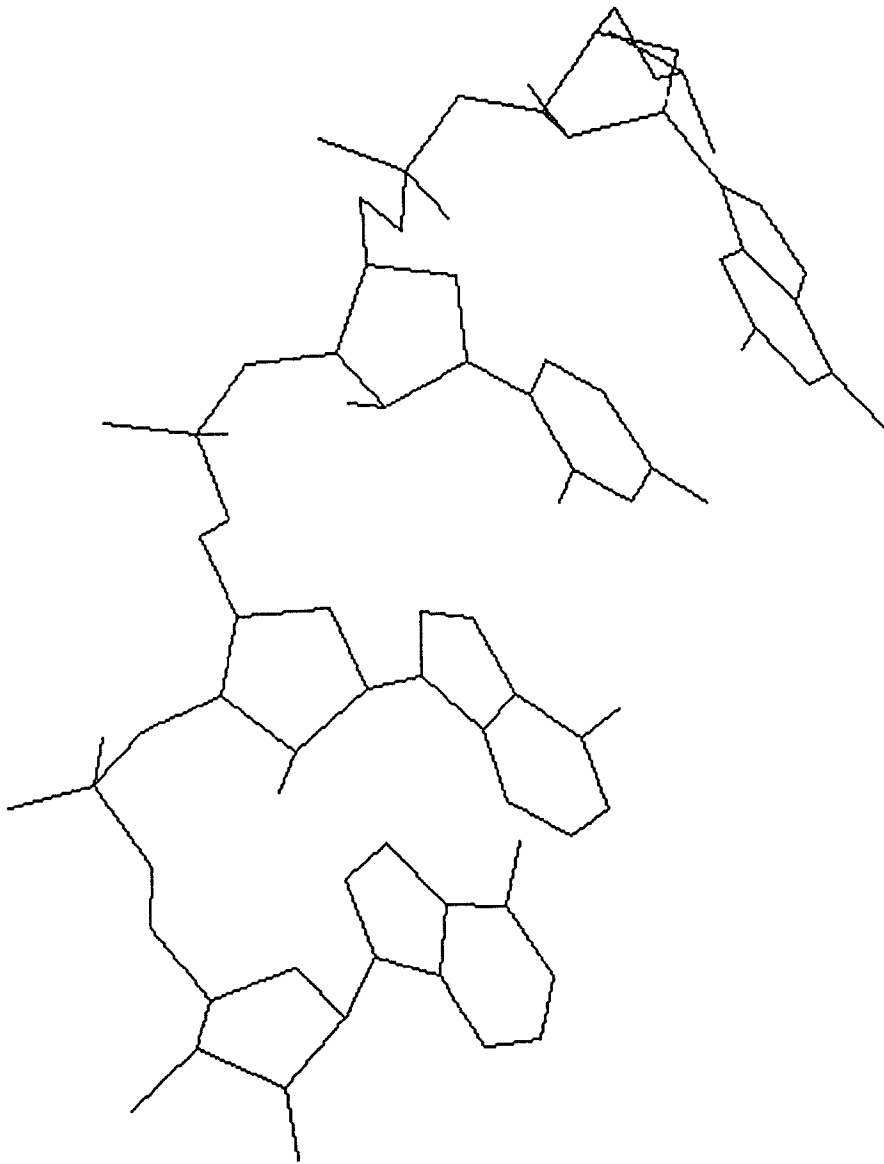


Figure 3.37: Model of GUAA as an A-form right-handed helix

to 1' sugar protons at 5.71 ppm, 5.79 ppm and 5.58 ppm, respectively (Figure 3.36). There are no ROEs seen from the peak at 5.72 ppm (U2 1' proton) to peaks at 8.06 and 8.09 ppm. Thus the sequential connection from U2 to A3 cannot be determined by the ROEs from 1' proton to aromatic protons. But a peak at 4.27 ppm clearly shows ROEs to two aromatic peaks at 7.66 ppm and 8.09 ppm. Assignment of the resonance at 4.27 ppm to sugar protons of A3 is not reasonable for an A-form right-handed helical RNA structure. Thus this peak belongs to sugar protons of U2. The connection between the resonance at 4.27 ppm and that at 8.09 ppm assigns the peak at 8.09 ppm to C8H of A3. Because of the ROE from 8.09 ppm (A3) to 5.71 ppm, the resonance at 5.71 ppm is assigned to the 1' sugar proton of A3. The remaining peaks at 8.06 ppm and 5.79 ppm are assigned to C8H and 1' proton of A4.

Other sugar protons were assigned by identifying the spin system within a sugar ring. The aromatic peak at 7.69 ppm (C8H of G1) is expected to have ROEs only to its own sugar protons. Thus resonances at 4.65, 4.57 and 4.20 ppm belong to the sugar protons of G1 (Figure 3.36). The peaks at 4.27, 4.51 and 4.30 ppm are assigned to the sugar protons of U2 based on their ROEs to the peak 7.66 ppm (C6H of U2). Here the 4.51 ppm peak also has a ROE to 8.09 ppm (A3) but it has no ROEs to other sugar protons of A3, eliminating the possibility of its being an A3 sugar proton. Several resonances contribute to the peak at 4.30 ppm. One of them shows a ROE to the resonance at 8.06 ppm (A4); it is probably from a proton of A4 sugar resonating at 4.30 ppm. The other four A4 sugar protons include 4.47, 4.57, 4.20 and 4.05 ppm, based on their ROEs to the aromatic peak of A4 (8.06 ppm). The peaks at 4.57, 4.30, 4.20 ppm contain multiple resonances.

ROEs between sugar protons are expected from the same sugar ring. Analysis

of ROE cross peaks in the sugar-sugar proton region identified the remaining sugar proton resonances, which do not have ROEs to their own aromatic peaks. For the G1 spin system, two more resonances, 3.74 ppm and 3.68 ppm, were identified. The peak at 3.74 ppm shows ROEs to peaks at 4.20, 4.57, 4.65 and 3.68 ppm. The peak at 3.68 ppm shows ROEs to peaks at 4.20, 4.65, 4.57 and 3.74 ppm. There is an extensive ROE network among the sugar protons of G1. Similarly two more resonances at 4.03 and 4.21 ppm were added to the U2 spin system based on their ROEs to other U2 sugar protons. All A4 sugar proton resonances have been identified previously and there are ROE networks among these resonances.

The spin system of A3 is not well defined because of a lack of ROE connectivities. The ROE from 5.71 ppm (A3) to 4.34 ppm put the the peak at 4.34 ppm to the A3 spin system. There is a ROE network among the remaining peaks 3.63, 3.50, 3.42 ppm, these resonances likely belong to A3 sugar protons.

In order to assign the individual sugar protons, a TOCSY experiments was carried out. In TOCSY experiments, one only observes cross peaks between protons separated by 3 bonds or less. Thus the TOCSY cross peaks could establish the connectivities of sugar ring proton resonances. Figure 3.38 shows the region containing sugar-sugar proton cross peaks of the TOCSY spectrum. The observed TOCSY cross peaks help to make several connectivities on sugar ring protons. Some of the cross peaks are so weak that they can only be seen at lower contour levels of the TOCSY spectrum. The connectivities from 5.72 ppm ($1'$ proton of U2) to 4.27 ppm to 4.51 ppm to 4.30 ppm to 4.21 ppm to 4.03 ppm assign the latter 5 resonances to $2'$, $3'$, $4'$, $5'$ and $5''$ of protons of U2. For the G1 sugar ring, there are NOE connectivities from 5.58 to 4.65 ppm, from 4.57 to 4.20 to 3.74 ppm and from 5.58 to 4.57 ppm. This

makes it difficult to determine whether the 4.65 ppm resonance or that of 4.58 ppm is from the 2' sugar proton of G1. For the A4 sugar ring, there is NOE connectivity from 4.57 to 4.30 to 4.05 to 4.20 ppm. No TOCSY cross peaks were observed among A3 sugar proton resonances. The proton assignments of free GUAA at 6 °C are listed in Table 3.4.

Table 3.4: Proton assignments of free GUAA

Proton	Aromatic	1'	2'	3'	4'	5'	5''
G1	7.69	5.58	4.65	4.57	4.20	3.74	3.68
U2	7.66	5.72	4.27	4.52	4.30	4.03	4.21
A3	8.09	5.71	4.34	4.13	3.63	3.50	3.42
A4	8.06	5.79	4.47	4.57	4.30	4.05	4.20

The assignments for all resonances of U2 and the aromatic and 1' sugar protons of the other nucleotides are definitive, but only tentative assignments for resonances of the 2', 3', 4', 5' and 5'' protons of G1, A3, A4 can be made at this time.

Structure of GUAA when bound to native tRNA^{Val} With the assignment of most resonances in the ¹H NMR spectrum of GUAA, it is possible to examine the spectral changes upon binding of GUAA to tRNA^{Val}. This is done by a transfer NOE experiment. In this experiment, 2.5 mg of native tRNA^{Val} were mixed with 2 mM GUAA in a D₂O solution containing 15 mM Mg²⁺, 100 mM NaCl and 10 mM phosphate. The transfer NOE experiment was performed with a mixing time of 0.15 seconds at 6 °C.

Figure 3.39 shows the region of the spectrum containing the aromatic to sugar proton cross peaks. Comparison of this map with the same region in the NOESY and ROESY maps (Figure 3.35 and 3.36) of free GUAA reveals substantial improvement in signal sensitivity. Many NOEs unobservable in the ROESY map now appear in

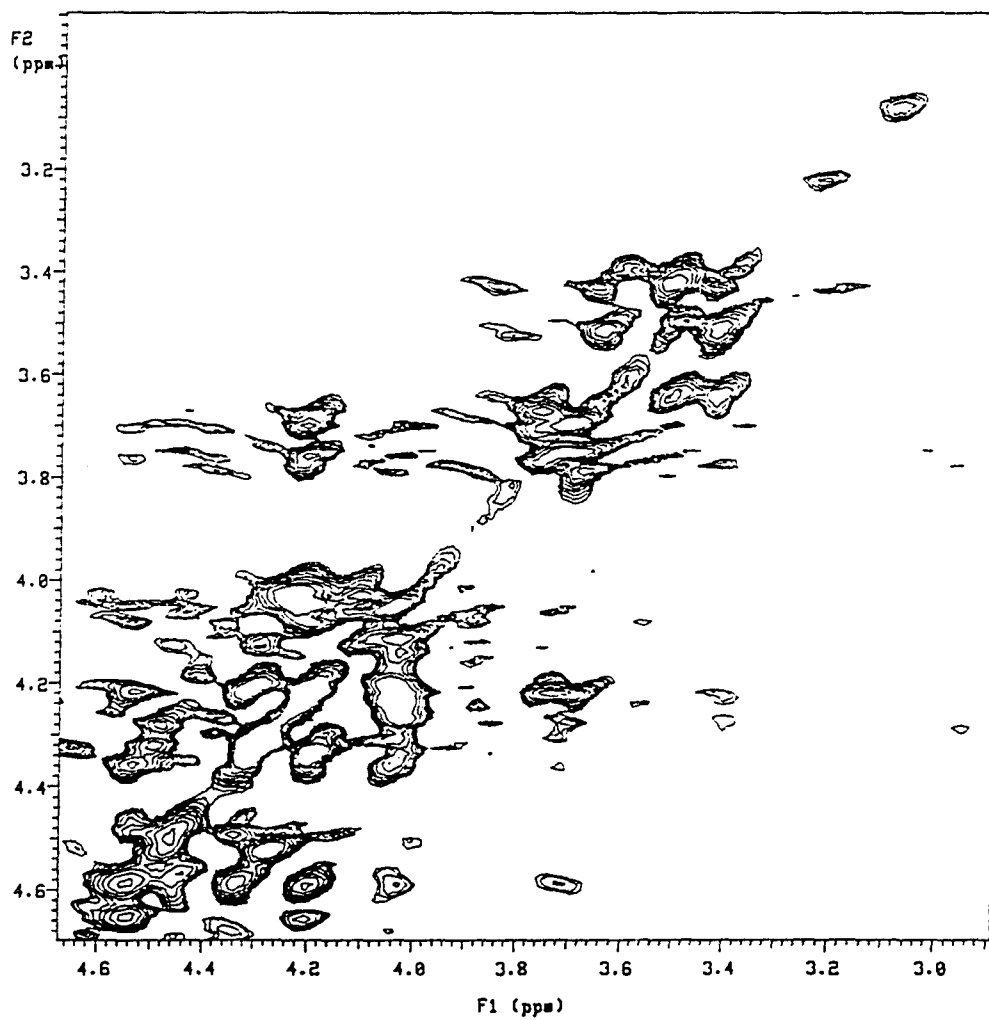


Figure 3.38: Portion of two-dimensional TOCSY spectrum of GUAA at 6 °C in D₂O containing 10 mM phosphate, 100 mM NaCl and 15 mM MgCl₂, showing NOE cross peaks between sugar protons

the presence of the tRNA. The transfer NOE experiment works well in this system. The general NOE pattern in the transfer NOE map is very similar to that of the ROESY experiment. But the relative intensities are different for some of the cross peaks. A few peaks shift slightly, for example, peaks at 4.26 ppm, 4.28 ppm and 4.34 ppm in the ROESY map (Figure 3.36) shift to 4.28 ppm, 4.32 ppm and 4.36 ppm in the transfer NOE spectrum respectively. In the ROESY map, C8H of G1 (7.66 ppm) shows about equal ROE intensities to peaks 4.30 and 4.26 ppm, while in the transfer NOE spectrum, the NOE from 7.66 ppm to 4.32 ppm (4.30 ppm in ROESY map) is very weak. The peak at 4.20 ppm in the ROESY map shows a ROE to 8.06 ppm, but shows a very weak NOE to 8.09 ppm in the transfer NOE map.

Other changes in NOE intensities were seen in the region containing cross peaks from 1' proton to other sugar protons. The two cross peaks in the ROESY map, which are from 5.62 ppm and 5.72 ppm to 4.57 ppm, are barely visible in the transfer NOE experiment. The cross peak from 5.62 ppm to 4.22 ppm becomes stronger in the transfer NOE map than in the ROESY map (in which it appears as a weak positive cross peak, not visible in Figure 3.36). The differences between ROE (free GUAA) and TNOE (bound GUAA) cross peak intensities indicate that the structure of GUAA in the bound state is different from that of free GUAA. Assignments of the transfer NOE spectrum of GUAA and quantitative measurements of the intensities of NOE cross peaks are required to determine the detailed structure of GUAA in the bound state. These studies are currently underway.

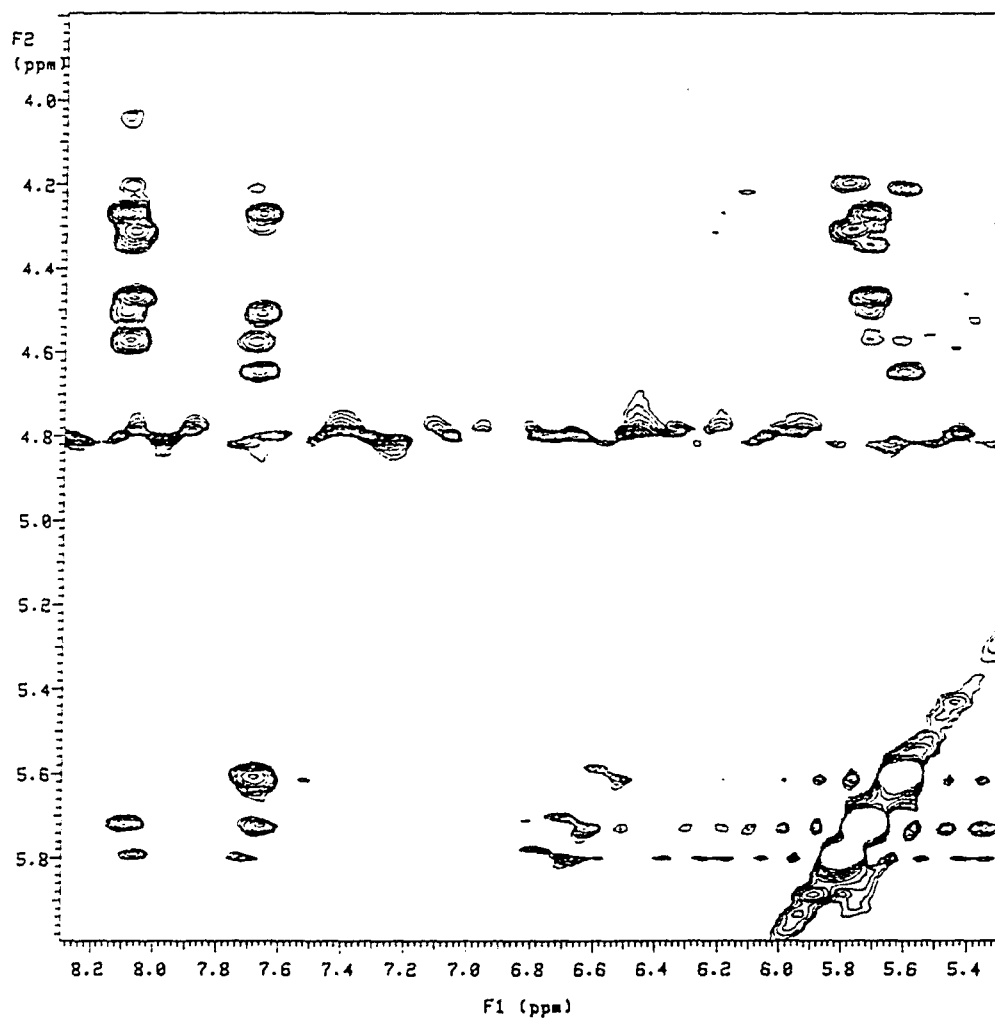


Figure 3.39: Portion of two-dimensional transfer NOE spectrum of GUAA in D_2O containing 10 mM phosphate, 100 mM NaCl and 15 mM $MgCl_2$ at 6 $^{\circ}C$, showing NOE cross peaks between aromatic and 1' sugar protons

CHAPTER 4. DISCUSSION

In *E. coli*, more than 50 genes (about 1% of the genome) encode tRNA modifying enzymes (Nishimura, 1979). The gene for m⁵U54-methyl transferase, not the transferase activity, is essential for viability (Persson *et al.*, 1992). Thus the gene product seems to have a second function, distinct from that of m⁵U54 synthesis in tRNA, which is vital. No modified nucleoside has been found essential for viability. The conserved presence of modified nucleosides in a large number of different organisms suggests they play important roles in tRNA function. To understand the role of nucleoside modification, the structures of modified and unmodified *E. coli* tRNA^{Val} were compared in this work.

Unmodified tRNA^{Val} was synthesized *in vitro* using T7 RNA polymerase. The *in vitro* transcribed tRNA^{Val} does not contain any modified nucleosides, yet it is fully active in aminoacylation (Table 3.1). Imino proton NMR was used to monitor the structure of tRNA^{Val} in solution. The imino proton NMR spectrum of unmodified tRNA^{Val} recorded in the presence of excess Mg²⁺ shows 28 imino proton intensities (Figure 3.2b). The excellent resolution of the spectrum allows assignment of the spectrum in a straight-forward fashion. The resonances of all imino protons involved in hydrogen bonds in the secondary and tertiary interactions were assigned using 2D NOESY and 1D NOE methods. Some aromatic C2 and C8 protons and one

amino proton resonance were also assigned. This work represents the first complete assignment of the imino proton NMR spectrum of an unmodified tRNA.

Comparison of the spectrum of unmodified tRNA^{Val} with the previously published spectrum of an unmodified tRNA — yeast tRNA^{Phe} (Hall *et al.*, 1989), shows that the former is much better resolved. There is no sign of sample aggregation up to 2 mM concentration in the presence of excess Mg²⁺ (Figure 3.3). In fact a spectrum of unmodified yeast tRNA^{Phe} (0.3 mM) was obtained under the same conditions (data not shown) whose resolution is as good as that in the spectrum of tRNA^{Val} (Figure 3.2b). Thus aggregation of *in vitro* transcribed RNA molecules is not a general phenomenon (Szewczak *et al.*, 1990).

In practice, at least 2 mg tRNA are required to obtain a spectrum with good signal-to-noise ratio on a 500 MHz NMR spectrometer in a reasonable time. For 1D NOE experiment, at least 5 mg tRNA are required. But for 2D NOESY experiments, about 20 mg sample are required. The 2D NOESY map shown in Figure 3.3 was obtained with 25 mg tRNA^{Val}. Some of the weak NOEs can only be seen at lower contours of the spectrum. Such large amounts of RNA sample were made possible by the development of an *in vitro* transcription method (Sampson and Uhlenbeck, 1988). Many tRNA^{Val} variants and 5FU substituted tRNA^{Val} preparations used in this work were synthesized by *in vitro* transcription with T7 RNA polymerase.

Although the ¹H NMR spectrum of native *E. coli* tRNA^{Val} was completely assigned (Hare *et al.*, 1985), it is necessary to have the exact same solution and instrument conditions when comparing the spectra of modified and unmodified tRNA^{Val}. Thus large amounts of native (modified) tRNA^{Val} are also required for NMR study. To obtain enough native tRNA^{Val}, a tRNA^{Val} overexpression system was con-

structed (see Chapter 2). The system uses the well-known T7 expression system (Studier and Moffatt, 1986) to increase the yield of tRNA^{Val}. The tRNA is processed to yield mature tRNA^{Val} by the *E. coli* cell. The tRNA^{Val} expression level is about 30-fold higher than in cells without the T7 RNA polymerase gene, 10 mg tRNA^{Val} can be purified from one liter of culture. Comparison the imino proton NMR spectrum of overexpressed tRNA^{Val} with that of commercial (Subriden) tRNA^{Val}, which was isolated from normal *E. coli* cells, showed no significant differences (Figure 2.2). The imino proton resonances of four modified nucleosides, s⁴U8, T54, Ψ55 and m⁷G46, have the same chemical shift positions in the spectrum of overexpressed tRNA^{Val} as in that of commercial tRNA^{Val}. Furthermore, the temperature dependence of the spectrum (data not shown) is the same as that of commercial tRNA^{Val} (Figure 3.7). These results strongly suggest that the overexpressed tRNA^{Val} has a structure very similar to that of commercial tRNA^{Val}, and is largely modified, at least at these 4 positions. The imino protons of the other 3 modified bases found in native tRNA^{Val}, D17, cm⁵U34, m⁶A37, cannot be observed because they are not involved in hydrogen bonding.

Whether overexpressed tRNA is fully modified or not differs for different tRNA species. During chromatographic purification of overexpressed *E. coli* tRNA^{Gln} (Perona *et al.*, 1988), the authors noted the presence of minor peaks and suggested that they might correspond to unmodified tRNA^{Gln} species. A similar result was obtained by Borel and his colleagues (1993) when they purified overexpressed *E. coli* tRNA₂^{Ser}. In this case, only half the A37 of tRNA₂^{Ser} was modified to 2-methylthio-N⁶-isopentenyl-adenisine (ms2i6A). However, in the case of overexpressed *E. coli* tRNA^{Asp} (Martin *et al.*, 1993), nucleoside analysis showed that base modification

is complete. This is not surprising because 15-fold overexpression of tRNA^{Asp} only increases total cell tRNA by 50%, and all the modified nucleosides in tRNA^{Asp} are simple and shared by many other tRNA species. For *E. coli* tRNA^{Val}, all 7 modified nucleosides (Figure 1.1) are simple and not unique; overexpression of tRNA^{Val} does not change the total cell tRNA concentration significantly, judged from the band intensities on gel electrophoresis of crude tRNAs from normal cells and overproducing cells (data not shown). Thus the activities of tRNA modifying enzymes should be sufficient to modify the overexpressed tRNA^{Val}.

The tRNA^{Val} expression system allows large quantities of native tRNA^{Val} to be obtained for biochemical and biophysical studies. Other tRNA sequences can be expressed with this system by replacing the tRNA^{Val} gene with the desired tRNA gene. tRNA^{Val} mutant G38 has been successfully overexpressed and purified (Figure 3.23). Because of the high level of expression of the cloned tRNA sequence, endogenous wild type tRNA^{Val} represents only 5% or less of total expressed tRNA molecules. Therefore, the major valine-accepting activity is due to the cloned tRNA. Such a system can also be used to produce ¹⁵N or ¹³C labeled tRNA for NMR studies.

Structures of modified and unmodified tRNA^{Val} were compared by looking at their imino proton NMR spectra. The chemical shift of an imino proton resonance is very sensitive to the immediate environment of that proton, therefore, any chemical shift differences between corresponding resonances of modified and unmodified tRNAs are indicative of structural differences. At high Mg²⁺ concentration, significant chemical shift differences were seen only for peaks B (U8), C (U54), K' (G46), U (U55) and X (G18 amino) (Figure 3.6). These peaks correspond to imino protons

on modified bases or to an amino proton (X) on a base that is paired to a modified base. The respective modified bases in native tRNA^{Val} are s⁴U8, T54, m⁷G46 and Ψ55. Base modification is expected to disturb the electronic distribution in the ring and account for the large chemical shift change of imino protons from modified bases. For example, dethiolation of s⁴U8 by chemical modification has been shown to cause a 0.6 ppm upfield shift of the resonance (Reid, *et al.*, 1975), and this is indeed the chemical shift difference between the signal for s⁴U8 and U8 observed when comparing the spectra of modified and unmodified tRNA^{Val} (Figure 3.6).

The amino proton of G18 is involved in hydrogen bonding with U55 (Kim *et al.*, 1974). Modification of U to yield Ψ at position 55 could affect the hydrogen bond from O2 of U55 to the G18 amino proton. Hydrogen bond strength is correlated with chemical shift (Wagner *et al.*, 1983), progressive down field shifts of the hydrogen bonded proton resonance is an indication of enhancement of the hydrogen bond strength. Thus, the upfield chemical shift of peak X in the ¹H NMR spectrum of unmodified tRNA^{Val} suggests a weaker hydrogen bond between U55 and G18. This conclusion is supported by the temperature dependence of the imino ¹H NMR spectra of modified and unmodified tRNA^{Val} (Figures 3.7 and 3.8).

At 15 mM Mg²⁺, all other chemical shift differences of corresponding peaks in the spectra of modified and unmodified tRNA^{Val} are less than 0.1 ppm. The similarity of the chemical shifts indicates that the global solution structure of modified and unmodified tRNA^{Val} are very similar at high Mg²⁺ concentration. Any differences in the two structures are localized to the vicinity of the modified bases.

Assignments of the imino proton NMR spectrum of unmodified tRNA^{Val} also provides a tool for monitoring conformational changes in tRNA^{Val} mutants resulting

from the base substitutions. The tRNA^{Val} variant U30A40 has a ¹H NMR spectrum similar to that of wild type tRNA^{Val} except for peak shifts near the mutation site (Figure 3.5), indicating it has a very similar structure to that of wild type tRNA^{Val}. Analysis of the spectrum of U30A40 allowed determination of the orientation of assignments in the anticodon stem. This confirmed the previous indirect assignments made in native tRNA^{Val} (Hare *et al.*, 1985).

In vitro transcribed tRNA is known to have a lower melting temperature (*T*_m) than the corresponding modified tRNA, even at high Mg²⁺ concentrations (Sampson and Uhlenbeck, 1988; Derrick and Horowitz, 1993). The available imino proton assignments for both the modified and unmodified *E. coli* tRNA^{Val} (Table 2.1) make it possible to compare the relative thermal stabilities of the tRNA molecules. In the spectrum of unmodified tRNA^{Val}, peaks C (U54), U (U55), I' (G19), F (44) and X (G18 imino) have disappeared at 60 °C. The loss of these tertiary marker resonances at 60 °C indicates the tertiary interactions involving these protons are largely disrupted. The presence of other tertiary resonances at 60 °C, peaks B (U8), K' (G46) and P (G15), indicates these tertiary interactions are stable at this temperature. These stable tertiary interactions are those involved in stabilizing the P10 loop.

In the case of the native tRNA^{Val}, only the tertiary resonance I' (G19) has disappeared from the spectrum at 60 °C (Figure 3.7), indicating disruption of this tertiary interaction (G19C56) between the D and T loops. Other tertiary resonances U (Ψ55), B (s⁴U8), C (T54), K' (m⁷G46) and P (G15) remain largely intact at 60 °C, indicating the corresponding tertiary interactions are still present at this temperature. Comparison of the temperature dependence of the intensity of peaks U (U55), B

(U8) and C (U54) in the spectra of modified and unmodified tRNA^{Val} suggests that nucleoside modifications at positions 8, 54 and 55 stabilize the associated tertiary interactions. These findings are consistent with previous studies on solution structure of tRNA by chemical modification and nuclease digestion. These studies showed the unmodified tRNA is more accessible than the corresponding native tRNA to nuclease attack, indicating the D loop and T loop interactions are weaker in unmodified tRNA (Derrick and Horowitz, 1993; Peret *et al.*, 1990).

All resonances of AU base pairs except C' (U29) are broadened or have disappeared in the spectrum of unmodified tRNA^{Val} at 60 °C (Figure 3.8). The imino proton resonances of the GU base pair, peak S (U64) and V (G50) are also broadened. Peak C' (U29) is still sharp at 60 °C, this is probably due to the better stacking interactions of this AU base pair in the center of the anticodon stem. Based on the broadening of resonances at higher temperature, the anticodon stem seems to be the most stable element of unmodified tRNA^{Val}. The D and T stems have about the same stability and the acceptor stem is the least stable element.

Assignment of the ¹H NMR spectrum of the unmodified tRNA at low Mg²⁺ showed that the resonances remaining are from base pairs in the acceptor stem, the T stem and the anticodon stem. No evidence for resonances or NOEs arising from the D stem and the tertiary interactions was found. Instead new NOEs between peak A (U67) and peak U (U64), peak v (G50) and peak q (G49) were observed. Peak L (U7) has shifted to the down field region of the spectrum at low Mg²⁺, and is visible as a shoulder on peak c' (U29) at room temperature. These observations indicate a substantial conformational change of unmodified tRNA^{Val} at the junction of the acceptor and T stems at low Mg²⁺.

Studies of the temperature dependence of the spectrum of unmodified tRNA^{Val} showed that the U67A6 base pair is unusually stable. This base pair interacts strongly with the G50U64 base pair to form a stable structural core even at 60 °C.

There are four strong Mg²⁺ binding sites in the crystal structure of yeast tRNA^{Phe} (Figure 1.2), two of them are in the D loop region, one in the D stem and one in the anticodon loop. Mg²⁺ ions bound to the D loop and D stem regions stabilize the tertiary interactions between the D and T loops and the P10 loop. Disruption of the D stem and tertiary interactions of unmodified tRNA^{Val} at low Mg²⁺ is consistent with the loss of bound Mg²⁺ ions at the D loop and the D stem. No such conformational changes are seen for native tRNA^{Val} at low Mg²⁺ concentrations. This indicates that Mg²⁺ ions bind to modified tRNA^{Val} more tightly than to unmodified tRNA^{Val}. Studies of the yeast tRNA^{Phe} anticodon stem region (Chen *et al.*, 1993) and of a DNA analog (Dao *et al.*, 1992) also indicate that modification of a cytosine base in the anticodon stem region facilitates site-specific Mg²⁺ binding, which in turn induces a conformational change in the anticodon loop. Thus, base modifications play important roles in stabilizing the Mg²⁺ binding sites.

Two slowly exchanging conformations of the unmodified tRNA molecule in solution at intermediate Mg²⁺ concentrations were observed during Mg²⁺ titration. With no added Mg²⁺, the imino proton of G39 shows two resonances (Figure 3.10) in slow exchange on the NMR time scale, which correspond to conformations with and without bound Mg²⁺. This indicates the existence of two slowly exchanging conformations near the anticodon loop. Under the same condition other parts of tRNA^{Val} are primarily in the conformation stable at low Mg²⁺. Thus the Mg²⁺ binding site in the anticodon loop is stronger than those in other parts of the tRNA. When the

molar ratio of Mg^{2+} to tRNA is 4, peak c'' (U24) starts to appear, indicating the lost D stem Mg^{2+} binding site is reforming. To completely restore the tRNA to the conformation present in excess Mg^{2+} , 40 Mg^{2+} ions per tRNA molecule are required (Figure 3.10).

The exchange between the metal-free and the metal-bound conformations of tRNA^{Val} is detected at a field strength of 500 MHz. Two resonances 10 Hz apart can be observed. The exchange rate must be much smaller than the smallest frequency difference between resonances corresponding to the two conformations. Thus the exchange rate, $K_{ex}=2\pi\nu$ is estimated to be $\ll 60 \text{ s}^{-1}$ when $\nu=10 \text{ Hz}$. This slow rate is consistent with the requirement of a significant conformational change upon binding and release of Mg^{2+} .

Previously Hall *et al.* (1989) reported the formation of a second GU base pair in unmodified yeast tRNA^{Phe} in the absence of Mg^{2+} , and speculated that this could be due to an interaction between G18 and U55. There is no evidence for a second GU base pair in unmodified tRNA^{Val} at low Mg^{2+} . In fact, base pairing between G18 and U55 is unlikely because of the disruption of the D loop/T loop interactions under these conditions. The absence of a second GU base pair in the low Mg^{2+} form of unmodified *E. coli* tRNA^{Val} may also reflect differences in the primary sequences of the two tRNA molecules.

The structures of modified and unmodified tRNA^{Val} were also compared at low pH with and without Mg^{2+} . In the presence of excess Mg^{2+} , no large changes in the spectra of modified and unmodified tRNA^{Val} are observed in the pH range 7.0 to 4.2, indicating that at high Mg^{2+} concentrations the tRNA structure is stable at low pH (Figure 3.14). In the absence of added Mg^{2+} , four peaks in the 15-

18 ppm region were seen in the spectrum of unmodified tRNA^{Val} at pH 4.2. In contrast, no such peaks were seen in the spectrum of native tRNA^{Val} under the same conditions (Figure 3.15). The appearance of these extremely low field resonances is accompanied by large spectral changes in the imino proton region, indicating large structural changes occur at low pH. Thus nucleoside modifications must somehow prevent these large structural changes from happening in the native tRNA.

pH induced structural changes in DNA have been demonstrated in many deoxy-oligonucleotides (Ahmed *et al.*, 1994; Jaishree and Wang, 1993; Feigon and Smith, 1992; Rajagopal and Feigon, 1989). These studies showed that at low pH, protonation occurs at the N1 of A and N3 of C. These protons resonate below 15 ppm when they are involved in hydrogen bonding. The extremely low field peaks are broad and become sharper at lower temperature, indicating the associated protons exchange with H₂O at a relatively fast rate. There is no evidence to show that these peaks are from the imino protons of Watson-Crick AU base pairs. Peaks 2, 3, 4 show no sharp NOEs to 7–8 ppm, indicating they are not from protons of A+. Peak 1 shows NOEs to two sharp peaks at 7.43 ppm and 7.65 ppm (Figure 3.16). Based on this observation and the fact that sharp peaks at 7–8 ppm are from the C2 proton of A, an AA+ base pair was proposed as the source of imino proton peak 1. This AA+ base pair contains only one hydrogen bond (Figure 3.17); the positions of the two As involved, are not known.

Spectra of tRNA^{Val} variants G38 and G9G12C23 (data not shown) also show four downfield peaks in low Mg²⁺ and low pH. But replacement of A6U67 with C6G67 prevents the appearance of peaks 3 and 4. In the same condition, the spectrum of yeast tRNA^{Phe} does not show such low field peaks (data not shown), indicating

that base protonation at low pH is not a general characteristic of tRNAs.

Recognition of the anticodon loop of *E. coli* tRNA^{Val} by VRS was investigated by analyzing the aminoacylation kinetic parameters of anticodon loop variants. The role of the known recognition site — the anticodon — was also examined further. tRNA^{Val} mutant G35 obtained by replacing A35 with G does not inhibit aminoacylation of wild type tRNA^{Val} (Figure 3.19). However, a truncated tRNA^{Val} molecule missing the 3' ACCA sequence but retaining the wild type anticodon (UAC) sequence is an inhibitor of VRS (Figure 3.19). These results strongly suggest that the anticodon contributes to tRNA^{Val} binding to VRS. Synthetase binding occurs even with a mutant tRNA^{Val} having the anticodon shifted one position in the 3' direction (Figure 3.18). Shifting the anticodon one position to the 5' side in the anticodon loop yields a mutant tRNA^{Val} with no aminoacylation activity. This is consistent with the fact that VRS binds to the inside of the L-shaped tRNA structure (Rich and Schimmel, 1977; Chu and Horowitz, 1991). Deleting all but the anticodon bases from the anticodon loop yields a tRNA^{Val} mutant with no detectable activity, the ¹H NMR spectrum of this mutant has very broad peaks, indicating a disrupted structure of this mutant (data not shown).

Aminoacylation kinetics of other anticodon loop mutants revealed that position 38 plays a role in the aminoacylation of tRNA^{Val} by VRS. A 12-fold reduction in the specificity constant (V_m/K_m) for aminoacylation of tRNA^{Val} mutant G38 was found (Table 3.2). Comparison of the ¹H NMR spectrum of tRNA^{Val} mutant G38 with that of wild type tRNA^{Val} shows extra imino proton intensity in the spectrum of mutant (Figure 3.22). This suggests that an extra base pair may be formed at the top of the anticodon loop between G38 and C at position 32. This base pair extends

the anticodon stem and changes the orientation of anticodon bases. Such base pair formation was supported by imino proton NMR studies of several other tRNA^{Val} variants. An extra imino proton resonance was observed in the ¹H NMR spectrum of tRNA^{Val} mutant C37G38 (data not shown) and in that of overexpressed tRNA^{Val} G38 (Figure 3.23).

Changes in the chemical shift positions of the resonances from FU33 and FU34 in the ¹⁹F NMR spectrum of FU-tRNA^{Val} mutant G38 suggests conformational changes in the anticodon loop. Chemical shift changes of resonances from the anticodon stem, the acceptor stem and T stem in the ¹H NMR spectra of unmodified and overexpressed tRNA^{Val} G38 indicate conformational changes in other parts of the tRNA molecules (Figures 3.22 and 3.23).

The structural changes in mutant G38 were further explored in the absence of Mg²⁺. The ¹H NMR spectrum of mutant G38 in the absence of Mg²⁺ at 22 °C shows two resonances corresponding to the imino proton of U29 (Figure 3.24). These two resonances presumably correspond to Mg²⁺-bound and Mg²⁺-free forms of the region of anticodon stem and anticodon loop. Based on the relative intensities of these two resonances, at least 75% of the molecules have Mg²⁺ at the Mg²⁺ binding site in the anticodon loop. The large chemical shift difference of peak 1 (U7) in the spectra of tRNA^{Val} mutant G38 and wild type tRNA^{Val} at low Mg²⁺ suggests that the conformation at the bottom of the acceptor stem differs in the two tRNAs. This difference is more visible in the spectra (at low Mg²⁺) recorded at 60 °C (Figure 3.25). The stable structural core found in wild type tRNA^{Val} has disappeared in the tRNA^{Val} mutant G38. Instead the acceptor stem and the anticodon stem are now the most stable elements. This dramatic structural change

is caused just by a single base substitution in the anticodon loop.

It is of interest to compare the structure of the tRNA^{Val} variant G38 and other mutants with base substitutions at positions 38 and 32. Of all 16 possible combinations, tRNA^{Val} variant G38 (having a C at position 32) is the only one that migrates more slowly on 16% PAGE (Figure 3.20). tRNA^{Val} mutant G32C38 behaves differently from mutant G38. There is no extra intensity in its ¹H NMR spectrum which could be derived from an imino proton resonance from a base pair involving G32 (data not shown). If there is formation of a base pair between G32 and C38, it must be weak. No chemical shift changes were seen for peaks from the acceptor stem and T stems in the ¹H NMR spectrum of G32C38, indicating the the mutation does not cause structural changes in these regions of the tRNA. Similar results were obtained from the ¹H NMR spectra of tRNA^{Val} mutants U32A38 and A32C38 (data not shown).

Conformational changes in the anticodon loop caused by mutations at positions 32 and 38 cannot be detected by imino proton NMR. ¹⁹F nuclei do not exchange with H₂O. Thus if a ¹⁹F nucleus is in fast exchange between several environments, the ¹⁹F NMR spectrum will show a peak at a position corresponding to the average of the chemical shifts. The results of ¹⁹F NMR studies of the tRNA^{Val} mutants with base substitutions at positions 32 and 38 demonstrate the effects of mutations at positions 32 and 38 on anticodon loop conformation. FU32 resonates at 7.11 ppm in the ¹⁹F NMR spectrum of FU-tRNA^{Val} mutant U32G38 (Figure 3.28). Peaks at such downfield positions are observed for FUs in a GU wobble base pair (Chu and Horowitz, 1989). This is thus strong evidence that G38 forms a base pair with FU32 in this FU-tRNA^{Val} mutant. Such results were not observed for peak FU38 in the

spectrum of FU-tRNA^{Val} mutant U38G32, indicating that the geometries of GU and UG produce different effects on anticodon loop conformation.

The geometry of UG pair resulting in an unusual stacking of its bases with its neighbors to the 5' and 3' sides was found by Mizuno and Sundralingam (1978). The overlap of the U to its 5' neighboring base and that the G to its 3' neighbor is much more extensive than to the bases at the 3' and 5' side, respectively. Thus an UG pair with G at the 3' end is preferred at the end of a helical region. This is consistent with the above results from ¹⁹F NMR studies of FU-tRNA^{Val} mutant U38G32 and U32G38. Examination of UG pairs in 16S rRNA reveals the same preference for stacked UG pairs (Van Knippenberg *et al.*, 1990).

There are other unexplained effects on the anticodon loop structure produced by mutations at positions 32 and 38. In the ¹⁹F NMR spectrum of FU-tRNA^{Val} mutant U32C38 (Figure 3.33), resonances of all three FUs in the anticodon loop are not in the central region of the spectrum. Thus their environments differ from those of the usual FU residues located in the single stranded regions of tRNA (Chu *et al.*, 1992). There must be some special stacking or other interactions causing these FUs to exhibit unusual chemical shifts. All these FU peaks are very sensitive to temperature, indicating the anticodon loop conformation is very flexible (Figure 3.33).

Accurate translation of the genetic code requires the recognition of anticodon triplets in mRNA by an appropriate tRNA. Because of the importance of codon-anticodon interactions in protein biosynthesis, the binding of complementary oligonucleotides to tRNA has been examined by many methods. The fluorescence data of Urbanke and Maass (1978) suggests a transition from a 3' stacked to a 5' stacked conformation of the anticodon. ¹H NMR studies demonstrated that four to five base

pairs are formed between the codon-containing pentanucleotide UUCAG and the anticodon loop of yeast tRNA^{Phe} (Geerdes *et al.*, 1980a). ¹H NMR studies of GGCU binding to *Bombyx mori* tRNA^{Gly}_{GCC} showed appearance of five new imino proton peaks, three GC base pairs and one UU base pair induced by codon-anticodon interaction (Amano and Kawakami, 1992). ¹⁹F NMR studies showed the position of the chemical shift for FU33 changes on GUAA binding to FU-tRNA^{Val}, but not GUAX (X=G, C or G), suggesting a possible interaction of the 3' A of GUAA with FU33 in the anticodon loop (Gollnick *et al.*, 1987). These NMR data indicate that the tRNA anticodon could become 5' stacked in the anticodon loop on codon binding. However, the structure of codon-anticodon complex remains unclear.

GUAA binds only to the anticodon loop of native FU-tRNA^{Val} (Gollnick *et al.*, 1987). Transfer NOE experiment also shows binding of GUAA to tRNA^{Val} (Figure 3.39). But no significant conformational changes were detected by imino ¹H NMR study of GUAA binding to native tRNA^{Val} (Figure 3.34). This study also failed to see the imino proton resonances from the codon-anticodon complex, indicating the binding and release of GUAA from the tRNA^{Val} is in fast exchange.

Further studies of the structure of the codon-anticodon complex by ¹H NMR have been initiated. The aromatic and 1' sugar protons of the codon-containing oligonucleotide GUAA have been assigned in a 2D ROESY experiment (Figure 3.36 and Table 3.4), assuming an A-form right-handed helical structure for GUAA. The U2 sugar protons have also been assigned by ROESY and TOCSY experiments (Figures 3.36 and 3.38, Table 3.4). Other sugar protons have been assigned to individual nucleotides. Complete assignment of spectrum of GUAA requires additional experimentation. Of the four sugar ring spin systems, that of A3 is not well defined, very

few NOEs were seen among protons of this residue. Thus A3 must be very flexible in this short oligonucleotide.

Preliminary transfer NOE experiment showed that certain NOE cross peaks of GUAA bound to tRNA^{Val} have different relative intensities compared to the ROE cross peaks of free GUAA. This indicates conformational changes in GUAA upon binding to tRNA^{Val}. Quantitative measurement of these cross peaks will help to determine the detailed structure of GUAA in the bound state. Then the structure of the codon-anticodon complex can be better described.

REFERENCES

- Amano, M. and Kawakami, M. (1992) *Eur. J. Biochem.* **210**, 671-681
- Bax, A. and Davis, D. G. (1985) *J. Magn. Reson.* **63**, 207-213
- Bertrand, K. and Yanofsky, C. (1976) *J. Mol. Biol.* **103**, 339-349
- Biou, V., Yaremchuk, A., Tukalo, M. and Cusack, S. (1994) *Science* **263**, 1404-1410
- Borel, F., Härtlein, M. and Leberman, R. (1993) *FEBS* **324**, 162-166
- Cavarelli, J., Rees, B., Ruff, M., Thierry, J.-C. and Moras, D. (1993) *Nature* **362**, 181-184
- Chao, Y. H. and Kearns, D. R. (1977) *Biochem. Biophys. Acta.* **427**, 20-26
- Chu, W.-C., Feiz, V., Derrick, W. B. and Horowitz, J. (1992) *J. Mol. Biol.* **227**, 1164-1172
- Chu, W.-C. and Horowitz, J. (1989) *Nucleic Acids Res.* **17**, 7241-7252
- Chu, W.-C., Kintanar, A. and Horowitz, J. (1992) *J. Mol. Biol.* **227**, 1173-1181
- Chu, W.-C. and Horowitz, J. (1991) *Biochemistry* **30**, 1655-1663
- Cleland, W. W. (1979) *Methods Enzymol.* **63**, 103-138
- Crick, F. H. C. (1966) *J. Mol. Biol.* **19**, 548-555

- Dao, V., Guenther, R. H. and Agris, P. (1992) *Biochemistry* **31**, 11012–11079
- DeBruijn, M. H. L., Schrier, P. H., Eperion, I. C. and Barrell, B. G. (1980) *Nucleic Acids Res.* **8**, 5231–5238
- Derrick, W. B. and Horowitz, J. (1993) *Nucleic Acids Res.* **21**, 4948–4953
- Driscoll, P. C., Clore, G. M., Beress, L., Gronenborn, A. M. (1989) *Biochemistry* **28**, 2178–2187
- Eidlic, L. and Neidhardt, F. C. (1965) *Proc. Nat. Acad. Sci. USA* **53**, 539–543
- Eisinger, J. (1971) *Biochem. Biophys. Res. Commun.* **43**, 854–861
- Eisinger, J. and Spahr, P. F. (1973) *J. Mol. Biol.* **73**, 131–137
- Francklyn, C. and Schimmel, P. (1989) *Nature* **337**, 478–481
- Fresco, J. R., Adams, A., Ascione, R., Henley, D. and Lindahl, T. (1966) *Cold Spring harbor Symp. Quant. Biol.* **31**, 527–537
- Gefter, M. L. and Russell, R. L. (1969) *J. Mol. Biol.* **39**, 145–157
- Giegé, R., Puglisi, J. D. and Florentz, C. (1993) *Progr. Nucl. Acids Res. Mol. Biol.* **45**, 129–206
- Gollnick, P., Hardin, C. C. and Horowitz, J. (1987) *J. Mol. Biol.* **197**, 571–584
- Greerdes, H. A. M., VanBoom, J. H. and Hilberc, W. (1980a) *J. Mol. Biol.* **142**, 195–217
- Greerdes, H. A. M., VanBoom, J. H. and Hilberc, W. (1980b) *J. Mol. Biol.* **142**, 219–230
- Griffey, R. H., Poulter, C. D., Yamaizumi, Z., Nishimura, S. and Hurd, R. E. (1982) *J. Am. Chem. Soc.* **104**, 5811–5813.
- Grodberg, J. and Dunn, J.-J. (1988) *J. Bact.* **170**, 1245–1253
- Gronenborn, A. M. and Clore, G. M. (1990) *Biochemical Pharmacology* **40**, 115–119
- Grosjean, H. J., Söll, D. G. and Crothers, D. M. (1976) *J. Mol. Biol.* **103**, 499–519

- Grundy, F. J. and Henkin, T. M. (1993) *Cell* **74**, 475–482
- Grundy, F. J., Rollins, S. M. and Henkin, T. M. (1994) *J. Bact.* **176**, 4518–4526
- Hall, K. B., Sampson, J. R., Uhlenbeck, O. C. and Redfield, A. G. (1989) *Biochemistry* **28**, 794–5801
- Hardin, C. C., Gollnick, P. and Horowitz, J. (1988) *Biochemistry* **27**, 487–495
- Hare, D. R., Rebeiro, N. S., Wemmer, D. E. and Reid, B. R. (1985) *Biochemistry* **24**, 4300–4306
- Hills, D. C., Cotten, M. L. and Horowitz, J. (1983) *Biochemistry* **22**, 1113–1122
- Hoagland, M. B., Zamecnik, P. C. and Stephenson, M. L. (1957) *Biochem. Biophys. Acta* **24**, 215–223
- Horowitz, J., Ofengand, J., Daniel, W. E. and Cohn, M. (1977) *J. Biol. Chem.* **252**, 4418–4420
- Hyde, E. I. and Reid, B. R. (1985) *Biochemistry* **24**, 4307–4325
- Jaishree, T. N. and Wang, A. H.-J. (1993) *Nucleic Acids Res.* **21**, 3839–3844
- Johnston, P. D. and Redfield, A. G. (1977) *Nucleic Acids Res.* **4**, 3599–3608
- Johnson, P. D. and Redfield, A. G. (1978) *Nucleic Acids Res.* **5**, 3913–3927
- Kaplan, S., Stretton, A. O. W. and Brenner, S. (1965) *J. Mol. Biol.* **14**, 528–533
- Kayne, M. S. and Cohn, M. (1974) *Biochemistry* 4159–4166
- Kessler, H., Geiwsinger, C., Kerssebaum, R., Wagner, K. and Ernst, R. R. (1987) *J. Am. Chem. Soc.* **109**, 607–609
- Kim, S.-H., Sussman, J. L., Suddeth, F. L., Quigley, G. J., Mcpherson, A., Wang, A. H. J., Seeman, N. N., Rich, A. (1974) *Proc. Nat. Acad. Sci. USA* **71**, 4970–4974
- LeRoy, J. L., Gueron, M., Thomas, G. and Favre, A. (1977) *Eur. J. Biochem.* **74**, 567–585

- Lindal, T., Adams, A. and Fresco, J. R. (1966) *Proc. Nat. Acad. Sci. USA* **55**, 941-945
- Maniatis, T., Fritsch, E. F. and Sambrook, J. (1989) *In Molecular Cloning - A laboratory Manual*, (Cold Spring Harbor Laboratory, Cold Spring Harbor, NY)
- Martin, F., Erian, G., Eiler, S., Moras, D., Dirheimer, G. and Gangloff, J. (1993) *J. Mol. Biol.* **234**, 965-974
- Miller, J. P., Hussoin, Z. and Schweizer, M. P. (1976) *Nucleic Acids Res.* **3**, 1185-1191
- Mizuno, H. and Sundaralingam, M. (1978) *Nucleic Acids Res.* **6**, 4451-4461
- Muramatsu, T., Nishikawa, K., Nemoto, F., Kuchino, Y. and Yokoyama, S (1988) *Nature* **336**, 179-181
- Nishimura, S. (1979) *In transfer RNA: Structure and properties and Recognition*, eds. Schimmel, P. R., Söll, D. and Abelson, J. N. (Cold Spring Harbor Laboratory, Cold Spring Harbor, NY), pp. 55-79
- Normanly, J., Ollick, T. and Abelson, J. (1992) *Proc. Nat. Acad. Sci. USA* **89**, 5682-5684
- Normanly, J., Orgden, R. C., Horvath, S. J. and Abelson, J. (1986) *Nature* **321**, 213-219
- Olson, T., Fournier, M. J., Langley, K. H. and Ford, N. J. (1976) *J. Mol. Biol.* **102**, 193-205
- Perret, V., Garcia, A., Puglisi, J., Grosjean, H., Ebel, J. P., Florentz, C. and Giegé R. (1990) *Biochimie* **72**, 735-744
- Persson, B. C., Gustafsson, C., Berg, D. E. and Björk, G. R. (1992) *Proc. Nat. Acad. Sci. USA* **89**, 3995-3998
- Peters, G. G. and Dahlberg, J. E. (1979) *J. Virol.* **31**, 398-407
- Peterson, R. D., Bartel, D. P., Szostak, J. W., Horvath, S. J. and Feigon, J. (1994) *Biochemistry* **33**, 5357-5366
- Plateau, P. and Guéron, M. (1982) *J. Am. Chem. Soc.* **104**, 7310-7311

- Pongs Bald, R. and Reinwoud, E. (1973) *Eur. J. Biochem.* **32**, 117–125
- Pallanck, L. and Schulman, L. H. (1991) *Proc. Nat. Acad. Sci. USA* **88**, 3872–3876
- Rajagopal, P. and Feigon, J. (1989) *Biochemistry* **28**, 7859–7870
- Rance, M. (1987) *J. Magn. Reson.* **74**, 557–564
- Redfield, A. G. (1978) *Methods Enzymol.* **49**, 253–287
- Reid, B. R., Ribeiro, N. S., Gould, G., Robillard, G., Hilbers, C. W. and Shulman, R. G. (1975) *Proc. Nat. Acad. Sci. USA* **72**, 2049–2053
- Rhodes, D. (1977) *Eur. J. Biochem.* **81**, 91–98
- Rich, A. and Schimmel, P. (1977) *Nucleic Acids Res.* **4**, 1649–1655
- Robertus, J. D., Ladner, J. E., Finch, J. T., Rhodes, D., Brown, R. S., Clark, B. F. C., Klug, A. (1974) *Nature* **250**, 546–551
- Rould, M. A., Perona, J. J., Söll, D. and Steitz, T. A. (1989) *Science* **246**, 1135–1142
- Rould, M. A., Perona, J. J. and Steitz, T. A. (1991) *Nature* **352**, 213–218
- Ruff, M., Krishnaswamy, S. Boegkin, M., Poterzman, A., and Moras, D (1991) *Science* **252**, 1682–1689
- Saenger, W. (1984) *Principles of Nucleic Acid Structure*, (Springer-Verlag, New York)
- Sampson, J. and Uhlenbeck, O. C. (1988) *Proc. Nat. Acad. Sci. USA* **83**, 1033–1037
- Sanger, F., Coulson, A. R., Barrell, B. G., Smith, A. J. H. and Roe, B. A. (1980) *J. Mol. Biol.* **143**, 161–178
- Schimmel, P. R., and Redfield, A. G. (1980) *Annu. Rev. Biophys. Bioeng.* **9**, 181–221
- Schulman, L. H. (1991) *Prog. Nucleic Acid Res. Mol. Biol.* **41**, 23–87

- Schulman, L. H. and Pelka, H. (1988) *Science* **242**, 765–768
- Schulman, L. H. and Chambers, R. W. (1968) *Proc. Nat. Acad. Sci. USA* **61**, 308–315
- Sklenar, V. and Bax, A. (1987) *J. Magn. Reson.* **74**, 469–479
- Smith, F. W. and Feigon, J. (1992) *Nature* **356**, 164–168
- Soffer, R. L. (1974) *Av. Enzymol.* **40**, 91–104
- Sprinzi, M. Wagner, T. Lorenz, D. and Erdmann, V. A. (1976) *Biochemistry* **15**, 3031–3039
- Stein, A and Crothers, D. M. (1976) *Biochemistry* **15**, 160–168
- Studier, F. W. and Moffatt, B. A. (1986) *J. Mol. Biol.* **189**, 113–130
- Szewczak, A. A., White, S. A., Gewirth, D. T. and Moore, P. B. (1990) *Nucleic Acids Res.* **18**, 4139–4142
- Taylor, J. W., Ott, J. and Eckstein, F. (1985) *Nucleic Acids Res.* **13**, 8765–8785
- Urbanke, C. and Maass, G. (1978) *Nucleic Acids Res.* **5**, 1551–1560
- Van Knippenberg, P. H., Formenoy, L. J. and Heus, H. A. (1990) *Biochimica et Biophysica Acta.* **1050**, 14–17
- Varshney, U., Lee, C.-P. and RajBhandary, U. L. (1991) *J. Mol. Biol.* **266**, 24712–24718
- Watanabe, K. Oshima, T and Nishimura, S. (1976) *Nucleic Acids Res.* **3**, 1703–1709
- Waters, L. C., Mullin, B. C., Ho, T. and Yang, W. K. (1975) *Proc. Nat. Acad. Sci. USA* **72**, 2155–2159
- Weigert, M. G., Lanka, E. and Garen, A. (1965) *J. Mol. Biol.* **14**, 522–527
- Yaniv, M. and Barrell, B. G. (1969) *Nature* **222**, 278–279

ACKNOWLEDGMENTS

I would like to express my deepest appreciation to my parents for their constant support, encouragement during my study here.

I thank Dr. Jack Horowitz, my major professor, for his superb guidance and hard pushing during my work in his laboratory.

To Dr. Agustin Kintanar, I would like to express my great appreciation for his introducing me to the NMR world. I thank Dr. Dave Scott for his assistance in obtaining the NMR spectra and data processing.

Finally, I thank all my friends at ISU, for their support and care.